Functional Analysis of Cellular STUbLs in the Replication Cycle of Human Adenovirus Type 5

DISSERTATION

with the aim of achieving a doctoral degree at the

Faculty of Mathematics, Informatics and Natural Sciences,

Department of Biology,

University of Hamburg

submitted

by

Sarah Müncheberg

August 2017 in Hamburg

Tag der Disputation: 15.11.2017

Gutachter: Prof. Dr. Thomas Dobner

Prof. Dr. Nicole Fischer

PD. Dr. Sabrina Schreiner

Prüfungsvorsitzende: Prof. Dr. Julia Kehr

Declaration on oath

I hereby declare on oath that I have written the present dissertation myself and have not used any other sources or aids than the ones indicated.

Hamburg,   Signature

Helmholtz Zentrum München · P.O. Box 11 29 · 85758 Neuherberg

Prof. Dr. Ruth Brack-Werner

Institute of Virology

Phone +49(0)89 3187-2923
Fax +49(0)89 3187-3329
brack@helmholtz-muenchen.de

08/28/17

I confirm that Sara Müncheberg's PhD thesis entitled

"Functional Analysis of Cellular STUbLs* in the Replication Cycle of Human Adenovirus Type 5" is fluently and understandably written and displays correct usage of English grammar and spelling. I give my support that the English language of the thesis meets the standard of international scientific English writing.

* *SUMO-targeted ubiquitin ligases*

HelmholtzZentrum münchen
Deutsches Forschungszentrum für Gesundheit und Umwelt (GmbH)

Institut für Virologie
Ingolstädter Landstr. 1 · 85764 Neuherberg

„We know something is happening, but we don't know what it is"

Bob Dylan - The Ballad of a Thin Man

Table of contents

Abbreviations

Ab	Antibody
AdV	Adenovirus
APL	Acute promyelocytic leukemia
ARM	Arginine rich motif
AS	Amino acid
As$_2$O$_3$	Arsen(III)-oxid
ATL	Adulte T cell leukemia
BRK	Baby rat kidney cells
CAR	Coxsackie/adenovirus receptor
DEPC	Diethylpyrocarbonat
DMEM	Dulbecco's Modified Eagle Medium
DMSO	Dimethylsulfoxid
ds	Double-stranded
DSB	DNA double-strand breaks
E.coli	*Escherichia coli*
EBV	Epstein-Barr Virus
ETOH	Ethanol
FCS	Fetal calf serum
ffu	*Fluorescence forming units*
FFU	Focus forming unit
fw	Forward
h p.i.	Hours post infection
h p.t.	Hours post transfection
HAdV	Human Adenovirus
HAdV-C5	Human Adenovirus species C Type 5
HCMV	Human Cytomegalovirus
HRP	Horseradish peroxidase
HTLV-1	Human T-lymphotropic Virus -1
IB	Isotonic buffer
IgG	Immunglobulin G
IP	IP
kb	kilobase
LB	Luria-bertani

Abbreviations

MOI	Multiplicity of infection
NES	Nuclear export signal
NEM	N-ethylmaleimide
NLS	Nuclear localization signal
PBS	Phosphate buffered saline
PCR	Polymerase chain reaction
PEI	Polyethylenimine
PFA	Paraformaldehyde
PTM	Posttranslational modifications
rcf	Relative centrifugal field
rev	Reverse
RF	RING-finger domain
RING	Really interesting new group of proteins
RSB	Reticulocyte standard buffer
RT	Room temperature
RT-PCR	Real time
SCS	SUMO conjugation site
SDC	Sodium desoxy cholate
SDS	Sodium dodecyl sulfate
SIM	SUMO interacting motif
SV40	Simian Virus 40
TBS-BG	Tris-buffered saline with BSA and glycine
TBE	Tris/Borate/EDTA buffer
UV	Ultra violet
WT	Wild type
(v/v)	Volume per volume
(w/v)	Weight per volume

1 Abstract

Human Adenovirus Type 5 from species C (HAdV-C5) represents a good model system for analyzing virus-host interaction pathways. The HAdV-C5 55 kDa gene product from early region 1B (E1B-55K) is a multifunctional phosphoprotein, which is a main factor for targeting antiviral cellular proteins for proteasomal degradation in cooperation with the viral early region 4 open reading frame 6 protein (E4orf6) and cellular components of a Cullin-5-dependent E3 Ubiquitin ligase. Many studies identified cellular targets of the viral E3 Ubiquitin complex, for example p53, Mre11, ATRX and SPOC1. Interestingly, the cellular transcription factor Daxx was identified as a target of a novel E1B-55K dependent degradation pathway, which is independent of E4orf6. To date, a new RF containing protein group called SUMO-targeted Ubiquitin ligases (STUbL) were recently connected to proteasomal degradation of SUMOylated protein. To date two cellular STUbL proteins have been identified: RNF4 and Arkadia/RNF111. The degradation of SUMOylated proteins via STUbL activity is important to prevent the accumulation of SUMOylated proteins upon high cellular stress, including DNA damage events, oxidative- and chemically-induced stress and cancer development.

The main part of this work investigated the role of RNF4 in the productive replication cycle of HAdV-C5. Since some viral factors (Tax from HTLV-1; Rta from EBV) have been described as targets of RNF4, this work unravels the role of RNF4 in the E1B-55K mediated degradation pathway of the PML associated protein Daxx. First, the interaction of E1B-55K and RNF4 could be confirmed in IP analyzes. Furthermore, RNF4 is relocalized in the nuclear matrix of infected cells juxtaposed to E1B-55K containing aggregates. Results of a RNF4 depleted cell line identified RNF4 as a positive factor for HAdV-C5 lytic replication. Interestingly, in transformation assays performed in primary BRK cells a negative effect of RNF4 on E1 region mediated transformation was observed.

The second part of this work focused on the cellular STUbL Arkadia during HAdV-C5 infection. Arkadia was identified as a new interaction partner of E1B-55K and a reduced amount of Arkadia could be detected at late time points of infection, which might indicate a HAdV-C5 dependent degradation of Arkadia during infection.

Abstract

In sum, this work revealed a HAdV-C5 dependent interaction with both cellular STUbLs for the establishment of an efficient viral infection. More experiments are needed to understand the direct link between the productive infection and the cellular SUMO dependent Ubiquitin machinery. However, the differences between the cellular STUbLs RNF4 and Arkadia during infection and the involvement of other viral proteins are of strong interest and subject for further investigations.

2 Introduction

2.1 Adenoviruses

2.1.1 Classification and pathogenesis

Adenoviruses (AdVs) were named after the adenoid tissue from which they were isolated in 1956 (1). AdVs were first characterized as respiratory disease causing agents but it became clear that AdVs are not the major agent of common cold in the general population, although they primarily infect the respiratory tract (2).

AdVs belong to the family *Adenoviridae* which are able to infect a wide range of vertebrates. Over 130 types are known and can be classified into five genera depending on their host specificity, the mammalian Mastadenovirus, bird Aviadenovirus, reptile Atadenovirus, amphibian Siadenovirus and Ichtadenovirus isolated from fish (3, 4) (Fig.1).
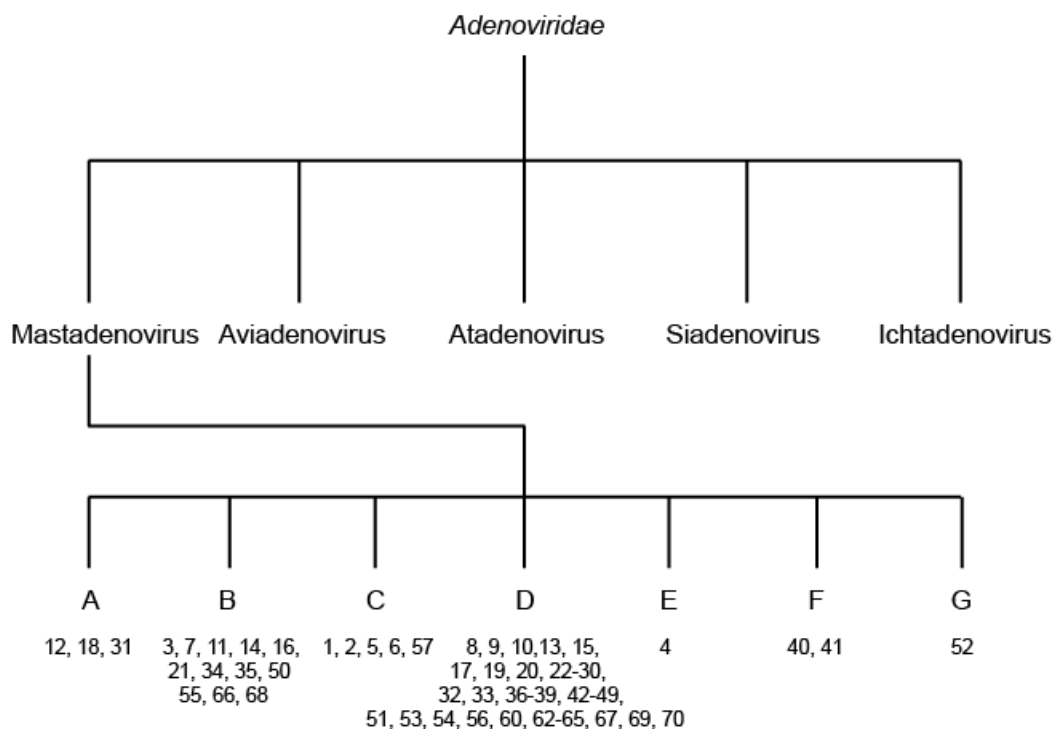
Fig. 1 Classification of HAdV

Simplified taxonomy illustration of the family of *Adenoviridae* including HAdV types 1-70 of different, so far investigated HAdV types. HAdV types are classified according to Davison *et al.* and the International Committee of the Taxonomy of Viruses (ICTV) (5).

Introduction

HAdV belong to the genus Mastadenovirus and are highly prevalent in the human population (4). According to their agglutination properties (6, 7) and since 2007 also by genomic data analysis (8), HAdV have been clustered into seven species A-G and until now over 70 different types were identified (5, 9). Within the seven species, HAdV types were subgrouped according to their sequence homology (GC content), hemagglutination and oncogenicity in immunosuppressed rodents (Fig. 1). HAdV types 2 and 5 of species C belong to the most investigated types and – due to their non-oncogenic properties – are mostly used as prototypes for clinical relevant vector studies (10). Historically, HAdV type 12 was the first human pathogenic virus that has been shown to have oncogenic properties, including induction of malignant tumors in rodents (11). This initial finding led to an astounding amount of research in the field of HAdV mediated transformation and furthermore the classification of HAdV as a DNA tumor virus.

Due to the tight host specificity, different HAdV types cause a wide range of diseases in humans, including pharyngitis (species B), pneumonia (species: A, E), gastroenteritis (specie: G), hemorrhagic cystis (species: A, B, E) or keratoconjunctivitis (species: D) (12-15). Especially in immunocompromised patients, including transplant, radiation and chemotherapy recipients, HAdV may cause life-threatening infections with medium up to high mortality (9, 16, 17). Despite, in immunocompetent patients, HAdV infections are self-limiting and usually cause only mild and local infections. Nevertheless, there are reports of epidemic and systemic HAdV infections with high fever and lethal outcome even in immunocompetent patients (18-21).

Until now, there is no specific treatment for HAdV infections and only general antiviral drugs, such as ribavirin, cidofovir and its derivative brincidofovir, are used to treat severe HAdV infections. Typically, this occurs in children and is usually associated with strong side effects (22, 23). Therefore, the basic research of AdV is still very crucial in order to enable a specific treatment, particularly for hospitalized immunocompromised patients.

Introduction

2.1.2 Structure and genome organization

HAdVs are non-enveloped viruses with an icosahedral capsid and an average size of 80-110 nm in diameter. They contain a linear ds DNA genome of 26-45 kbp with inverted terminal repeats (ITR) at the end of the genome, ranging from 36 up to 200 bp in size (24, 25). Additionally, the 5' end of the genome is associated with terminal proteins (TP), which serve as a primer for viral DNA synthesis (5). The viral capsid is formed by antenna-like extensions (spikes), 240 trimeric hexons and 12 pentons, which are non-covalently linked to the fiber proteins (Fig. 2).
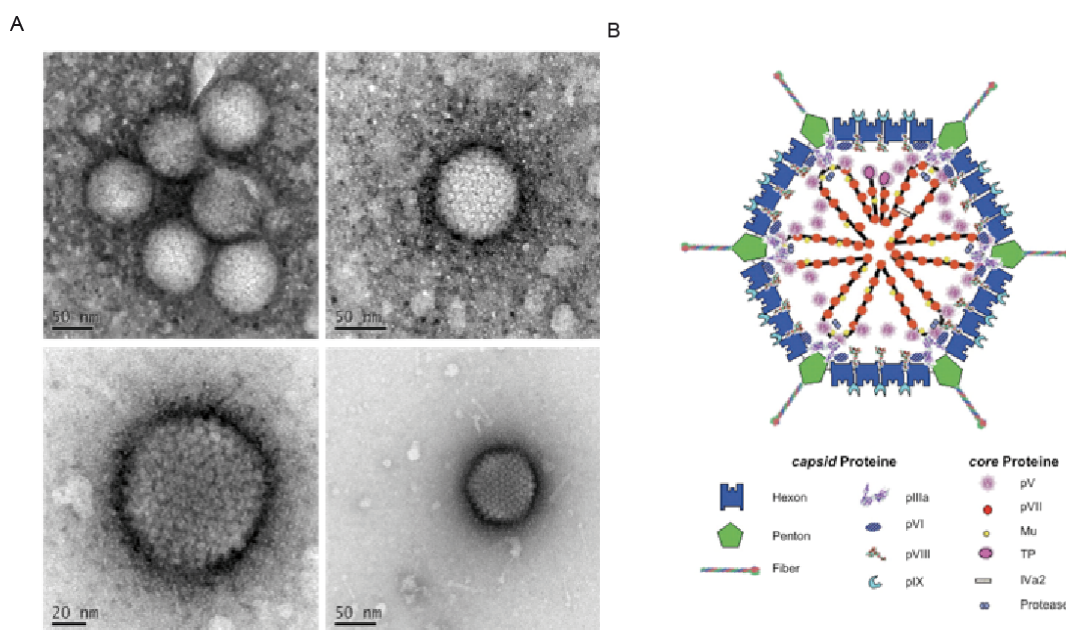
Fig. 2 Schematic representation of HAdV

(A) Electron micrograph of HAdV-C5 particles, showing the icosahedral capsids with the fibers (Technology platform: Microscopy and Image Analysis, Heinrich Pette Institute, Leibniz Institute for Experimental Virology, Hamburg). (B) Schematic cross section of an HAdV particle based on cryoelectronmicroscopic analysis (26).

The HAdV core proteins can be grouped into capsid associated (pIIIa, pVI, pIII and pIX) (27) and genome associated proteins (pV, pVII, Mu, IVa2 and TP) (26, 28). The fiber proteins, especially the C-terminal fiber knob and the penton base protein, mediate the attachment of the virion to the host cell receptors followed by clathrin mediated endocytosis of the virus particle via secondary interaction with the host cell membrane. Besides CD46 (29), the coxsackie/adenovirus receptor (CAR) is the most relevant receptor for the largest group of HAdV (30, 31). Initially, the capsid-associated proteins were thought to solely act as cement proteins for capsid

Introduction

stabilization. However, pVI was found to have an additional function by antagonizing the intrinsic antiviral cell response (32).

The HAdV genome contains nine transcription units, which encode for approximately 40 different regulatory and structural proteins as well as two virus-associated RNAs (VA RNAs). They can be divided in five early (E1A, E1B, E2, E3 and E4), three intermediate early (IX, IVa2 and E2 late) and one major late transcription unit (MLTU). During the course of infection the MLTU primary transcript is further processed into five late mRNAs (L1-L5) (Fig. 3). All HAdV genes are transcribed by the cellular RNA polymerase II, with the exception of the VA RNAs (33). Sequence comparison with other types show that all HAdV have a similar genome organization and express a conserved set of gene products (5, 10).
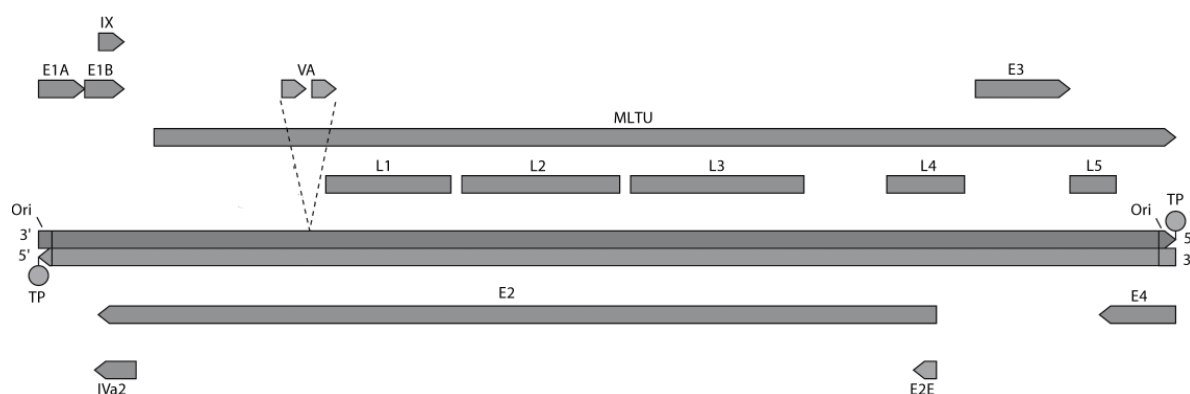
Fig. 3 Genome organization of HAdV-C5

Schematic organization of early proteins (E1A, E1B, E2, E3, E4, pIX, IVa2) and major late transcription unit (MLTU). Arrows indicate the direction of the transcription. The late genes (L1 to L5) are transcribed from a common promoter (MLP) after the onset of viral DNA replication and encode mainly for structural proteins of the virion. The early viral transcription units are already active before DNA synthesis and have regulatory functions related to DNA replication (E2), immune system modulation (E3), transcription, RNA processing, and cell cycle control (E1A, E1B and E4). VA RNAs: virus associated RNAs; TP: terminal protein; Ori: origin of replication; ITR: inverted terminal repeats (modified; from (34)).

2.1.3 Productive replication cycle of HAdV

HAdV types 2 and 5 have been favored for intensive virus replication studies, due to the fact that they can be easily propagated in cell culture. In general, all HAdV mainly infect different types of post mitotic resting cells of the epithelium, the gastrointestinal tract, the central nervous system as well as primary and immortalized cells, where they usually cause lytic infections (35).

Introduction

The replication cycle of HAdV-C5 is divided into the immediate early, early and late phase of infection. Upon clathrin-mediated endocytosis of the virus, the uncoated virus particle is transported to the nucleus where the viral DNA is imported into the nucleus through the nuclear pore complex (NPC). Prior to DNA synthesis, expression of the immediate early protein E1A activates transcription of other viral genes from the E1- and E4-region, which are subsequently spliced in order to produce viral early regulatory proteins. These early regulatory proteins are necessary to favor an optimal environment for efficient virus replication (10). Upon these initial steps, the viral E2A/DBP, the viral DNA polymerase (E2B) and the precursor terminal protein (pTP) are expressed (10).

After synthesis of immediate early and early proteins, the late phase of the infection is induced by the onset of viral DNA synthesis. The transcription of the MLTU is initiated by activation of the major late promoter (MLP), where the late viral mRNAs L1-L5 are generated by differential splicing of the 29 kb major late precursor mRNA (36). The current model favors the shut-off of host cell mRNAs transport and translation to ensure an efficient expression of viral mRNA (37). The HAdV replication cycle is completed by the release of up to 10^4 progeny virions per cell 24-36 h p.i. by cell lysis.

2.1.4 HAdV-C5 protein E1B-55K during lytic infection

In HAdV-C5 infected cells, the E1B-55K protein is involved in several steps in the early and late phase of infection (38). During the early phase, E1B-55K establishes an optimal environment for virus replication by inducing repression of promoter bounded p53 and counteracting the cellular DNA damage response. In order of this, E1B-55K acts as a multifunctional protein, which is known to shuttle between nucleus and cytoplasm. This mechanism is dependent on the internal leucine-rich NES and a SCS at lysine 104 (39-41) (Fig. 4). As already mentioned above, E1B-55K also counteracts the cellular DNA damage response and antiviral factors, which are part of the intrinsic antiviral immune response. Therefore, E1B-55K forms an E3 Ubiquitin ligase complex with the viral protein E4orf6 and the cellular proteins Elongin B and C, Cullin 5 and RING-box proteins (Rbx-1, RCO1, Hrt1) by which E1B-55K serves as the substrate recognition factor while E4orf6 binds Elongin C via the BC-Box motif (42) (Fig. 4). This complex promotes the Ubiquitinylation and hence proteasomal degradation of several cellular proteins that are part of the DNA

Introduction

damage response, including p53, the MRN-complex, chromatin remodeling factors like X-linked α-thalassaemia retardation syndrome (ATRX) and Survival-time associated PHD protein in ovarian cancer 1 (SPOC1) (43-47). Furthermore, DNA ligase IV, the α3 subunit of the cellular surface receptor protein Integrin, the acetyltransferase Tip60 as well as the DNA repair protein Bloom helicase (BLM) were identified as cellular substrates of the E1B-55K/E4orf6 E3 Ubiquitin ligase (48-50). Interestingly, a novel E1B-55K dependent degradation pathway for the cellular death domain associated factor (Daxx) was identified, which is independent of the E4orf6 (51). The exact degradation pathway of Daxx has not been clarified to date. However, it is known that SUMOylated E1B-55K is necessary for the degradation of Daxx in HAdV-C5 infected cells (52) (Fig. 4). Daxx is constitutively associated with the PML nuclear bodies (PML-NBs) and plays a major role in the intrinsic antiviral immune response. Currently, there are numerous indications for Daxx-dependent repression of HAdV-C5 replication, which is reflected in a significant increase of viral gene expression after depletion of Daxx (46, 51). This negative effect of Daxx on viral gene expression is closely related to its interaction with ATRX. Both factors are capable for recruiting histone acetyltransferases (HDACs) to condense chromatin structure at the respective promoters (53, 54). This process prevents the efficient attachment of transcription factors to the DNA and leads to a negative regulation of HAdV-C5 gene expression (46).
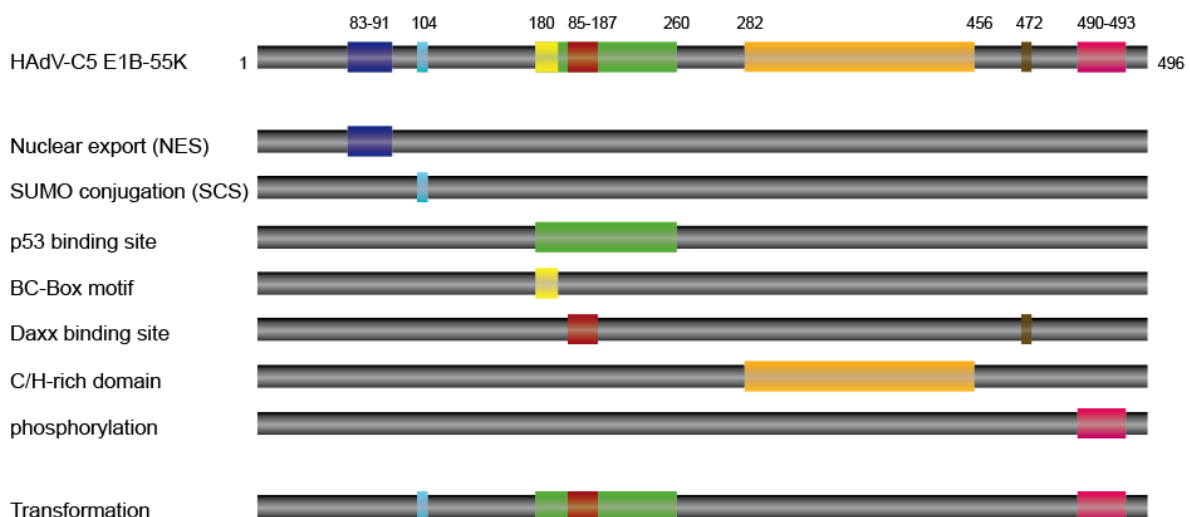
Fig. 4 Structural and functional domains of HAdV-C5 E1B-55K

Schematic representation of structural and functional domains of the HAdV-C5 E1B-55K protein. NES: nuclear export signal; SCS: SUMO conjugation site; BC-Box: Elongin B and C-Box; C/H-rich domain: cysteine/histidine-rich region.

Introduction

2.1.5 Transforming potential and oncogenicity of HAdV

HAdV usually perform a lytic replication cycle in human cells, however in rodents, HAdV induces asymptomatic infections (10). The observation that HAdV-A12 is able to induce solid tumors in newborn hamsters, resulted in the classification of HAdVs as DNA tumor virus (11). Nevertheless, a HAdV dependent malignant tumor development in humans has never been observed (55-57), apart from the presence of low amounts of HAdV DNA in some pediatric brain tumors (35). So far, the HAdV mediated transformation of primary human cells is thought to be very inefficient (58). Nevertheless, some studies confirm the oncogenic potential of certain types (HAdV-A12, HAdV-A18, HAdV-A31) (59). However, a recent publication demonstrated the efficient transformation of human mesenchymal stromal cells (hMSC) by HAdV-C5 early region 1 oncoproteins (60). Until now, HAdVs from species 1-51 have been classified regarding their tumorigenic potential in non-oncogenic, low or highly oncogenic (Fig. 5).
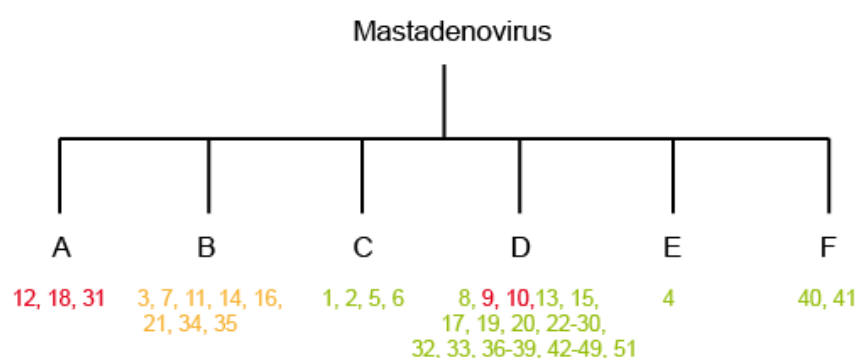
Fig. 5 Oncogenicity of HAdV types in rodents

Classification of HAdV types according to their oncogenic potential in primary rodent cells. So far, only HAdV types 1-51 have been tested. Red = highly oncogenic, yellow = low oncogenic, green = non-oncogenic.

Most HAdV transformed cell lines are characterized by the chromosomally integrated viral DNA of E1A and E1B, which simultaneously leads to the stable expression of corresponding viral proteins (59). Interestingly, several single AS exchange mutations in both proteins can alter the transformation potential (61). Overall, HAdV mediated transformation follows the classical concept of viral oncogenesis, where the viral genes persist within the transformed cells and maintain the oncogenic phenotype. The expression of the E1 region is almost invariably

detectable in all transformed cells and underscores the importance of the encoded proteins (61). E1A interacts with E2F transcription factors, thereby deregulating the cell cycle and pushing the cell into S-phase, while preventing p53 mediated G1-arrest (61). Particularly, E1B blocks the onset of apoptosis to favor an optimal milieu for viral replication. In primary rodent cells however, the same events promote oncogenic transformation. Although a lot of studies carried out the molecular mechanism of this process, it still remains elusive why primary rodent cells can be efficiently transformed, whereas transformation of primary human cells is rather inefficient (62, 63). Besides E1 proteins, E4 gene products are also associated with transformation of primary rodent cells (64, 65). The E4 proteins act through a complex network of protein-protein interactions with cellular factors involved in apoptosis, cell cycle control, DNA repair mechanisms and the integrity of PML-NBs.

2.1.6 Role of HAdV-C5 E1B-55K protein during transformation

Upon infection, E1A induces p53 dependent apoptosis, which is counteracted by E1B-55K and E1B-19K through interaction with apoptosis regulating proteins to keep the cell in the S-phase for optimal virus replication (66, 67). The E1B-55K protein directly interacts with p53 and triggers proteasomal degradation of p53 by the viral E3 Ubiquitin ligase complex, thus inhibiting activation of p53 regulated genes and in consequence also induction of apoptosis (68, 69). A further mechanism of p53-inhibition is the E1B-55K mediated relocalization of p53, due to the shuttling-properties of E1B and the E1B dependent alteration of p53 PTM, like SUMOylation and acetylation (41, 70-74) (Fig. 5). Besides, E1B-55K mediates transformation through several other different functions, including the interaction with several cellular proteins involved in DNA repair, apoptosis and transcription. Interestingly, it was shown that the E1B-55K dependent Daxx degradation is important for the transformation potential of HAdV-C5 E1 gene products. Additionally, the interaction of E1B-55K and Daxx also seems to play an important role for the HAdV-C5 E1A/E1B mediated transformation (Fig. 4), since E1B-55K mutants that are not able to degrade Daxx show no focus forming potential (52).

2.2 The cellular PTM machinery

2.2.1 General pathways of cellular PTM

PTM of proteins is the main mechanism of the cell to regulate several processes, including cell cycle progression, cell growth, signal transduction, protein stability and control, the DNA damage response but also viral infections (75-77). The best-known protein for PTM is Ubiquitin, the founding member of the Ubiquitin-like (Ub) modifier superfamily. Ubiquitin is essential in most organisms and plays a central role in targeting proteins for proteolytic degradation by the 26S proteasome. Despite that, regulation of protein localization and/or activity as well as crucial steps in the cell cycle can also be regulated by covalent attachment of Ubiquitin to proteins. Additionally, in 1996 the small-Ubiquitin-related modifier (SUMO) was identified and has been shown to covalently modify several proteins upon cellular stress to maintain chromatin structure and/or genome stability in the same way as Ubiquitin (78). Upon identification, the SUMOylation system was not thought to be related to the Ubiquitin system. Rather, both Ubs were supposed to be part in competitive functions by targeting identical lysine residues within the protein sequence (78). However, it soon became clear that both systems were linked in a very specific manner, first and foremost in the process of SUMO dependent Ubiquitinylation (79). This very specific modification of proteins with SUMO and Ubiquitin plays an important role in UV irradiation-induced DNA damage as well as genome and protein stability (80-83).

The Ubiquitin and SUMO conjugation pathway is a three-step enzymatic cascade that shares a lot of similarities. Upon PTM stimulation, the SUMO/Ub-activating enzyme (E1) leads to an ATP dependent activation of the Ub C-terminus. Thereby, the active site cysteine in the E1 protein is forming a high energy thiolester bond with the C-terminus of the Ub, releasing adenosinmonophosphat (AMP) (84). The activated Ub is then transferred to a cysteine in the SUMO/Ub conjugating enzyme (E2), where it forms an Ub/E2 thiolester intermediate (85). With the help of a SUMO/Ub protein ligase (E3), the Ub gets transferred from the E2 protein to the substrate, where it is conjugated to a specific lysine residue in the target protein sequence (Fig. 6).

Introduction
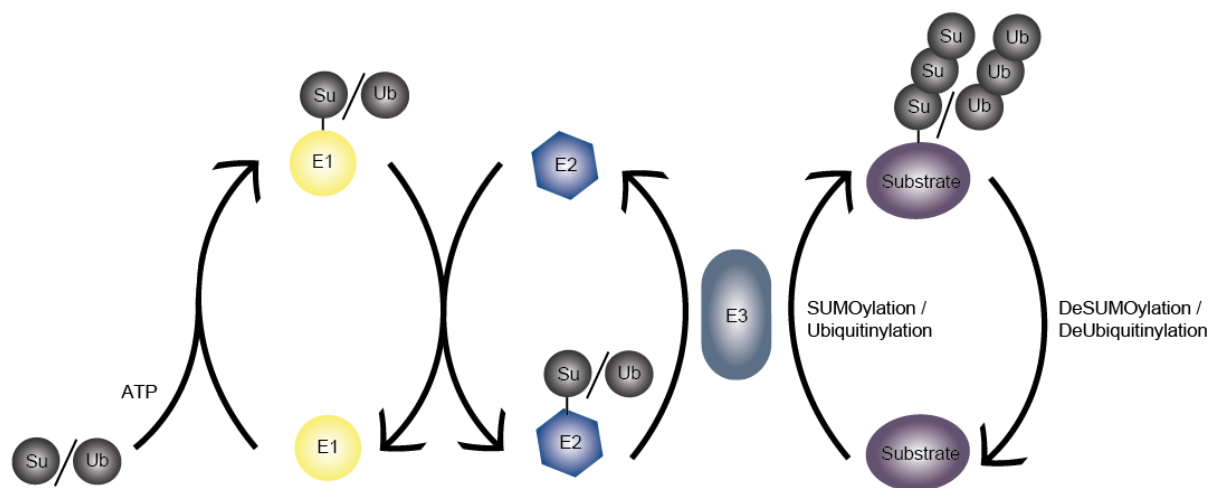
Fig. 6 Pathway of the cellular SUMO/Ubiquitin machinery

Intersection of the SUMO/Ubiquitin pathway, which shows the similarities of the three-step enzymatic cascade of SUMO (Su) and Ubiquitin (Ub) conjugation. Adapted from Garza *et al.* (86).

Ubiquitinylation and SUMOylation are both covalent protein modifications. They are attached to the protein via an isopeptide bond between a C-terminal glycine in the Ub and a lysine residue in the substrate. For SUMO, the consensus motif $\psi(I/V/L)KX(D/E)$ was identified, where ψ represents a hydrophobic AS and K is the main lysine residue for SUMO conjugation (87). Noteworthy, the SUMO consensus motif harbors a direct binding site for the SUMO-conjugating enzyme Ubiquitin carrier protein 9 (Ubc9), which is the only known E3 SUMO ligase so far (78). Many studies from the last years conclude that almost half of the known SUMO substrates are modified at a minimal KxE motif. However, upon cellular stress, lysine residues in non-SCS are also used for modification (88). So far, five different isoforms of SUMO, SUMO-1-5, were identified. However, SUMO-1-3 are the most studied SUMO isoforms so far and are expressed in all human tissues. Interestingly, SUMO-1 and SUMO-2/3 share a 97% sequence identity, but only 50% sequence homology and seem to be expressed in all tissues (89) (Fig. 7). NMR studies have shown that SUMO-1 and Ubiquitin have a similar 3D-structure, although charge distribution on the protein surface differs a lot despite sharing 18% sequence identity (90) (Fig. 7). Both SUMO and Ubiquitin are reversible PTMs and can be removed by enzymes of the Ubiquitin cleavage protease (Ulp) family by cleaving Ubs from the substrate (78, 91). Ubiquitin is able to form polymeric chains by covalent attachment to one another. Further Lys 48-linked poly-Ubiquitinylation is strongly linked to proteasomal degradation of the targeted protein (92). In contrast, SUMO was initially

12

Introduction

thought to function as a monomer, however SUMO-2 and 3 harbor an internal SCS at lysine 11 and both proteins are able to form polymeric chains (93) (Fig. 7). The function of this SUMO chains are not fully understood so far, but there are strong indications that they might be essential for degradation of SUMO- and Ubiquitinylated proteins upon cellular stress. SUMO-1 conjugation to cellular or viral substrates mainly causes an altered affinity to other proteins, which affects localization and/or activity.
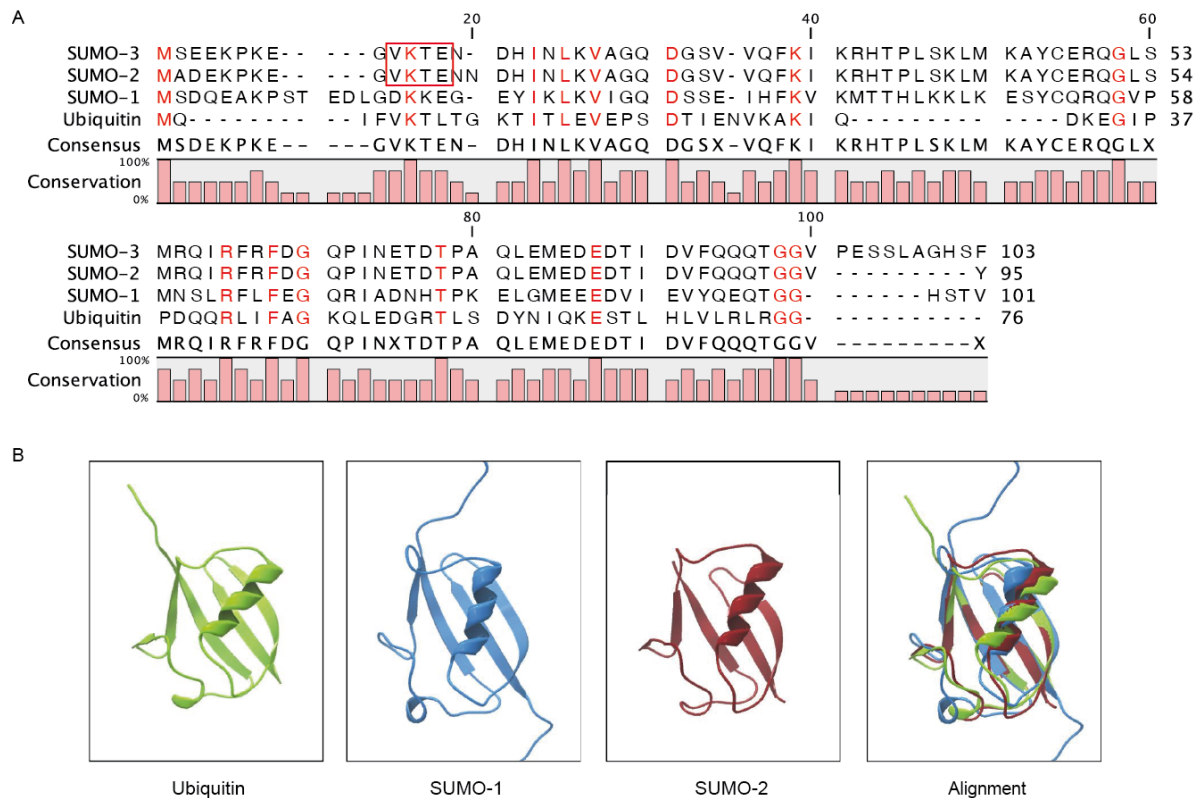
Fig. 7 Ubiquitin and SUMO protein structures and alignment

(A) AS sequence alignments of Ubiquitin and SUMO-1, SUMO-2 and SUMO-3. Identities are indicated in red. A SCS for polymeric chain elongation present in SUMO-2 and SUMO-3 is boxed in red. (B) Schematic protein structures with data obtained from the protein data bank (PDB; (94)) highlight the similarities (alignment) of the three-dimensional structures from Ubiquitin, SUMO-1 and SUMO-2. PBD-IDs: Ubiquitin, green: 1ubq; SUMO-1, blue: 1a5r; SUMO-2, red: 1wm3. Graphics and alignment were generated with the CLC main workbench 7.

2.2.2 Modulation of the cellular Ubiquitin and SUMO machinery in HAdV-C5 infected cells

PML-NBs are multi-protein complexes, which are present in nearly all cell types and can perform diverse functions depending on their composition (95). To date, more than 80 proteins are known to transiently localize to PML-NBs (96-99). Previous studies show that the cellular factors promyelocytic leukemia protein (PML), Daxx, ATRX, speckled protein 100kDa (Sp100) and SUMO-1 are the main components of PML-NBs. A direct interaction with PML has so far only been confirmed for a very small number of proteins, such as p53, Daxx, Sp100, Ubc9 as well as SUMO-1 (100, 101). It is known that all components of the core structures can be conjugated to SUMO-1, which is necessary for assembling the PML-NBs (102-104). In HAdV-C5 infected cells, viral proteins target the PML-NBs to directly prevent the intrinsic antiviral immune response mediated by PML-NB components. An interaction of E1B-55K with PML-NB key components, like Daxx and Sp100A was already observed in HAdV-C5 infected cells (51, 105, 106). This interaction leads to proteasomal degradation of cellular proteins, triggered by the viral E1B-55K/E4orf6 E3 Ubiquitin ligase complex. In the same moment, E4orf3 relocalizes key components of the PML-NB into track-like structures (107, 108), making antiviral factors such as Daxx accessible for degradation. Interestingly, it could be shown that the repressive properties of Daxx are inhibited as long as the protein can be detected in the PML-NBs (109). In sum, the multifunctional transforming properties of E1B-55K depend on several factors, however most of all on the direct SUMO modification of E1B-55K (110).

2.2.3 HAdV-C5 E1B-55K protein and the cellular PTM machinery

A strong interplay between E1B-55K and the cellular PTM machinery has been first observed by the interaction of E1B-55K with Ubc9 (111). Furthermore an E3 SUMO ligase activity towards p53 of a PML-NB associated E1B-55K was also described in 2008 (72, 73, 112). Additionally, Härtl and coworkers identified a putative cysteine and histidine rich RING (really interesting new group of proteins) motif in E1B-55K (113) (Fig. 4). RING motifs are important for Ubiquitin ligase activity of E3 Ubiquitin ligases (114) and are essential for the cellular Ubiquitinylation pathway (115, 116). Moreover, the RING motif enables a putative interaction/dimerization of E1B-55K with other Ubiquitin ligases, which reinforces the hypothesis of an influence of E1B-

Introduction

55K on the cellular PTM machinery. Nevertheless, the exact function of the RING motif in E1B-55K is still unknown and needs to be further investigated (113).

Additionally, it has been shown that E1B-55K itself undergoes SUMO-1 conjugation at a SCS at lysine 104 (40), which is directly linked to its Phosphorylation at the C-terminus mediated by casein kinase 2 (CK2) (117) (Fig. 4). In latest findings show that E1B-55K can be modified by SUMO-2 and SUMO-3 in addition to SUMO-1. The extent of this PTM is also closely related to the degree of Phosphorylation of E1B-55K (111). Inactivation of these PTM leads to a strong impact on E1B-55K functions, including impaired nucleo-cytoplasmic shuttling, inefficient repression of p53, inability of Daxx degradation and, as already described before, diminished focus forming properties of primary mammalian cells (52, 111, 118). Finally, overexpression of SUMO-1 leads to an accumulation of E1B-55K at characteristic nuclear structures, presumably PML-NBs, at least observed in HAdV-C5 E1A7E1B transformed rodent cells (110).

As mentioned above, it has been shown that E1B-55K is able to posttranslationally modify Daxx, which subsequently causes proteasomal degradation in the absence of E4orf6 (119). Further, some reports indicate that cellular stress or treatment with arsenic trioxide (AS$_2$O$_3$) also result in an increased recruitment of Daxx to PML-NBs. In line with this, it could be observed that Daxx becomes SUMOylated and recruited to PML-NBs upon UV-induced apoptosis (120, 121). This supports the assumption that the nuclear localization of Daxx to PML-NBs and thus the interaction of SUMOylated Daxx with PML are crucial for the repression of HAdV5-replication. Therefore, HAdV-C5 might target SUMOylated Daxx for proteasomal degradation with the help of the recently identified SUMO-targeted Ubiquitin ligase protein family.

Introduction

2.3 Cellular SUMO-targeted Ubiquitin ligases

2.3.1 Human RING-finger protein 4 (RNF4; SNURF)

SUMO-targeted Ubiquitin ligases (STUbL) or E3 Ubiquitin ligases for SUMOylated proteins (ULS) represent a new class of Ubiquitin ligases, which link SUMO modification to the Ubiquitin/proteasome system.

Non-covalent SUMO/SIM interactions between the SUMOylated target and the STUbL mediates the Ubiquitinylation of SUMOylated proteins for proteasomal degradation (122) (Fig. 8). So far, only two human STUbLs are identified, the RF protein 4 (RNF4, Small nuclear finger protein; SNURF) and the RF protein 111 (RNF111, Arkadia) (122, 123). At least for RNF4, the SIM motifs 2, 3 and 4 are supposed to form β-strand confirmation upon SUMO interaction and bind to SUMO between the second β-strand and the following α-helix (124). In this process, SUMO-1 and SUMO-2/3 are preferred similarly, although chains of at least three SUMO forms are favored (125).
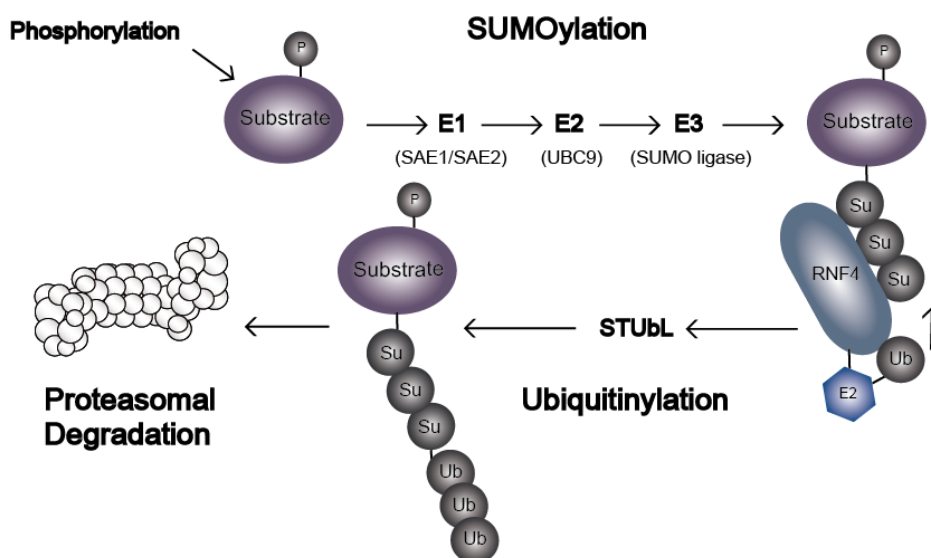
Fig. 8 STUbL mediated Ubiquitinylation of SUMOylated proteins.

Schematic representation of STUbL/RNF4 triggered proteasomal degradation of SUMO modified proteins via Ubiquitinylation. Adapted from J. L. Staudinger (126).

Introduction

To date, RNF4 is the most studied STUbL and represents the smallest characterized STUbL with a size of only 190 AS. Originally, RNF4 was discovered as a coactivator of a steroid receptor (127). For the first time, in 2004, an E3 Ubiquitin ligase activity was detected for RNF4 (128). By analysis of RNF4 levels in human tissues, a high expression of RNF4 mRNA was detected in testis, although low levels of RNF4 mRNA were examined in all other human tissues (129). RNF4 comprises four consensus sequences for SIM domains (SIM1-SIM4; between AS 36 and 110) and a RING domain at the C-terminus (125, 130) (Fig. 9). Additionally, a contiguous hydrophobic region connecting the SIM4 and the RING domain was identified via NMR spectroscopy (124). Mutational analysis of this putative SIM showed no effect on the interaction with SUMO-2 chains and thus SIM5 is unlikely to be a *bona fide* SIM domain (124). RNF4 acts as a homodimer, which gets activated via dimerization of the RING domain. This is essential for the ligase function of the protein and thus for the Ubiquitinylation of SUMOylated proteins (131). For the transfer of Ubiquitin to the SUMOylated target protein, RNF4 binds the E2 charged Ubiquitin and thereby activates this bond for catalysis (114, 132, 133). Moreover, it was recently published that RNF4 also binds to phosphorylated proteins via an ARM, leading to proteasomal degradation of these proteins (134) (Fig. 9). Additionally, *in silico* sequence analysis identified a putative nuclear localization signal (NLS) at the N-terminus of the protein (Fig. 9).
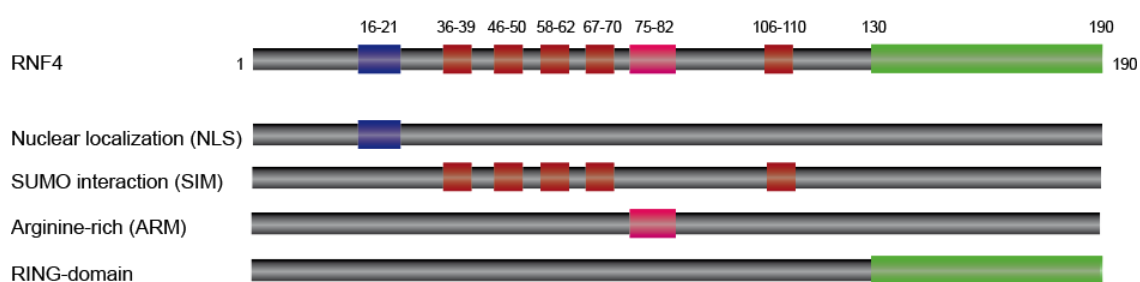
Fig. 9 Structural and functional domains of RNF4

Schematic representation of structural and functional domains of RNF4. NLS: nuclear localization signal; SIM: SUMO interaction motif; ARM: Arginine rich motif; RING domain: Really Interesting New Group of proteins domain.

Introduction

The degradation of SUMOylated proteins via STUbL activity is important to prevent the accumulation of SUMOylated proteins inside the cell upon high cellular stress, including DNA damaging events, oxidative and chemically induced stress and cancer development. Therefore, it is not surprising that PML and the oncogenic fusion PML/RARα (retino acid receptor α) proteins were identified as the first targets of RNF4 (135). Previously, it was shown that RNF4 is recruited to the PML-NBs via SUMO-1 modification (136). RNF4 was shown to bind SUMO-1 non-covalently and in this course localizes to NBs containing PML and SUMO-1. SUMO-1 overexpression markedly enhances colocalization between PML and RNF4, but the direct SUMO-1 modification of both proteins is not crucial for this interaction (136). RNF4 binds to polySUMOylated PML via a non-covalent SUMO/SIM interaction and consequently leads to proteasomal degradation of PML (137). Interestingly, As_2O_3 triggers the RNF4-dependent proteasomal degradation of PML. In this context, patients with APL are treated with As_2O_3 to activate the SUMO/RNF4/Ubiquitin mediated signaling pathway. APL is characterized by a PML/RARα fusion protein with altered functions, which are required for development of leukemia. As_2O_3 induces a SUMO-2/3 modification of PML, which then leads to RNF4 mediated Ubiquitinylation and thus induces the proteasomal degradation of PML/RARα isoforms I-VII (80, 138).

So far, over 300 potential RNF4 target proteins were identified via a non-denaturing affinity pull down approach (139). Some of them where directly linked to the DNA damage checkpoints, DNA repair pathways and other important regulatory metabolic pathways. Work from Kuo and coworkers revealed a phosphor/SUMO/RNF4 interaction for the transcriptional corepressor and chromatin remodeling protein transcription intermediary factors 1-beta (KAP1) via the RNF4-ARM region. Upon DSB, KAP1 undergoes multiple PTMs leading to proteasomal degradation via RNF4 recruitment (134). Besides KAP1, RNF4 also targets other proteins of the DNA repair complex for degradation. DSB are detected by the Mre11/Rad50/Nbs1 (MRN) complex, which keeps the fractional ends of the DNA in close proximity and recruits the serine protein kinase (ATM). This process also activates E3 Ubiquitin ligases, which lead to Ubiquitinylation of chromatin components (140). The recruitment of RNF4 in response to DSB depends on the functional domains of the protein as well as other factors like DNA repair and telomere maintenance protein (Nbs1), RF protein 8 (RNF8) and breast cancer type 1 susceptibility protein (BRCA1) (141, 142). A very recent publication showed that the

PTM dependent recruitment of RNF4 to KAP1 regulates the tenancy of BRCA1 at DSB sites in a cell cycle dependent manner. Interestingly, irradiation induced DSBs lead to enhanced RNF4 levels during S-/G2-phase, whereas RNF4 expression was suppressed in the G0-/G1-phase (143).

2.3.2 Role of RNF4 during virus infections

Apart from its function in cellular processes, it has been shown recently that RNF4 also plays an important role in viral infections. For HTLV-1 infection, the exact function of the viral oncoprotein Tax is still unknown, but the nuclear localization is dependent on the SUMOylation status of the protein (144). Recently, it could be shown that RNF4 binds to Tax and regulates the nucleocytoplasmic localization of the viral protein. It was further shown that an RNF4-induced modification of Tax leads to a relocalization of the oncoprotein from the nucleus into the cytoplasm (145). This relocalization leads to an increased NF-κB response, which might support Tax induced cell transformation (145). Furthermore, Dassouki and coworkers observed a RNF4 dependent degradation of PML-NB located Tax protein upon As_2O_3 treatment of ATL-cells (146). The STUbL dependent degradation of Tax during HTLV-1 infection could have an immense therapeutic value on degradation of SUMOylated pathogenic proteins. Furthermore, it was shown in EBV infected mammalian cells that the SUMO-2 conjugated viral transcription factor Rta is Ubiquitinylated via a SUMO/SIM by directly interacting with RNF4. In contrast, EBV infections are promoted in RNF4 depleted cells (147). Very recently it could be observed that a viral microRNA (miR-BHRF-1) is essential for the down regulation of RNF4 during productive EBV infection, which leads to an accumulation of SUMO proteins and interestingly induces an increased viral progeny production (148).

Introduction

2.3.3 Human RING-finger protein 111 (RNF111; Arkadia)

The cellular E3 Ubiquitin ligase Arkadia was identified through a string search approach identifying novel polySUMO-binding proteins to associate via an internal SIM/SUMO interaction to SUMOylated substrate proteins (149). Arkadia harbors three SIM domains (between AS 300 and 392) and a RING domain at the C-terminus (between AS 933 and 978; Fig. 10).
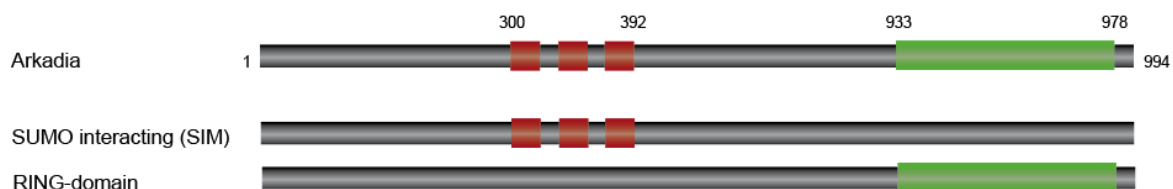
Fig. 10 Structural and functional domains of Arkadia

Schematic overview of structural and functional domains of Arkadia. SIM: SUMO interaction motif; RING domain: Really Interesting New Group of proteins domain.

In the current literature it is intensively discussed whether the STUbL activity of Arkadia is essential for the degradation of cellular substrates. A recent study showed that Arkadia induces activation of the transforming growth factor β (TGF-β) signaling pathway by degradation of regulator proteins (150), which consequently leads to an increased transcription of target genes. However, Erker and coworkers have shown that the STUbL function of Arkadia is on the one hand essential for the degradation of polySUMOylated PML upon As_2O_3 treatment, but on the other hand the STUbL characteristic SIM domains are not necessary for the degradation of TGF-β regulators (123). However, Sun and coworkers claimed that the specific role of Arkadia in the TGF-β pathway is attributable to SUMO binding and RING domain mediated Ubiquitin ligase activity of Arkadia (149). Nevertheless, Arkadia seems to be involved in the cellular DNA damage recognition (151). For example, xenoderma pigmentosum C (XPC) protein, an important regulator of nucleotide excision repair (NER), gets polySUMOylated and further Ubiquitinylated upon UV irradiation, which triggers the Arkadia mediated recruitment of XPC to UV damaged DNA.

3 Material

3.1 Cells

3.1.1 Bacterial Strains

Strain	Genotype
DH5α	*sup*E44, Δ*lac*U169, (φ80d*lacZ*ΔM15), *hsd*R17, *rec*A1, *end*A1, *gyr*A96, *thi*-1, *rel*A1 (152).

3.1.2 Mammalian cell lines

Cell line	Genotype
H1299	Human lung carcinoma cell line, p53 negative (153).
H1299 shscramble	H1299 cell line with non-target mammalian shRNA.
H1299 shRNF4	H1299 cell line with shRNA against RNF4; 5'CCGGACGTATATGTGACTACCCATACTCGAGTATGGGT AGTCACATATACGTTTTTTG -3' (NM_002938.3-650s21c1).
HeLa	Human cervix carcinoma cell line, p16 negative (154).
HeLa-Su2	HeLa cell line stably expressing His-SUMO-2 (155).
HEK 293	HAdV-C5 transformed human embryonic kidney cell line stably expressing HAdV-C5 E1 region gene products (62).
HEK 293T	HEK 293 cell line stably expressing large T antigen from SV40.
pBRK	Freshly isolated primary BRK.

3.2 Viruses

#	Adenovirus	Characteristics
100	H5*pg*4100	WT HAdV-C5 containing an 1863 bp deletion (nt 28602-30465) in the E3 region (156).
149	H5*pm*4149	HAdV-C5 E1B-55K null mutant containing four stop codons at the AS position 3, 8, 86 and 88 of the E1B-55K sequence (156).
154	H5*pm*4154	HAdV-C5 E4orf6 null mutant containing a stop codon at AS 66 within the E4orf6 sequence (157).

Material

3.3 Nucleic acids

3.3.1 Oligonucleotides

The following oligonucleotides were used for sequencing, PCR, RT-PCR and site-directed mutagenesis. All nucleotides were ordered from Metabion and numbered according to the internal group *Filemaker Pro* database.

#	Name	Sequence	Purpose
635	pcDNA3-fwd	ATGTCGCGCTAACAACTC	Sequencing
782	E1B-central	CAAGGATAATTGCGCTAATGAGC	Sequencing
1319	E1B-C-Terminus	GGACATGCTCTCGGGCTCAAG	Sequencing
110	E1B 361-389 rev	CGGTGTCTGGTCATTAAGCTAAAA	RT-PCR
64	E1B bp 2043 fwd	CGCGGGATCCATGGAGCGAAGAAACCATCTGAGC	RT-PCR
1441	Hexon-qPCR-fwd	CGCTGGACATGACTTTTGAG	RT-PCR
1442	Hexon-qPCR-rev	GAACGGTGTGCGCAGGTA	RT-PCR
1573	E1A-qPCR-fwd	GGTAGGTCTTGCAGGCTCCG	RT-PCR
1574	E1A-qPCR-rev	ATGAGGACCTGTGGCATGTTTG	RT-PCR
1371	18S rRNA fwd	CGGCTACCACATCCAAGGAA	RT-PCR
1372	18S rRNA rev	GCTGGAATTACCGCGGCT	RT-PCR
2917	RNF4 rev >143	GCTCTAAAGATTCACAAGTGAGG	Sequencing
2918	RNF4 fwd >460	GCGGCCATGTCTTCTGTAGCC	Sequencing
2919	RNF4 fwd > 54	CGAACTCGGGAAGCAACCTCC	Sequencing
2965	RNF4 fwd K18R	CAAGCTCAGAGGCGAACTCGG	site-directed mutagenesis

2966	RNF4 rev K18R	CCGAGTTCGCCTCTGAGCTTG	site-directed mutagenesis
2978	RNF4 fwd RTR192021AAA	CAAGCTCAGAAGGCAGCGGCGGAAGCAACCTCC	site-directed mutagenesis
2979	RNF4 rev RTR192021AAA	GGAGGTTGCTTCCGCCGCTGCCTTCTGAGCTTG	site-directed mutagenesis
3070	RNF4 fwd K5R	GCTCCATGAGTACAAGAAGGCGTCGTGG	site-directed mutagenesis
3071	RNF4 rev K5R	CCACGACGCCTTCTTGTACTCATGGAGC	site-directed mutagenesis
3263	Daxx fwd K142R	GCCA AAAAGAGGCT GAACTTGG	site-directed mutagenesis
3264	Daxx rev K142R	CCAAGTTCAGCCTCTTTTTGGC	site-directed mutagenesis
3265	Daxx fwd K277R	GCTCATCAAC AGGCCAGGGCC	site-directed mutagenesis
3266	Daxx rev K277R	GGCCCTGGCCTGTTGATGAGC	site-directed mutagenesis
3267	Daxx fwd K634R	CCCTGCAAAAAATCTCG GAGAGAGAAG AAGC	site-directed mutagenesis
3268	Daxx rev K634R	GCTTCTTCTCTCTCCGAGATTTTTTGCAGGG	site-directed mutagenesis
3279	Daxx n'term	GGAGTTCTGCAACATCCTCTCTAGG	Sequencing
3280	Daxx central	GGATTCTGGTGAGGGCCCTA	Sequencing
3289	RNF4 fwd C132/135S	GGTACTGTCAGTTCTCCCATCTCCATGGACGG	site-directed mutagenesis
3290	RNF4 rev C132/135S	CCGTCCATGGAGATGGGAGAACTGACAGTACC	site-directed mutagenesis
3356	RNF4-qPCR fwd	GGTGGAGCAATAAATTCTAGACAAGC	RT-PCR
3357	RNF4-qPCR rev	CCACCACAGGCTCTAAAGATTCACAAGTGAGG	RT-PCR

Material

3.3.2 Recombinant plasmids

The following recombinant plasmids were used for cloning and transfection experiments. All vectors are numbered according to the database.

#	Name	Vector	Insert	Reference
608	pCX-15	pXC15	HAdV-C5 E1 region (1-5790).	Group database
737	pE1A	pML	HAdV-C5 E1A.	Group database
1319	pcDNA-E1B-55K	pcDNA3	HAdV-C5 E1B-55K Promoter.	Group database
1022	E1B-55K-SCS	pcDNA3	HAdV-C5 E1B-55K-K104R.	Group database
1023	E1B-55K-NES	pcDNA3	HAdV-C5 E1B-55K-L83/87/91A.	Group database
1276	E1B-55K-RF1	pcDNA3	HAdV-C5 E1B-55K-C283SC288S.	Group database
1277	E1B-55K-RF2	pcDNA3	HAdV-C5 E1B-55K-H344LC348S.	Group database
1280	E1B-55K-RF4	pcDNA3	HAdV-C5 E1B-55K-H373LH377L.	Group database
1281	E1B-55K-RF5	pcDNA3	HAdV-C5 E1B-55K-C393SH396L.	Group database
1282	E1B-55K-RF6	pcDNA3	HAdV-C5 E1B-55K-C454SC456S.	Group database
1521	E1B-55KDa-delP	pcDNA3	HAdV-C5 E1B-55K-S490/91A, T495A.	Group database
2068	E1B-55K-pM	pcDNA3	HAdV-C5 E1B-55K-S490/91D, T495D.	Group database
2193	E1B-55K-RTR	pcDNA3	HAdV-C5 E1B-55K-R448/449/450AAA.	Group database
1968	pCMV-VSV-G	pCMV	Core protein G (VSV-G) from SV40.	(158)
1969	pRSV-Rev	pRSV	HIV-*Rev*.	(159)
1970	pMDLg/pRRE	pMDL	HIV-1 *Gag*, HIV-1 *Pol*.	(159)
2058	Flag-PML-IV	pLKO	Flag-tagged human PML-IV isoform.	R. Everett
2894	6His-Ubiquitin	pMT107	6His-tagged human Ubiquitin 8 copies.	R. Hay (M.Treier)
3201	shRNF4	pLKO	shRNA against human RNF4 protein NM_002938.3-650s21c1, TRCN0000272669.	Sigma-Aldrich
3011	SFB-RNF4-WT	unknown	N-terminal flag-tagged human RNF4-WT.	Dr. Junjie Chen

Material

3012	SFB-RNF4-K18R	unknown	N-terminal flag-tagged human RNF4-K18R mutant.	this work
3013	SFB-RNF4-RTR192021AAA	unknown	N-terminal flag-tagged human RNF4-RTR mutant.	this work
3113	SFB-RNF4-SIM	unknown	N-terminal flag-tagged human RNF4-SIM mutant.	Dr. Junjie Chen
3114	SFB-RNF4-ARM	unknown	N-terminal flag-tagged human RNF4-ARM mutant.	Dr. Junjie Chen
3115	SFB-RNF4-SIM/ARM	unknown	N-terminal flag-tagged human RNF4-SIM/ARM double mutant.	Dr. Junjie Chen
3116	SFB-RNF4-K5R	unknown	N-terminal flag-tagged human RNF4-K5R mutant.	this work
3117	SFB-RNF4-K5/18R	unknown	N-terminal flag-tagged human RNF4-K5/18R double mutant.	this work
3248	SFB-RNF4-C132/135S	unknown	N-terminal flag-tagged human RNF4 C132/135S mutant.	this work
3209	Flag-Daxx-WT	pRK5	N-terminal flag-tagged human Daxx-WT.	Xiaolu Yang (addgene # 27974)
3210	Flag-Daxx-K142R	pRK5	N-terminal flag-tagged human Daxx-K142R (SUMO-mutant).	this work
3211	Flag-Daxx-K277R	pRK5	N-terminal flag-tagged human Daxx-K277R (SUMO-mutant).	this work
3212	Flag-Daxx-K634R	pRK5	N-terminal flag-tagged human Daxx-K634R (SUMO-mutant).	this work

3.4 Antibodies

3.4.1 Primary antibodies

#	Name	Properties
131	M73	Monoclonal mouse Ab against E1A-proteins (E1A-12S, E1A-13S) of HAdV-C5 (160).
1	2A6	Monoclonal mouse Ab against N-terminal E1B-55K of HAdV-C5 (161).

Material

113	B6-8	Monoclonal mouse Ab against E2A/DBP of HAdV-C5 (162).
94	RSA3	Monoclonal mouse Ab against E4orf6 (E4orf6/7) of HAdV-C5 (163).
275	6B10	Monoclonal rat Ab against L4-100K of HAdV-C5 (164).
88	α-actin (AC-15)	Monoclonal mouse Ab against β-actin (Sigma, Catalog number: A5441).
551	α-6His	Monoclonal mouse Ab against 6xHis-tag (Clontech)
155	α-Ubiquitin	Monoclonal mouse Ab against Ubiquitinylated proteins (Affiniti Research; Catalog number: PW8810, clone FK2)
247	α-Mre11	Polyclonal rabbit Ab against human Mre11 (Novus Biologicals, Inc, Catalog number: pNB 100-142).
62	α-p53 (DO-1)	Monoclonal mouse Ab against the N-terminal AS 1-25 of human p53 (Santa Cruz Biotechnology, Catalog number: sc126) (165).
624	α-pVI	Polyclonal antiserum against purified pVI (166).
536	α-RNF4 (A01)	Polyclonal mouse Ab against human RNF4 (Abnova, catalog number: H00006047-A01).
598	α-RNF4	Monoclonal mouse Ab against human RNF4 (kindly provided by Mr. Takeshi Urano).
370	α-Daxx	Polyclonal rabbit Ab against human and rat Daxx (Upstate/Millipore, Catalog number: 0747).
566	α-PML	Polyclonal rabbit Ab against human PML (Novus Biologicals, Inc., pAB NB100-59787).
452	α-Capsid	Rabbit antiserum against HAdV-C5 capsid, L133.
158	α-Flag	Monoclonal mouse Ab against the flag-tag (Sigma-Aldrich, Inc., mAB Flag-).
621	α-proteasome	Polyclonal rabbit Ab against human proteasome 19S S5A subunit (Novus, NBP2-19952).
533	α-Arkadia (H-16)	Polyclonal goat Ab against human Arkadia (Santa Cruz, sc-21588).
535	α-Arkadia /RNF111	Monoclonal mouse Ab against human RNF111/Arkadia (Abcam, ab88535).
405	α-CK2α	Polyclonal rabbit Ab against human CK2α (Abcam, ab13410).

Material

3.4.2 Secondary antibodies

3.4.2.1 Antibodies for Western Blot analysis

Product	Properties
HRP-anti-mouse IgG	HRP-coupled, sheep anti-mouse (Jackson)
HRP-anti-rat IgG	HRP-coupled, sheep anti-rat (Jackson)
HRP-anti-rabbit IgG	HRP-coupled, sheep anti-rabbit (Jackson)
HRP-anti-goat IgG	HRP-coupled, sheep anti-goat (Jackson)
HRP-anti-mouse IgG (light chain specific)	HRP-coupled, sheep anti-mouse (Jackson)
HRP-anti-rabbit IgG (light chain specific)	HRP-coupled, sheep anti-rabbit (Jackson)

3.4.2.2 Antibodies for immunofluorescence staining

Product	Properties
Cy3 anti-mouse IgG	Affinity purified, Cy3-coupled, donkey anti-mouse (H+L; Dianova)
Cy3 anti-rabbit IgG	Affinity purified, Cy3-coupled, donkey anti-rabbit (H+L; Dianova)
Cy3 anti-rat IgG	Affinity purified, Cy3-coupled, donkey anti-rat (H+L; Dianova)
Cy3 anti-goat IgG	Affinity purified, Cy3-coupled, donkey anti-goat (H+L; Dianova)
Alexa™ 488 anti-mouse IgG	Alexa 488 goat anti-mouse (H+L, F(ab')s Fragment, Invitrogen)
Alexa™ 488 anti-rabbit IgG	Alexa 488 goat anti-rabbit (H+L, F(ab')s Fragment, Invitrogen)

3.5 Commercial systems

Product	Company
Plasmid Purification Mini, Midi, Maxi Kit	Qiagen
SuperSignal® West Pico Chemiluminescent	Substrate Pierce
ProFection-Kit	Promega; Catalog number: E1200

Material

3.6 Chemicals, enzymes, reagents, equipment

Chemicals, enzymes and reagents used in this study were obtained from AppliChem, Biomol, Hartenstein, Invitrogen, New England Biolabs, Merck, Roche and Sigma Aldrich. Cell culture materials, general plastic material as well as equipment were supplied by PAA, Pan, BioRad, Biozym, Brand, Eppendorf GmbH, Sarstedt, Whatman and VWR.

3.7 Standards and markers

Product	Company
1 kb / 100bp DNA ladder	New England Biolabs
PageRuler Plus Prestained Protein Ladder	Pierce

3.8 Software and Databases

Software	Purpose	Source
Acrobat 9 Pro	PDF data processing	Adobe
CLC Main Workbench	Sequence data and protein structure processing	CLC bio
Endnote X7	Reference management	Thomson
Filemaker Pro 14	Database management	FileMaker, Inc.
Illustrator CS5	Layout processing	Adobe
Photoshop CS5	Layout processing	Adobe
Word 2011	Text processing	Microsoft
PowerPoint	Layout processing	Microsoft
PubMed	Literature database open sequence, analysis software	Open Software (provided by NCBI)
Fiji	Image processing	(167)

3.9 Experimental animals

Classical transformation experiments (4.2.5) were performed in primary BRK cells. Therefore, the kidneys were taken from three to five days old Sprague Dawley (Crl:CD (SD) rats (Charles River; Kißlegg).

4 Methods

4.1 Bacteria

4.1.1 Culture and storage

For liquid *E.coli* bacteria cultures, sterile LB was inoculated with a single bacteria colony. With the appropriate antibiotic (100 µg/ml ampicillin) the culture was incubated over night at 30 °C/37 °C at 200 rpm in an *Inova 4000 Incubator* (New Brunswick). For solid cultures, bacteria were plated on an LB medium containing dish with the appropriate antibiotic (100 µg/ml ampicillin) and incubated over night at 30 °C/37 °C. If necessary, bacteria concentrations were determined by measuring the optical density (OD) at 600 nm (*SmartSpec Plus;* BioRad) against plain medium.

Solid cultures can be stored at 4 °C sealed with Parafilm (*Pechiney Plastic Packaging*). For long-term storage, liquid cultures were centrifuged at 4000 rpm for 5 min (*Multifuge 5417 R*, Eppendorf GmbH) at RT. The pellet was resuspended in 0.5 ml LB medium containing and 0.5 ml sterile glycerol, transferred into *CryoTubes*™ (Sarstedt) and stored at -80 °C for several years.

LB Medium	Trypton Yeast extract NaCl *Autoclaved	10 g/l 5 g/l 5 g/l
Antibiotic solution	Ampicillin (500x) *Sterile filtered *Stored at -20 °C	50 mg/ml in H_2O_{bid}

4.1.2 Chemical transformation of *E.coli*

For transformation of *E.coli*, 100 µl of chemically competent DH5α bacterial cells were transferred into a 15 ml *Falcon 2059* tube together with 1-10 µl diluted DNA (~200 ng). After 30 min on ice, a heat shock was performed by incubating the bacteria in a water bath at 42 °C for 45 s. The cells were immediately chilled on ice for 2 min before addition of 1 ml LB medium without antibiotics, followed by incubation for 1 hour at 37 °C and 220 rpm in an *Inova 4000 Incubator* (New Brunswick). The bacteria were pelleted (4000 rpm, 3 min; *Cryo centrifuge 5417R*, Eppendorf), resuspended in 100 µl LB, plated on LB agar containing appropriate antibiotics and incubated at 30 °C/37 °C over night.

Methods

4.2 Mammalian Cells

4.2.1 Cultivation and determination of cell number

Adhesive mammalian cells were grown as monolayers on polystyrene cell culture dishes (6-well/100 mm/150 mm tissue culture dishes; Sarstedt/Falcon) in DMEM (Sigma) containing 0.11 g/l sodium pyruvate, 10% FCS (PAN) and 1% of penicillin/streptomycin solution (1000 U/ml penicillin & 10 mg/ml streptomycin in 0.9% NaCl; PAN). For cultivation of human cervix carcinoma cell lines (HeLa), the medium was additionally supplemented with puromycin (1 μg/ml). The cells were incubated at 37 °C in *Heraeus incubators* with 5% CO_2 atmosphere. To split confluent cells, the medium was removed, cells were washed with sterile PBS and incubated with trypsin/EDTA (PAA) for 3-5 min at 37 °C. Trypsin activity was inactivated by adding standard culture medium and detached cells were transferred to a 50 ml tube following 3 min centrifugation at 1500 rpm (*Multifuge 3S-R*; Heraeus). The supernatant was removed and cells were resuspended in an appropriate amount of culture medium. Depending on the experimental conditions, cells were counted and seeded in a definite amount for further experiments or split in an appropriate ratio. For counting, cells were trypsinized, pelleted and resuspended in an appropriate volume of fresh medium (4.2.1). 50 μl cell suspension were mixed with 50 μl Trypan Blue solution and placed in a *Neubauer hemocytometer* (Marienfeld). After determination of the mean number of cells in 16 small squares using a *Leica DMIL* light microscope, the total number of viable cells was calculated by applying the following formula:

$$\text{cell number/ml} = \text{counted cell} \times 2 \text{ (dilution factor)} \times 10^4$$

PBS (pH 7.3)	NaCl	140 mM
	KCL	3 mM
	Na_2HPO_4	4 mM
	KH_2PO_4 in H_2O	1.5 mM
	*Autoclaved	
Trypan Blue solution	Trypan Blue	0.15%
	NaCl	0.85%

Methods

4.2.2 Storage

For long-time storage of mammalian cell lines, subconfluent cultures were trypsinized and pelleted as described previously (4.2.1). The cells were resuspended in pure FCS with 10% DMSO and transferred to *CryoTubes* (Nunc). The samples were frozen slowly using a *Mr. Frosty* freezing container (Nalgene Labware) before storage in liquid nitrogen. For re-cultivation, cells were rapidly thawed in a water bath at 37 °C and immediately resuspended in pre-warmed culture medium. Cells were pelleted once by centrifugation to remove the DMSO containing medium, resuspended in 1 ml of fresh culture medium, seeded in an appropriate cell culture dish and incubated at standard conditions (4.2.1).

4.2.3 Transfection of mammalian cells

4.2.3.1 Transfection with Polyethylenimine

For stable transfection of mammalian cells, PEI (Polysciences) was dissolved in ddH$_2$O at a concentration of 1 mg/ml, neutralized with 0.1 M HCl (pH of 7.2), sterile filtered (0.2 µm pore size), aliquoted and stored at -80 °C. Cells were seeded in 6-well or 100 mm tissue culture dishes 24 h before transfection. The transfection solution composed of a mixture of DNA, PEI and pre-warmed culture medium without supplements in a ratio of 1:10:100 was vortexed and incubated for 20 min at RT. The culture medium of the cells was replaced by fresh culture medium without supplements before application of the transfection solution. After incubation of the cells for 4-6 h at standard conditions, transfection mixture was replaced by standard culture medium, since PEI is toxic to mammalian cells. Transfected cells were harvested 24-72 h p.t.

4.2.3.2 Transfection with calcium phosphate

pBRK cells were seeded in 100 mm tissue culture dishes for transfection 48 hours after isolation (*ProFection-Kit*; Promega). DNA mixture was covered with calcium phosphate, which would be absorbed by cells via endocytosis. For this, DNA was first diluted with deionized water to a final volume of 300 µl/500 µl after adding 37 µl/62 µl 2M CaCl$_2$. Additionally, 300 µl/500 µl of 2xHBS was prepared in a 15 ml conical centrifuge tube. Prepared DNA solution was added slowly to the tube with 2xHBS while it was vortexed continuously. The transfection solution was incubated 30 min before it was added to seeded cells.

4.2.4 Cell harvesting

Harvesting of transfected or infected adherent mammalian cells was performed with cell scrapers before transfer into 15 ml tubes and centrifugation at 2000 rpm for 3 min at RT (*Multifuge* 3 S-R; Heraeus). After removing the supernatant, the cell pellet was washed once with PBS and stored at -20 °C for following experiments.

4.2.5 Stable knock-down cells

4.2.5.1 Generation of recombinant lentiviral pseudo-particles

For the generation of stable knock.down cells, lentiviral pseudo-particles were used for the integration of genetically modified matrial into the target cell. For this, replication incompetent lentiviral pseudo-particles were produced in the helper cell line HEK 293T, which was cotransfected with scrambled shRNF4 or shRNF4 and the packaging plasmids pCMV-VSV-G, pMDLg/pRRE and pRSV-Rev. Approximately 6-12 hours after transfection, the medium was replaced by 8 ml culture medium supplemented with 10% FBS. Supernatant containing viral particles was collected 24 h and 48 h post transfection. Therefore, supernatant was harvested with a syringe and sterile filtered (0.45 µm) into 2 ml reaction tubes. Virus particle containing supernatant was quickly frozen in liquid nitrogen and stored at -80 °C (168).

4.2.5.2 Transduction of mammalian cells with lentiviral pseudo-particles

For transduction with lentiviral pseudo-particles, appropriate cells were grown to a confluence of 50-70% in 100 mm culture plates. Media was replaced by culture medium without supplements and 100 µl lentiviral particles were added drop-wise to the cells. After 1-2 hours post transduction, standard DMEM supplemented with 10% FBS was added. 48 h p.t., puromycin (1 µg/ml) was added for selection of depleted cells. Cells were cultured and propagated under these conditions and knockdown efficiency was examined via Western Blot analysis.

Methods

4.2.6 Transformation of pBRK cells

For transformation assays with HAdV-C5 oncoproteins, pBRK cells were cultured and seeded in 100 mm tissue culture dishes 48 h before transfection in standard culture medium. The cells were transfected as described (4.2.3.2). After three weeks, most non-transfected cells died, whereas cells transfected with adenoviral gene products were considered transformed, resulting in multi-layered cell colonies (*foci*). These could be stained with a crystal violet staining solution and counted afterwards. The number of *foci* is a measure of the efficiency with which cellular and viral oncogenes can initiate the transformation process.

Crystal Violet Staining Solution	Crystal Violet	1% (w/v)
	Methanol	25% (v/v)
	* in $H_2O_{bid.}$	

4.3 Adenovirus

4.3.1 Infection with adenovirus

Mammalian cells were infected at a confluency of 50-70%. Prior to infection, cells were washed in PBS and medium without supplements was applied to the cells. Virus dilutions were prepared in an appropriate volume of culture medium without supplements and added to the cells. Following formula was used for determination of the volume of virus stock solution:

$$\text{volume virus stock solution (µl)} = \frac{\text{total-cell number}}{\text{virus titer (FFU/µl)}} \times \text{MOI}$$

After an incubation of 2 h at standard culture conditions, the infection medium was replaced with standard culture medium. The infected cells were harvested at desired time points post infection according to the experimental setup described in (4.2.4).

Methods

4.3.2 Determination of virus progeny production

To determine the virus progeny production of infected cells, cells were infected as described (4.3.1) and harvested 24, 48 and 72 h p.i. as described (4.2.4). The harvested cells were resuspended in 300-500 µl culture medium without supplements and stored at -80 °C. Cells were lysed by three freeze and thaw cycles and afterwards centrifuged for 10 min (4500 rpm, 10 min; *Multifuge 3S-R*, Thermo) at RT. Virus containing supernatant was transferred into a sterile 1.5 ml tube (Eppendorf) and stored at -4 °C. The number of infectious particles in the supernatant could be determined as indicated (4.3.3) and the number of progeny viruses was calculated taking into account the dilution and number of cells.

4.3.3 Titration of virus stocks

Virus titer determination is based on the number of *ffu* after immunofluorescence staining of the adenoviral E2A/DBP. Therefore, each virus stock was diluted with DMEM by a factor of 1.0, 0.1, 0.01 to infect $4x10^5$ HEK-293 cells/6-well with each virus dilution. 24 h p.i., the cells were washed once with PBS and fixed by applying ice-cold methanol for 15 min at -20 °C. The methanol was then removed, the cells were air dried at RT and non-specific-Ab binding sites were blocked with TBS-BG for 1 h at RT. Each well was incubated for 2 h with an Ab solution containing the E2A/DBP specific-Ab B6-8 (1:10 in TBS-BG), washed three times for 10 min with TBS-BG before adding *Alexa Fluor* 488 coupled secondary Ab (Invitrogen; 1:500 in TBS-BG) for 2 h at RT. Finally, the secondary Ab was removed, each well was washed three times for 10 min with TBS-BG and infected cells were counted using a fluorescence microscope (DMIL, Leica). The total number of infectious particles was calculated as the mean value of at least three independent countings, taking into account the infected cell numbers, virus dilutions and microscope magnification.

TBS-BG	Tris/HCL, pH 7.6	20 mM
	NaCl	137 mM
	KCl	3 mM
	MgCl$_2$	1.5 mM
	Tween-20	0.05% (v/v)
	Sodium-Azide	0.05% (w/v)
	Glycine	5% (w/v)
	BSA	5% (w/v)

Methods

4.4 DNA techniques

4.4.1 Preparation of plasmid DNA from *E.coli*

For preparative isolation of Plasmid-DNA from *E.coli,* a liquid bacterial culture was used. For this, 0.5 l of LB medium supplemented with the appropriate antibiotics was inoculated with 200-500 µl of a pre-culture derived from a single bacteria colony. After incubation for 16-20 h at 30 °C/37 °C (*Inova 4000 Incubator*; New Brunswick), the bacteria were pelleted at 6000 rpm for 10 min (*Avanti J-E*; Beckman & Coulter). Plasmid DNA was extracted according to the manufacturer's protocol using a plasmid extraction kit (*MaxiKit*, Qiagen).

4.4.2 Quantitative determination of nucleic acid concentrations

For determination of DNA/RNA concentrations a *NanoDrop 1000* spectrophotometer (PEQLAB) was used at a wavelength of 260 nm. In the case of ds DNA, absorption of 1.0 corresponds to an absorption maximum of 260 nm at a concentration of 50 µg/ml. For single-stranded oligonucleotides, the approximation is 1.0 OD260 = 33 µg/ml. In case of RNA, absorption of 1.0 corresponds to an absorption maximum of 260 nm at a concentration of 40 µg/ml. DNA purity was assessed by calculation of the OD260/OD280 ratio, which should be located at 1.8 for highly pure DNA and at 2.0 for highly pure RNA.

4.4.3 Agarose gel electrophoresis

Agarose gels were prepared by dissolving agarose (Biozym) in 1xTBE buffer to a final concentration of 0.6-1.2%, melting the agarose solution in a microwave (Siemens) and finally adding ethidium bromide to a final concentration of 0.5 µg/ml before pouring the liquid agarose solution in a gel tray. DNA samples were mixed with 6x loading dye and subjected to agarose gel electrophoresis at a voltage of 5-10 V/cm gel length. DNA was visualized by applying UV light at 312 nm using the *G:BOX transilluminator system* (SynGene). For DNA extraction, the gel was sliced and after centrifugation at 20000 rpm for 2 h (*RC 5B Plus*; Sorvall), the DNA was precipitated from the obtained supernatant with isopropanol, washed, dried and rehydrated as described for plasmid DNA. To minimize harmful UV irradiation for preparative purposes, agarose gels were supplemented with 1 mM guanosine.

Methods

5 x TBE	Tris (pH 7.8)	0.45 M
	Boric acid	0.45 M
	EDTA	10 mM
6x Loading Dye	Bromphenol Blue	0.25% (w/v)
	Xylencyanol	0.25% (w/v)
	Glycerol	50% (v/v)
	50 x TAE	2% (v/v)
Ethidium Bromide-Stock Solution	Ethidium Bromide *Storage at 4 °C	10 mg/ml

4.4.4 PCR

The PCR is a method for amplification of a defined nucleic acid sequence *in vitro (169)*. For standard amplification of a DNA template, a 50 µl PCR reaction was prepared by mixing 50-100 ng DNA template, 0.2 µM forward primer, 0.2 µM reverse primer, 1 µl dNTP mixture (dATP, dTTP, dCTP, dGTP; each 1 mM; New England Biolabs), 5 µl 10 x PCR reaction buffer (Omnilab) and 5 U Taq-polymerase (Roche) in a 0.2 ml PCR tube. Following PCR program was performed using a thermocycler (*Flexcycler*; Analytic Jena):

DNA denaturation	1 min	95 °C
Primer annealing	45 s	55-70 °C
Extension	1 min/kb	72 °C (27-33 cycles)
Final extension	10 min	72 °C
Storage	∞	4 °C

To determine PCR efficiency, 5 µl PCR reaction was analyzed by gel electrophoresis (4.4.3). The fragment size and yield was examined under UV light with the *G:BOX transilluminator system* (SynGene).

Methods

4.4.5 Site-directed mutagenesis

Plasmid mutations were inserted using the *In vitro QuikChange Site-Directed Mutagenesis Kit* (Agilent) according to the manufacturer's instructions. Forward and reverse primers were designed with the desired mutations and ordered from Metabion (Munich). Depending on the introduced mutation, the PCR program was as followed:

DNA denaturation	1 min	95 °C
Primer annealing	45 s	55 °C
Extension	1 min/kb	68 °C (15-17 cycles)
Final extension	10 min	68 °C
Storage	∞	4 °C

To determine PCR efficiency, 10 µl PCR reaction were analyzed by gel electrophoresis (4.4.3). The remaining 40 µl of PCR product were incubated with 1 µl restriction enzyme *DpnI* (New England Biolabs) for 1 h at 37 °C to remove methylated template DNA. 10 µl were transformed into chemical competent *DH5α* (4.1.2), single clones were picked, cultured in 5-10 ml LB medium and prepared plasmid DNA (4.4.1) was analyzed by sequencing (4.4.6).

4.4.6 DNA sequencing

For DNA sequencing 0.5-1.0 µg of DNA and 20 pmol of sequencing primer were mixed with ddH$_2$O in a total volume of 7 µl and sent to Seqlab (Göttingen).

4.5 RNA techniques

4.5.1 Preparation of total RNA from mammalian cells

For isolation of RNA from mammalian cells, previously seeded cells were harvested and lysed in 100 µl RIPA buffer. Cells were then incubated for 2 min on ice before

Methods

centrifugation at 500 rcf for 5 min (*5417R,* Eppendorf) at 4 °C. The pellet was resuspended in 1 ml Trizol reagent (Invitrogen*)* and incubated for 5 min at RT. Afterwards, 200 µl Chloroform (Sigma) was added to the remaining pellet, vortexed shortly, incubated for another 2-3 min at RT and centrifuged at 12000 rcf for 15 min (*5417R,* Eppendorf) at 4 °C, in order to discard the cell debris. The RNA containing supernatant was transferred into a new 1.5 ml reaction tube and RNA was precipitated with 600 µl isopropanol at 12000 rcf for 15 min (*5417R,* Eppendorf) at 4 °C. The RNA pellet was washed once with 1 ml 75% (v/v) EtOH (7500 rcf, 15 min, 4 °C; *5417R,* Eppendorf) air-dried and re-hydrated in 20 µl DEPC treated H_2O at 55 °C for 10 min. The amount of total RNA was determined with the *NanoDrop* spectrophotometer (PEQLAB; 4.4.2). RNA was stored at -20 °C or subjected to reverse transcription for quantitative RT-PCR (4.5.2).

4.5.2 Quantitative reverse transcription RT-PCR

For investigation of the mRNA synthesis, 1 µg of RNA was reverse transcribed using the *Transcriptor High Fidelity cDNA Synthesis Sample Kit* (Promega*).* Quantitative reverse transcription (RT)-PCR was performed with a *Rotor-Gene 6000* (Corbett Life Sciences, Sydney, Australia) in a 0.5 ml reaction tube with cDNA template (diluted 1:50), 10 µM of each primer and 5 µl *2x Sensi Mix*^{TM} *SYBR-Green* (Bioline). The PCR conditions were as followed:

DNA denaturation	10 min	95 °C
Primer annealing	30 s	95 °C
Hybridization	30 s	60 °C (40 cycles)
Polymerization	30 s	72 °C
Storage	∞	4 °C

The average Ct-value was determined from triplicate reactions and levels of viral mRNA relative to cellular 18S rRNA were calculated. The identities of the products obtained were confirmed by melting curve analysis.

Methods

4.6 Protein techniques

4.6.1 Preparation of total-cell lysates

The lysis of cells was performed using a highly stringent RIPA lysis buffer supplemented with protease inhibitors (PMSF 1 mM, aprotinin 10 U/ml, leupeptin 1 µg/ml and pepstatin A 1 µg/ml). Depending on the pellet size, cells were resuspended in 100-500 µl ice-cold RIPA lysis buffer and incubated for 30 min on ice while vortexed every 10 mins. RIPA lysis buffer ensured a proper solubilisation of matrix associated proteins, such as E1B-55K and eliminated unspecific or weak protein interactions. To ensure efficient cell disruption, lysates were sonified (*output* 0.8 Impulse/s; Branson Sonifier 450) for 30 s at 4°C. Cell debris and insoluble components were centrifuged (14000 rpm, 5 min; *5417R,* Eppendorf) at 4 °C and the protein concentration of the supernatant was determined by spectrophotometry (4.6.2). Finally, proteins were denatured by addition of 5x SDS sample buffer and subsequent boiling at 95 °C for 3 min. Protein lysates were stored at -20 °C until analysis by SDS-PAGE/Western Blot (4.6.3; 4.6.4). For analysis of Ubiquitinylated proteins, cells were treated with N-ethylmaleimide (25 mM; Sigma Aldrich) and MG-132 (10 mM; Merck) 4 h before harvest to accumulate and stabilize ubiqitinylated proteins. Afterwards, cells were lysed and Ubiquitinylated proteins were isolated and analyzed as described (4.6.3; 4.6.5).

RIPA (highly stringent)	Tris/HCL, pH 8.0	50 mM
	NaCl	150 mM
	EDTA	5 mM
	Nonidet P-40	0.15% (v/v)
	Sodium deoxycholat	0.50% (v/v)
	Protease inhibitors	freshly added
5x SDS sample buffer (Laemmli)	Tris/HCL, pH 6.8	100 mM
	Glycerol	20% (v/v)
	SDS	10% (w/v)
	Bromphenol blue	200 mM

4.6.2 Quantitative determination of protein concentrations

Protein concentrations of total-cell lysates were determined by measuring the absorption of protein bound chromogenic substrate at 595 nm using the Bradford based *BioRad Protein-Assay* (170). For each sample, 1 µl protein lysate was mixed with 800 µl ddH$_2$O and 200 µl *Bradford Reagent* (BioRad), incubated for 5 min at RT and

measured in a *SmartSpec Plus* spectrophotometer (BioRad) at 595 nm against a blank. Protein concentrations were determined by interpolation from a standard curve with BSA (concentrations of 1-16 µg/µl; New England Biolabs).

4.6.3 SDS polyacrylamide gel electrophoresis (SDS-PAGE)

Protein samples were separated according to their molecular weights by SDS-PAGE (Biometra). The negatively charged SDS accumulates at constant weight ratios to the proteins and thus compensates for their positive charge. In this way, the rate of migration of the proteins to the anode is determined solely by its size. The quality of the protein separation is increased by the use of a discontinuous stacking gel. The proteins concentrate in the low percentage concentration gel and migrate from there into the separating gel (171). Polyacrylamide gels were made using 30% acrylamide/bisacrylamide solution (37,5:1 *Rotiphorese Gel 30*; Roth), diluted to a final concentration of 8-15% with ddH$_2$0. The gels were run at 20 mA/gel in TGS-buffer. The *PageRuler Prestained Protein Ladder Plus* (Fermentas) was used for protein weight comparison.

Acrylamide Stock Solution (30%)	Acrylamid N, N'Methylenbisacrylamid	29% (w/v) 1% (w/v)
Stacking Gel (5%)	Acrylamide stock solution Tris/HCL, pH 6.8 SDS APS Temed	17% (v/v) 120 mM 0.1% (w/v) 0.1% (w/v) 0.1% (v/v)
Separating Gel (10%)	Acrylamide stock solution Tris/HCL, pH 8.8 SDS APS Temed	34% (v/v) 250 mM 0.1% (w/v) 0.1% (w/v) 0.04% (v/v)
TGS Buffer	Tris Glycine SDS	25 mM 200 mM 0.1% (w/v)

Methods

4.6.4 Western Blot analysis

A wet procedure for the transfer of separated proteins from a polyacrylamide separation gel to a nitrocellulose membrane (*Millipore Immobilon NC pure*, Merck-Millipore) was performed using a *Trans-Blot® Electrophoretic Transfer Cell* (BioRad) according to the manufacturer at a current intensity of 400 mM for 90 min in *Towbin* buffer. The denatured proteins migrate in the direction of the anode, corresponding to their negative charge and are then immobilized on the nitrocellulose membrane.

PBS-Tween	Tween-20	0.1% (v/v)
	* in 1x PBS	200 mM
Towbin Buffer	Tris/HCL, pH 8.3	25 mM
	Glycine	200 mM
	SDS	0.05% (w/v)
	Methanol	20% (v/v)

To saturate non-specific-Ab binding sites, the membranes were incubated for 2 h at RT or over night at 4 °C in PBS-Tween containing 5% (w/v) non-fat dry milk powder (Frema). Afterwards, the blocking solution was discarded, membranes were washed briefly to remove remaining blocking solution and incubated for 2 h at RT with the primary Ab diluted in PBS-Tween. The primary Ab dilutions were established for each individual Ab. After primary Ab incubation, the membranes were washed three times for 5 min and incubated for 2 h at 4 °C in PBS-Tween with the HRP-coupled secondary Ab (1:10000; Amersham) containing 3% (w/v) non-fat dry milk powder (Frema) before three final washes in PBS-Tween for 5 min each. Protein bands were visualized by enhanced chemiluminescence using *SuperSignal West Pico Chemiluminescent Substrate* (Pierce) according to the manufacturer's instructions and detected by X-ray films (*RP New Medical X-Ray Film*; CEA) using a *GBX Developer* (Kodak). X-ray films were scanned, cropped using *Photoshop CS5* (Adobe) and figures were prepared using *PowerPoint* (Microsoft) and *Illustrator CS5* (Adobe).

Methods

4.6.5 IP

Equal amounts of total-cell lysates (0.5-1 mg) were used to investigate direct interaction between proteins via IP. The lysates were precleared by addition of pansorbin for 2 h at 4 °C in a rotator (GFL) to reduce unspecific binding. Simultaneously, appropriate amounts of Ab were coupled to 3 mg of sepharose/IP for 2 h at 4 °C in a rotator (GFL). Ab-coupled sepharose beads were washed three times with 1.0 ml of RIPA lysis buffer and added to the precleared protein lysate in a 1.5 ml reaction tube after removing the pansorbin by centrifugation (600 rcf, 5 min, 4 °C; *5417R,* Eppendorf). IP was performed at 4 °C in a rotator (GFL) for 2 h. Sepharose beads with precipitated protein complexes were pelleted (600 rcf, 5 min; *5417R,* Eppendorf) at 4 °C before washing three times with 1.0 ml RIPA lysis buffer. Finally, 15 µl *2x SDS sample buffer* was added to the samples before boiling them at 95 °C for 5 min. Eluted protein samples were stored at -20 °C for further Western Blot analysis (4.6.4).

2 x SDS Sample Buffer (Laemmli)	Tris/HCL, pH 6.8	100 mM
	SDS	4% (w/v)
	DTT	200 mM
	Bromphenol Blue	0.2% (w/v)
	Glycerol	20% (v/ v)

4.6.6 Subcellular fractionation

For subcellular fractionation, cells were freshly harvested and resuspended in 500 µl isotonic buffer (IB) and lysed by the addition of 33.33 µl 10% NP-40. 5 min after incubation, the crude nuclei were centrifuged (100 rpm, 3 min) at 4 °C and the supernatant was transferred to a new 1.5 ml reaction tube as the cytoplasmic fraction (F1). Next, the cell nuclei containing pellet was resuspended in F2 buffer (IB buffer, 10 % NP-40, 10 % SDC), gently vortexed and centrifuged (1000 rpm, 3 min) at 4 °C. The supernatant was transferred into a new 1.5 ml reaction tube as the soluble nuclear fraction (F2) (172). The remaining pellet was resuspended in 0.5 ml RSB buffer and 5 µl 10 mg/ml RNase-free DNase I was added. After 30 min incubation, the pellet was centrifuged as before and the supernatant was transferred into a new reaction tube as the nuclear membrane fraction (F3). To digest the chromatin from the nuclei, the pellet was resuspended in 2 ml RSB and 0.25 ml 5 M NaCl was added (173, 174). The chromatin-depleted nuclei were centrifuged (2000 rpm, 5 min) at 4 °C

and the supernatant was collected in a new tube as the chromatin fraction (F4). The remaining pellet was solubilized in isotonic buffer by adding 0.2% SDS and 10 mM EDTA, to isolate the nuclear matrix fraction (F5). Appropriate *5x SDS sample buffer* was added to the samples before boiling them at 95 °C for 3 min. Eluted protein samples were stored at -20 °C for further Western Blot analysis (4.6.4).

IB	Tris/HCL, pH 7.5 (1M)	10 mM
	NaCl (5M)	150 mM
RSB	Tris/HCL, pH 7.5 (1M)	10 mM
	NaCl (5M)	10 mM
	MgCl$_2$ (1M)	3 mM
F5B	EDTA (250mM)	10 mM
	SDS	0.2%
	IB buffer	*ad 15 ml
NP-40		10% in ddH$_2$O
SDC		10% in ddH$_2$O

4.6.7 Denaturing-purification and analysis of conjugates

HeLa cells stably expressing 6His-SUMO-2 (155) were infected/transfected according to the experimental setup. After infection/transfection cells were harvested, washed once with 1x PBS and lysed in 5 ml Guanidinium Hydrochloride containing lysis buffer. 10% of the cells were lysed with RIPA Buffer for total protein analysis (4.6.1). Lysates in Guanidinium buffer were incubated over night at 4 °C with 25 µl Ni-NTA agarose (Qiagen) prewashed with lysis buffer. The beads/protein solution was washed once with lysis buffer, then once with each wash buffer pH 8.0/pH 6.3. 6His-SUMO conjugates were eluted with 40 µl elution buffer and afterwards boiled at 95 °C for 5 min. Eluted protein samples were stored at -20 °C for further Western Blot analysis (4.6.4).

Methods

Guanidinium Lysis Buffer	Guanidinium-HCL	6 M
	Na_2HPO_4	0.1 M
	NaH_2PO_4	0.1 M
	Tris/HCL, pH 8.0	10 mM
	Imidazol	20 mM
	β-mercaptoethanol	5 mM
Wash Buffer pH 8.0	Urea	8 mM
	Na_2HPO_4	0.1 mM
	NaH_2PO_4	0.1 mM
	Tris/HCL, pH 8.0	10 mM
	Imidazol	20 mM
	ß-mercaptoethanol	5 mM
Wash Buffer pH 6.3	Urea	8 mM
	Na_2HPO_4	0.1 mM
	NaH_2PO_4	0.1 mM
	Tris/HCL, pH 6.3	10 mM
	Imidazol	20 mM
	β-mercaptoethanol	5 mM
Elution Buffer	Imidazol	200 mM
	SDS	0.1% (w/v)
	Tris/HCL, pH 6.3	150 nM
	Glycerol	30% (v/v)
	β-Mercaptoethanol	720 mM
	Bromphenol Blue	0.01% (w/v)

4.6.8 Immunofluorescence analysis

For immunofluorescence analysis, mammalian cells were grown on coverslips in 6-well plates and transfected or infected depending on the experimental setup. Afterwards, cells were fixed in ice-cold methanol at -20 °C for 10 min, or with 4% PFA at 4 °C for 20 min followed by permeabilization with PBS containing 0.5% Triton X-100 for 5 min at RT. After 15 min blocking in TBS-BG buffer (4.3.5), coverslips were treated for 30 min with the primary Ab diluted in PBS and washed three times with TBS-BG buffer. Subsequent, coverslips were incubated with the corresponding Fluor-*Alexa488* (Invitrogen) or Cy3-conjugated (Dianova) secondary antibodies for 20 min at RT. Coverslips were washed twice with TBS-BG buffer and chromatin was stained with 1:2000 DAPI. Finally, coverslips were washed once with PBS and mounted in *Glow medium*. Digital images were acquired with a confocal laser-scanning microscope (Nikon-*C2*). Images were sampled according to Nyquist-sampling theorem and analyzed using Fiji (167).

5 Results

5.1 RNF4 is a novel interaction partner of HAdV-C5 E1B-55K

5.1.1 RNF4 levels are modulated during HAdV-C5 productive infection

HAdV-C5 has been shown to represent a suitable model for analyzing the intrinsic immune response during the very early infection with DNA viruses. Although the viral response on cellular antiviral strategies is still not completely understood, HAdV-C5 provides very good insight in the molecular mechanisms to counteract cellular antiviral proteins such as Mre11, Rad50, Nbs1 and Daxx by using the cellular Ubiquitin-, and SUMO machineries (45, 51).

The viral protein E1B-55K is known as a multifunctional protein that regulates the productive replication and oncogenic transformation in non-permissive mammalian cells. These functions depend on E1B-55K's PTM and its binding to E4orf6. Both early viral proteins recruit specific host factors to form an E3 Ubiquitin ligase complex by which E1B-55K serves as the substrate recognition factor while E4orf6 binds Elongin C via the BC-Box motif (157). Recently it was reported that the PML-NB-associated transcription factor Daxx, which represses efficient HAdV-C5 productive infection, was proteasomally degraded via a SUMO-E1B-55K dependent, E4orf6 independent pathway (119). Recently, two cellular STUbLs were identified, both targeting Ubiquitinylated proteins for proteasomal degradation (122, 151, 175). Since it has been shown that RNF4 also plays an important role in viral infections, this work mainly focused on RNF4 and its function during HAdV-C5 life cycle, especially on the E1B-55K dependent Daxx degradation.

To analyze the protein function of RNF4 in HAdV-C5 infected cells, RNF4 protein levels were analyzed by Western Blot analysis. H1299 were infected with WT virus or E1B-55K mutant virus, and cells were harvested at the indicated time points (Fig. 11). Consistent with published results, Daxx and Mre11 were degraded at late time points only in the presence of E1B-55K (Fig. 11A and Fig. 11B; lanes 4-6) (45, 51). Interestingly, RNF4 levels were also decreased upon 48 h p.i. with WT virus (Fig. 11A; lanes 5-6), whereas E1B-55K protein levels started to increase at this time points (Fig. 11A; lanes 5-6). No reduction of RNF4 protein levels were observed in the E1B-55K mutant virus (Fig. 11B; lanes 1-6), which raised the question whether E1B-55K might use RNF4 STUbL functions in HAdV-C5 infected cells for its own benefit.
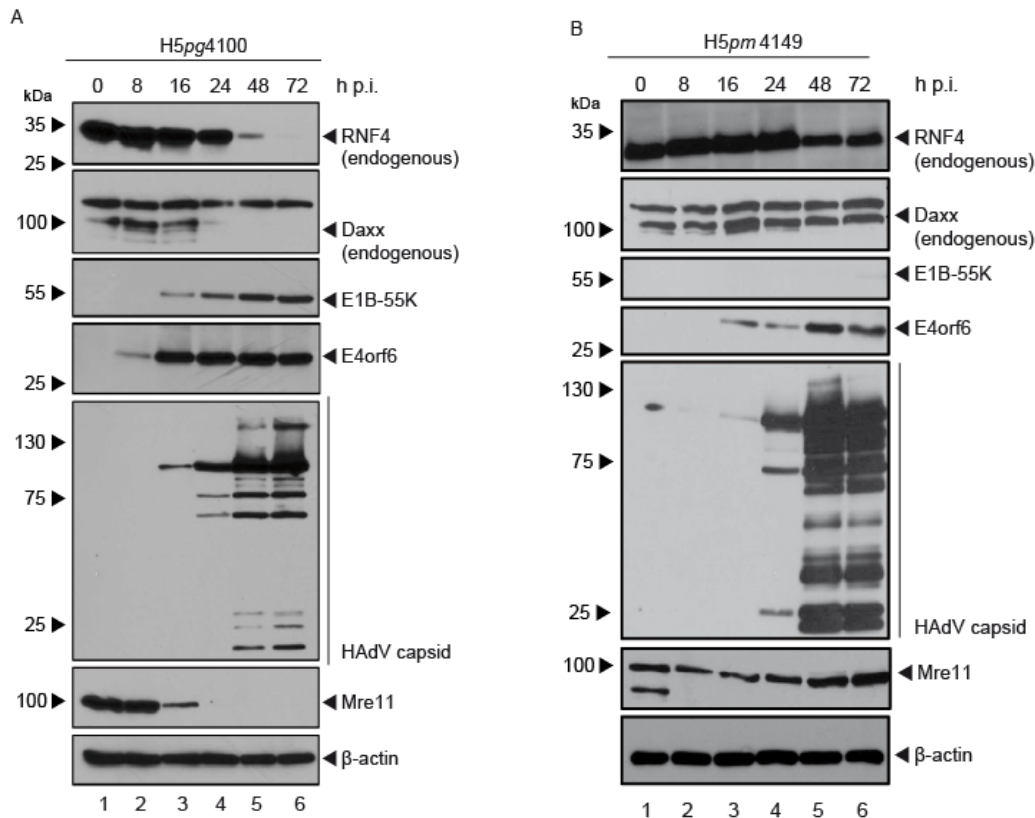
Results

Fig. 11 RNF4 levels are modulated during HAdV-C5 productive infection

H1299 cells were infected with WT virus (H5*pg*4100) or E1B-55K mutant virus (H5*pm*4149) at a MOI of 50 and harvested at the indicated time points post infection. Total-cell extracts were prepared, separated by SDS-PAGE and subjected to immunoblotting using RNF4 mouse mAb, Daxx rabbit pAb, E1B-55K mouse mAb, E4orf6 mouse mAb (163), HAdV-C5 rabbit polyclonal serum (40), Mre11 rabbit pAb and β-actin mAb as loading controls. Molecular weights in kDa are indicated on the *left*, relevant proteins on the *right*. These blots represent the result of several repeated experiments.

5.1.2 RNF4 is relocalized into the insoluble nuclear matrix fraction during HAdV-C5 infection

In the next experiment fractionation assays were performed to analyze the RNF4 protein localization in HAdV-C5 infected cells, since decreased RNF4 protein levels were observed at late time points of infection. Cell lysates from WT virus and E1B-55K mutant virus infected cells were separated into a cytoplasmic fraction (Fig. 12A; lanes 1-3, Fig. 12B; lanes 1-2) and an insoluble nuclear matrix fraction (Fig. 12A; lanes 4-6, Fig. 12B; lanes 3-4). The data show that RNF4 is mainly localized in the cytoplasmic fractions in uninfected cells and 8 h p.i. (Fig. 12A; lanes 1, 2, 4 and 5), whereas at late time points of infection RNF4 was relocalized into the insoluble nuclear matrix fraction (Fig. 12A; lanes 3 and 6). E1B-55K was detected in the nucleus and modified forms of E1B-55K were mainly detected in the insoluble nuclear matrix fraction (Fig. 12A; lane 6). As expected, no relocalization of RNF4 into the insoluble

47

Results

matrix fraction was observed during E1B-55K mutant virus infection compared to WT virus (Fig. 12B; lanes 3-4). In accordance with earlier results (176), Daxx was also observed in the insoluble matrix fraction. Additionally, a decrease of Daxx protein levels at 72 h p.i. could only be detected in the presence of E1B-55K (Fig. 12A; lane 6, Fig. 12B; lanes 3-4), which is consistent with published data illustrating Daxx degradation in HAdV-C5 infected cells in an E1B-55K dependent manner (46, 51). Many studies revealed that adenoviral proteins counteract host cell factors, such as PML and PML-associated proteins, to establish a favorable environment for productive viral replication. It is therefore not surprising that viral proteins often localize in the vicinity of nuclear matrix bound protein complexes, such as PML-NBs (108). In HAdV-C5 infected cells, antiviral proteins are furthermore known to relocalize into HAdV-C5 protein containing aggregates to block their antiviral activities (177).
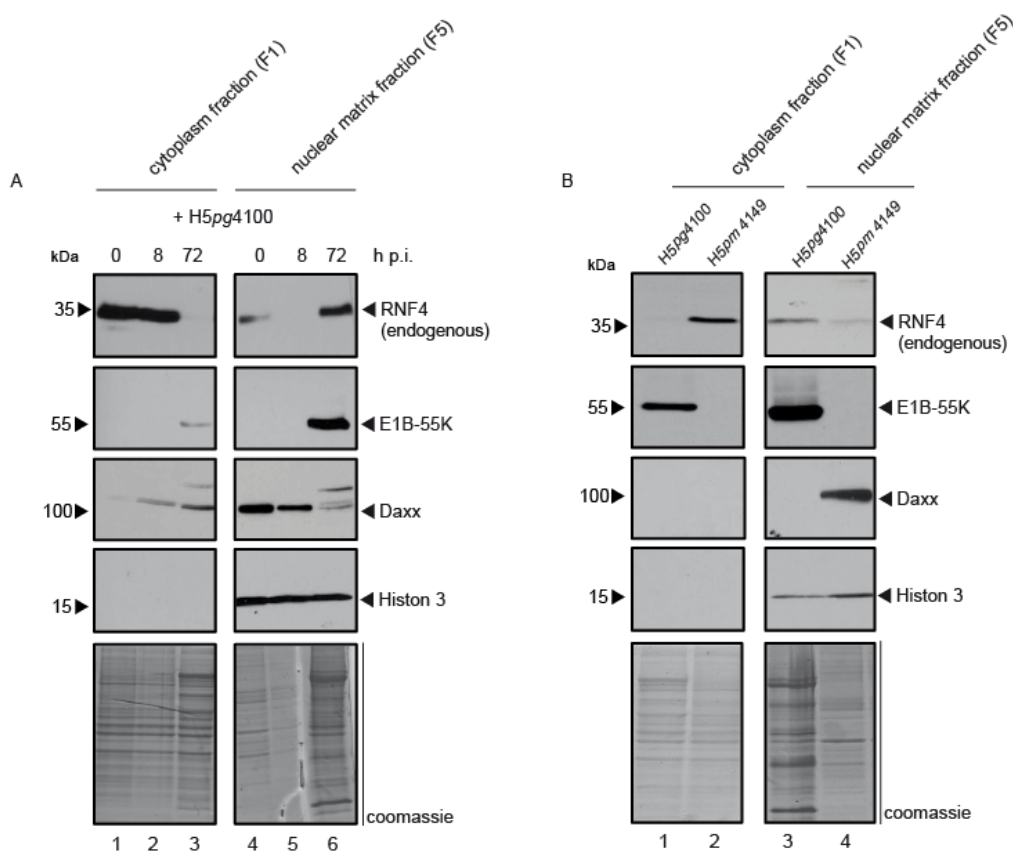

Fig. 12 RNF4 is relocalized into the insoluble nuclear matrix fraction dependent on virus infection

(A) H1299 cells were infected with WT virus (H5*pg*4100) at a multiplicity of 50 FFU/cell and harvested at the indicated time points post infection. (B) H1299 cells were infected with WT virus (H5*pg*4100) and E1B-55K mutant virus (H5*pm*4149) and harvested at 48 h p.i. Cell extracts from both experiments were fractionated into cytoplasmic, soluble nuclear, nuclear membrane, chromatin and insoluble nuclear factions, separated by SDS-PAGE and subjected to immunoblotting using the Ab indicated. α-histone 3 rabbit mAb and coomassie staining serve as loading controls. Molecular weights in kDa are indicated on the *left*, relevant proteins on the *right*. These blots represent the result of several repeated experiments.

Results

5.1.3 E1B-55K localizes juxtaposed to RNF4 during HAdV-C5 infection

For further analysis of the HAdV-C5 dependency on nuclear RNF4 relocalization, immunofluorescence analyzes were performed to visualize the localization of RNF4. Unfortunately, no RNF4 specific-Ab is commercial available for detection of endogenous RNF4 in immunofluorescence, therefore exogenous Flag-tagged RNF4 were used for all immunofluorescence analyzes.

Plasmid coding for Flag-RNF4-WT was overexpressed in H1299 HAdV-C5 infected cells and were subsequently stained after fixation 48 h p.i. Uninfected cells were used as a control. As expected, no E1B-55K staining was observed in the mock cells, whereas RNF4 exhibited a characteristic punctate nuclear staining (Fig. 13; panels b and c). This was to be expected, since it has been shown that upon cellular stress, RNF4 is recruited to the PML-NBs, inducing the proteasomal degradation of SUMOylated PML via Ubiquitinylation (178, 179). Interestingly, in the majority of HAdV-C5 infected cells, RNF4 is relocalized from its punctate nuclear form into larger round-shaped structures (Fig. 13; panels f, g and i). The E1B-55K localization is also worth mentioning, since E1B-55K seems to localize juxtapose to the RNF4 structures during HAdV-C5 infection (Fig. 13; panels h and i).
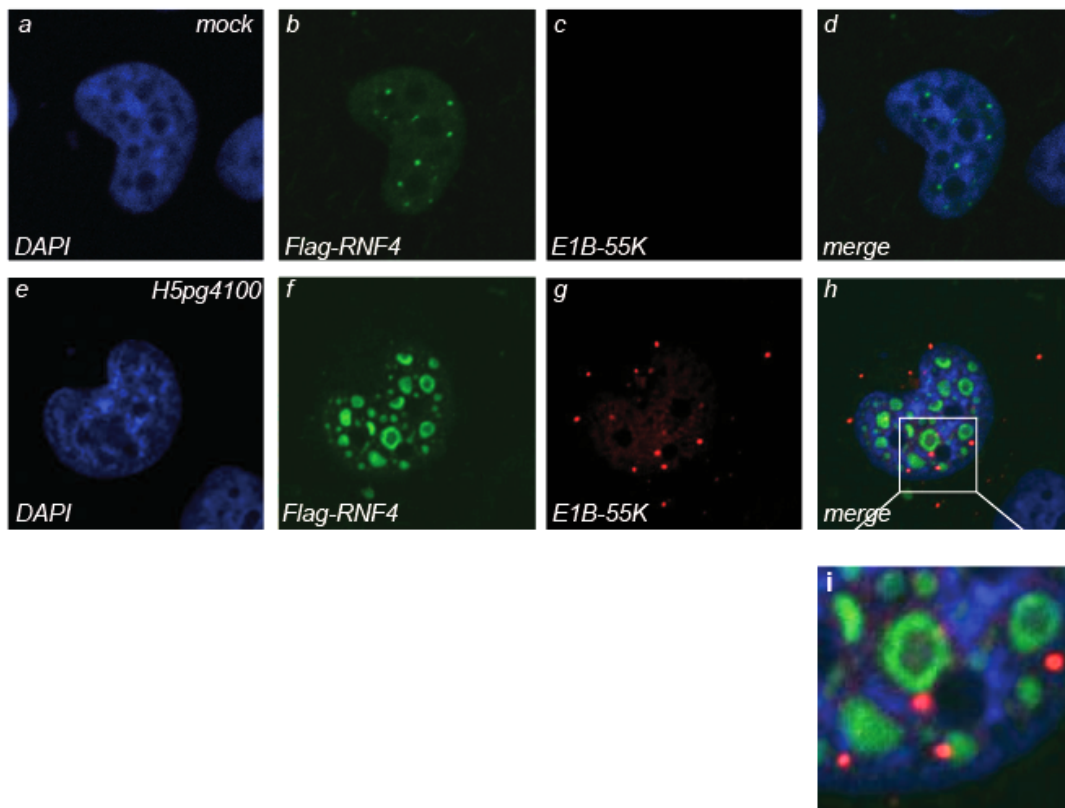
Fig. 13 E1B-55K localizes juxtaposed to RNF4 during HAdV-C5 infection

H1299 cells were transfected with a Flag-RNF4 coding plasmid and were infected 24 h p.t. with WT virus (H5*pg*4100) at a MOI of 20. Cells fixed with 4% PFA 24 h p.i/48 h p.t. Cells were labeled with α-Flag mouse mAb, detected with Alexa488 (α-Flag; green) conjugated secondary Ab and E1B-55K mouse mAb, detected with Cy3 (α-E1B-55K; red) conjugated secondary Ab. Nuclei were labeled with DAPI. α-Flag (green; Ab, Af), α-E1B-55K (red; Ac, Ag), DAPI (blue; Aa, Ae) staining patterns, overlay of the single images (merge; Ad, Ah) and enlarged overlay (merge; Ai) are shown (magnification x 7600). The represented phenotypes were observed in the major amount of analyzed cells from repeated experiments.

5.1.4 RNF4 interacts with E1B-55K protein in transient transfection and during infection

To investigate whether RNF4 is interacting with E1B-55K in HAdV-C5 infected cells, IP experiments in infected and transfected cells were performed (Fig. 14A). H1299 cells were infected with WT virus or transfected with a plasmid encoding the E1B-55K WT protein. As anticipated, in infected cells IP experiments with E1B-55K and RNF4 revealing an interaction between both factors (Fig. 14A, lane 6). No E1B-55K signal was observed in the corresponding negative control (Fig. 14A, lane 5). In line with the data obtained in infected cells, a RNF4 binding to E1B-55K in the absence of any viral background could be detected (Fig. 14A, lane 8). By using immunofluorescence analysis, a timely coordinated and E1B-55K concentration dependent relocalization of RNF4 into E1B-55K containing aggregates was additionally detectable (Fig. 14B; panels Bd, Bh, Bl, Bp, Bt and Bx).
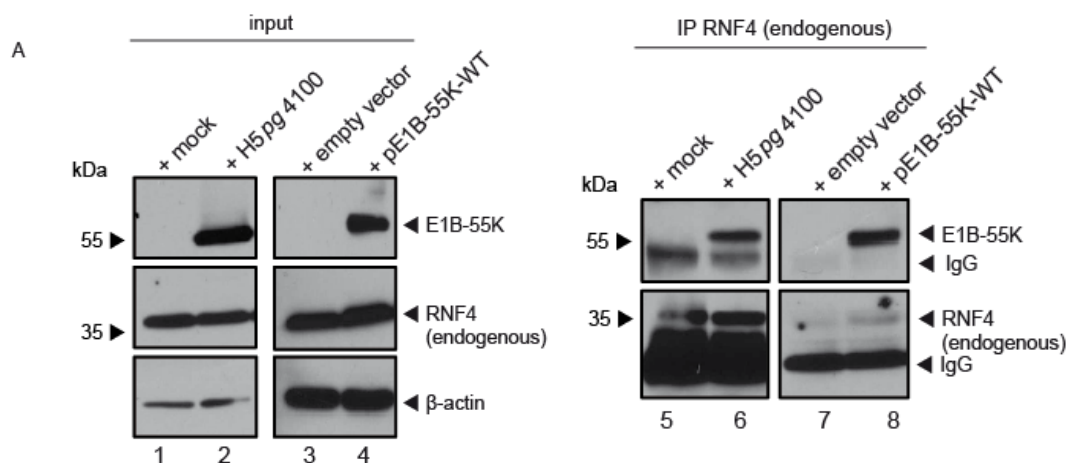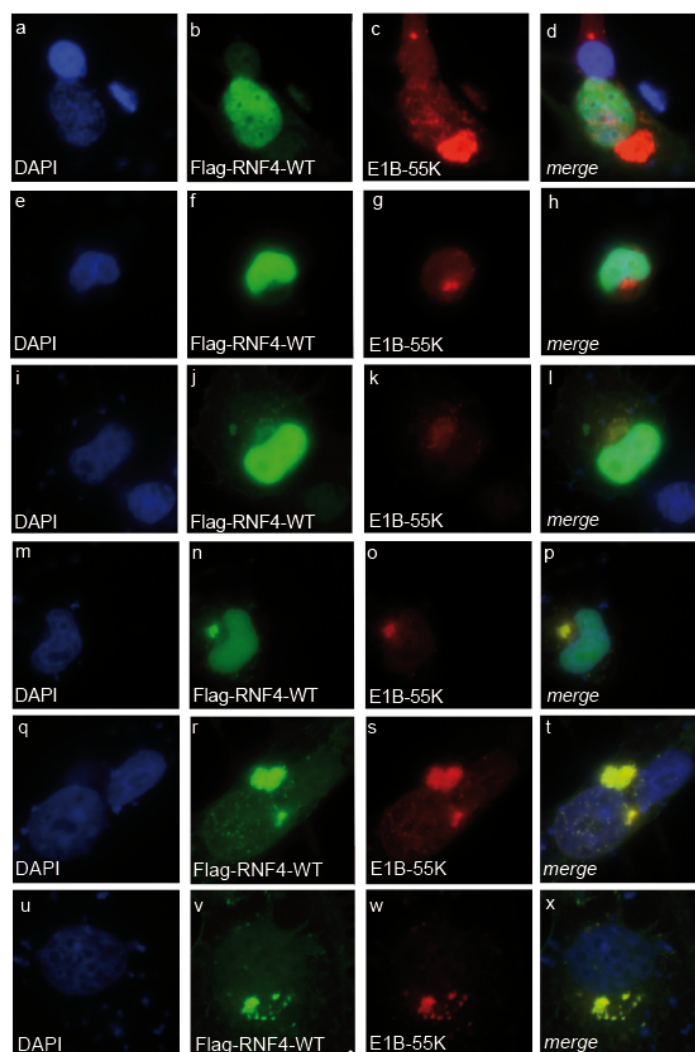
Fig. 13 RNF4 interacts with E1B-55K protein in transient transfection and infection

(A) H1299 cells were transfected with an empty vector control or a plasmid encoding E1B-55K and harvested 48 h p.t., or were infected with WT virus (H5*pg*4100) at a MOI of 50, harvested 24 h p.i. and total-cell extracts were prepared. IP of endogenous RNF4 was performed using RNF4 mouse pAb. Proteins were separated by SDS-PAGE and subjected to immunoblotting. Input levels of total-cell lysates and IP proteins were detected using E1B-55K mouse mAb, RNF4 mouse pAb and β-actin mouse mAb as loading controls. Note that heavy chains (IgG) were detected at 55 kDa and light chains (IgG) were detected at 25 kDa. Molecular weights in kDa are indicated on the *left*, relevant proteins on the *right*. These blots represent the result of several repeated experiments. (B) H1299 cells were cotransfected with 2 μg Flag-RNF4-WT and 2 μg pE1B-55K. 48 h p.t., cells were fixed with ice-cold methanol and labeled with α-Flag mouse mAb, detected with *Alexa488* (α-Flag; green) conjugated secondary Ab and E1B-55K mouse mAb, detected with Cy3 (α-E1B-55K; red) conjugated secondary Ab. Nuclei are labeled with DAPI. α-Flag (green; Bb. Bf, Bj, Bn, Br, Bv), α-E1B-55K (red; Bc, Bg, Bk, Bo, Bs, Bw), DAPI (blue; Ba, Be, Bi, Bm, Bq, Bu) staining patterns and overlays of the single images (merge; Bd, Bh, Bl, Bp, Bt, Bx) are shown (magnification x 7600). The represented phenotypes were observed in the major amount of analyzed cells from repeated experiments.

5.1.5 RNF4 interaction and relocalization is independent on SUMOylation of E1B-55K

Previous published data illustrate that SUMOylation can regulate the intranuclear targeting and nuclear export of E1B-55K (40). In order to investigate the importance of E1B-55K SUMOylation on RNF4 relocalization, complex formation between both proteins was analyzed with the E1B-55K SCS mutant. In addition, the E1B-55K NES mutant was also tested in IP and fractionation assays since inactivation of the E1B-55K NES results in higher SUMOylation of lysine 104 (40) (Fig. 15A+B). H1299 cells were cotransfected with plasmids encoding E1B-55K-WT, -SCS or -NES as well as Flag-RNF4. Binding of RNF4 to E1B-55K WT and E1B-55K NES was observed (Fig. 15A; lower panel, lanes 6 and 8). Weaker binding to E1B-55K was seen in the E1B-55K SCS mutant likely due to the lower steady state concentrations of the viral mutant protein (Fig. 15A, lower level, lane 7). Likewise, no SCS dependent relocalization of RNF4 into the nuclear matrix could be detected (Fig. 15B, lanes 2-4). In sum, these data suggest that RNF4 binds to E1B-55K in a SUMO independent manner.
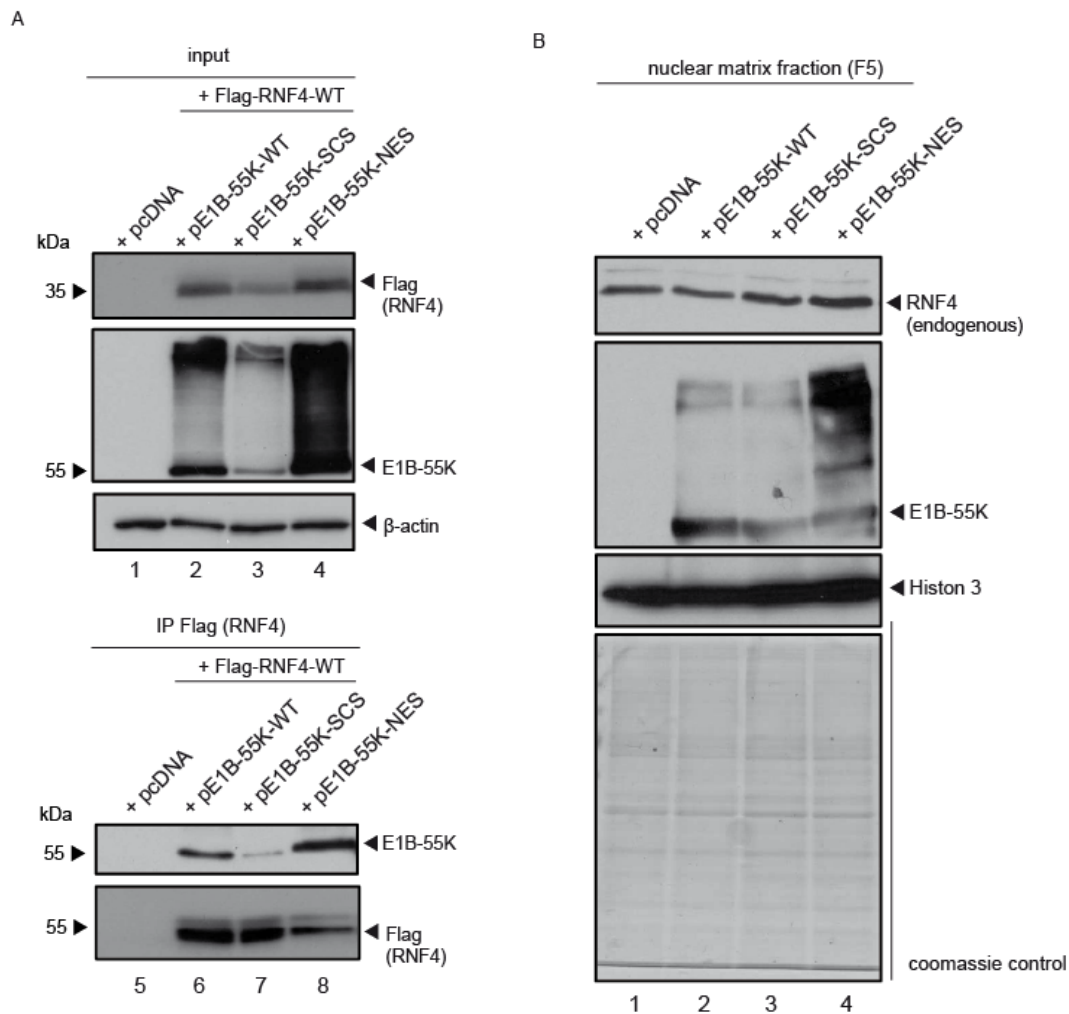
Fig. 15 RNF4 interaction and relocalization is independent on SUMOylation of E1B-55K

(A) H1299 cells were cotransfected with 2 μg Flag-RNF4-WT and 2 μg pE1B-55K-WT, -SCS or -NES NES and harvested 48 h p.t. and total-cell extracts were prepared. IP of Flag-RNF4 was performed using α-Flag mouse mAb, proteins were separated by SDS-PAGE and subjected to immunoblotting. Input levels of total-cell lysates and IP proteins were detected using the Ab indicated in (Fig. 18A). (B) H1299 cells were transfected with pE1B-55K-WT, -SCS or -NES and harvested 48 h p.t. Cell extracts were fractionated into cytoplasm, soluble nuclear, nuclear membrane, chromatin and insoluble nuclear factions, separated by SDS-PAGE and subjected to immunoblotting using the Ab indicated in (Fig. 12). Protein levels in the insoluble nuclear faction are shown. Molecular weights in kDa are indicated on the *left*, relevant proteins on the *right*. These blots represent the result of several repeated experiments.

Results

5.1.6 RF domain of E1B-55K is not necessary for RNF4 interaction

Recently, it was published that the RF domain of RNF4 is necessary for the dimerization of the protein and consequently for its Ubiquitin ligase activity (114, 180). E1B-55K itself exhibits a putative RF domain as well (113). To investigate a possible interaction of the two proteins via their RF domains, E1B-55K RF domain mutants were examined for their RNF4 binding in a first step. For this, H1299 cells were transfected with plasmids encoding for E1B-55K-WT or E1B-55K-RF1 to –RF6. After precipitating endogenously expressed RNF4 and subsequent staining for E1B-55K, interactions with all tested E1B-55K mutants could be observed (Fig. 16). Note that the extra higher migrating bands in the E1B-55K IP blot are most likely non-specific-Ab signals (Fig. 16; lane 2-5).
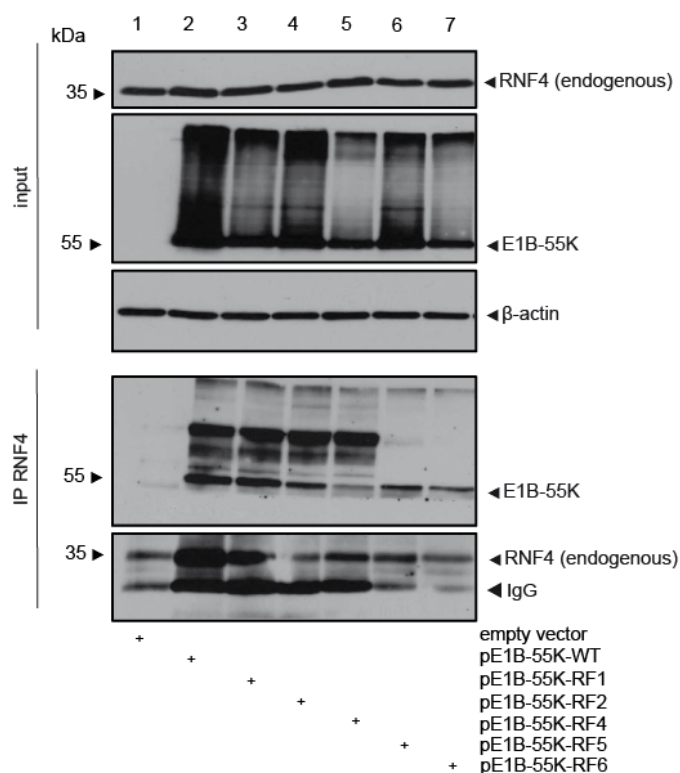
Fig. 16 Putative RF domain of E1B-55K is not necessary for interaction with RNF4

H1299 cells were transfected with an empty vector control or a plasmid encoding pE1B-55K-WT Flag-RNF4-RF1 to -RF6 and harvested 48 h p.t. and total-cell extracts were prepared. IP of endogenous RNF4 was performed using RNF4 mouse pAb, proteins were separated by SDS-PAGE and subjected to immunoblotting. Input levels of total-cell lysates and IP proteins were detected using E1B-55K mouse mAb, RNF4 mouse pAb and β-actin mouse mAb as loading controls. Note that light chains (IgG) were detected at 25 kDa. Molecular weights in kDa are indicated on the *left*, relevant proteins on the *right*. These blots represent the result of several repeated experiments.

Results

5.1.7 RNF4 RF domain mutant interacts with E1B-55K

As seen in Figure 16, the E1B-55K RF mutants still bind to RNF4. Consequently, the RF domain of E1B-55K is not necessary for the interaction with RNF4. Therefore it was examined, if the RF domain of RNF4 is important for the binding ability to E1B-55K. To identify the putative E1B-55K binding site in the RNF4 protein, plasmids encoding for Flag-RNF4-WT and a Flag-RNF4-RF mutant were used for further analyzes (Fig. 17A). The Flag-RNF4-RF mutant was generated by site-directed mutagenesis where two cysteine residues at position 132 and 135 were replaced by two serines (3.3.1).

Since the RF domain of RNF4 is important for its Ubiquitin ligase function, the functionality of the Flag-RNF4-RF mutant was verified by immunofluorescence analysis, regarding PML disruption. As expected, PML track-like structures were visible in the majority of RNF4-WT transfected cells (Fig. 17B; panels Ba, Bb), whereas punctate staining of PML was still visible in the Flag-RNF4-RF transfected cells (Fig. 17B; panels Bc, Bd). This result revealed that the Flag-RNF4-RF mutant might not be able to disrupt and degrade PML as described in the literature (114, 180). However, precipitating Flag-tagged RNF4 and subsequently staining for E1B-55K revealed a specific interaction between E1B-55K and both RNF4 variants (Fig. 17C; lanes 2-4). No E1B-55K signal was observed in the corresponding negative control (Fig. 17C; lane 1). In sum this result indicates a RF independent interaction between RNF4 and E1B-55K.
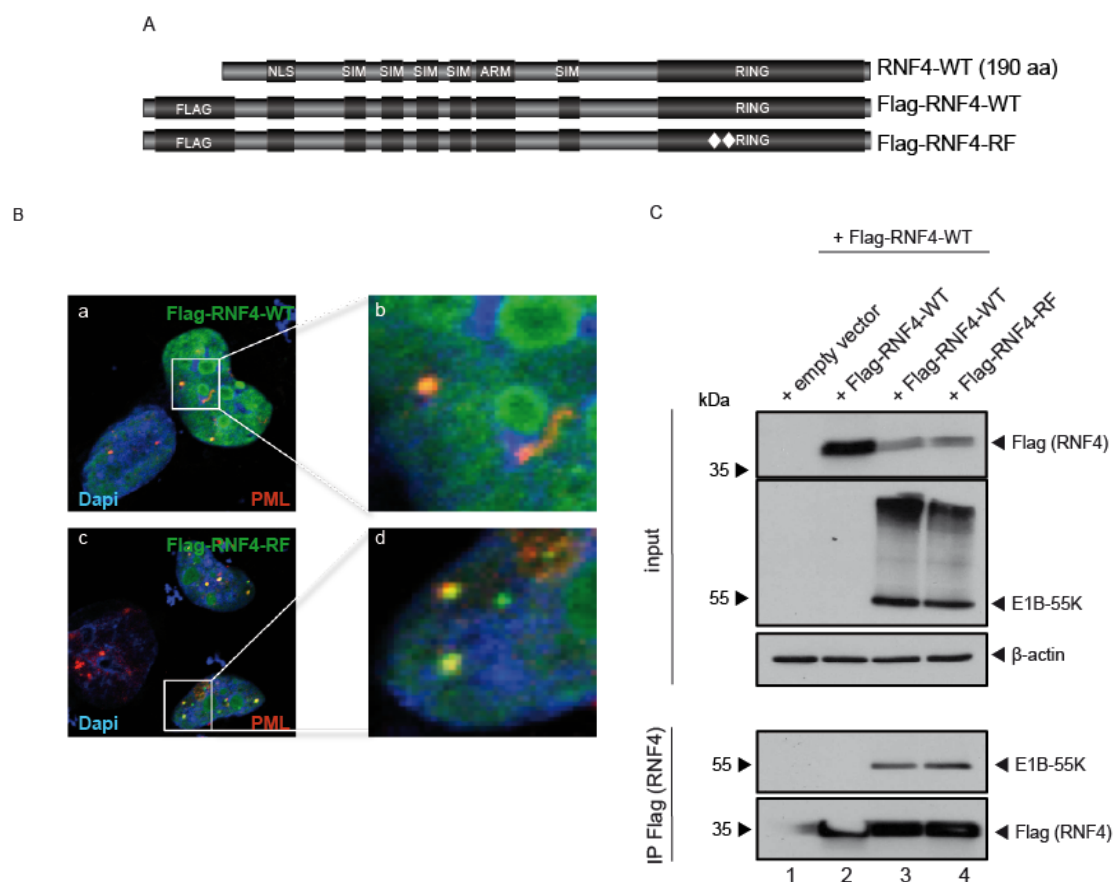
Fig. 17 RNF4 RF domain mutant interacts with E1B-55K

(A) Schematic representation of the mutated Flag-RNF4 constructs WT and RF (mutation of C132/135S). (B) H1299 cells were transfected with 10 μg of Flag-RNF4-WT or Flag-RNF4-RF-mutant. Cells were fixed with 4% PFA 48 h p.t. and labeled with α-Flag mouse mAb detected with *Alexa488* (α-Flag; green) conjugated secondary Ab and anti-PML rabbit pAb, detected with Cy3 (α-PML; red) conjugated secondary Ab. Overlay of images (merge; Ba, Bc) and corresponding enlarged overlay (merge; Bb, Bd) staining patterns are shown (magnification x 7600). The represented phenotypes were observed in the major amount of analyzed cells from repeated experiments. (C) H1299 cells were cotransfected with a plasmid encoding E1B-55K and Flag-RNF4-WT Flag-RNF4-RF and harvested 48 h p.t. and total-cell extracts were prepared. IP of Flag-RNF4 was performed using α-Flag mouse mAb and proteins were separated by SDS-PAGE and subjected to immunoblotting. Input levels of total-cell lysates and IP proteins were detected using E1B-55K mouse mAb, α-Flag mouse mAb and β-actin mouse mAb as loading controls. Molecular weights in kDa are indicated on the *left*, relevant proteins on the *right*. These blots represent the result of several repeated experiments.

Results

5.1.8 AS changes in the putative RNF4 NLS show an effect on RNF4 subcellular localization

After previous precipitation experiments with several RNF4 and E1B-55K mutants could not reveal the E1B-55K binding site in the RNF4 protein, a site directed mutagenesis screen of RNF4 was performed. Various studies have identified RNF4 domains with different functions. In addition to the functional SIM and RING domains of RNF4 (125, 130, 134, 181), a classical monopartite nuclear localization signal (cNLS) in RNF4 (16-AQKRTR-21) was identified by *in silico* analysis.

Therefore a correlation between the putative NLS in RNF4 and its relocalization to the insoluble nuclear matrix fraction in HAdV-C5 infected cells was assumed. To address this question, RNF4-NLS mutants were generated and immunofluorescence analyzes were performed (Fig. 18). In the first NLS mutant, the lysine at position 18 was replaced by an arginine (K18R) and in the second NLS mutant the RTR motif was replaced by a triple alanine motif (AAA) at position 19-21 (3.3.1) (Fig. 18A; AAA-mutant named as Flag-RNF4-RTR). As anticipated, immunofluorescence analysis of both RNF4-NLS mutants showed a more diffuse cytoplasmic localization, compared to the WT (Fig, 18B; panels Bd, Bg, Bj). Especially, the RTR mutant showed a significantly stronger and clearer cytoplasmic localization compared to the WT (Fig. 18B; panels Bd, Bj).

Results
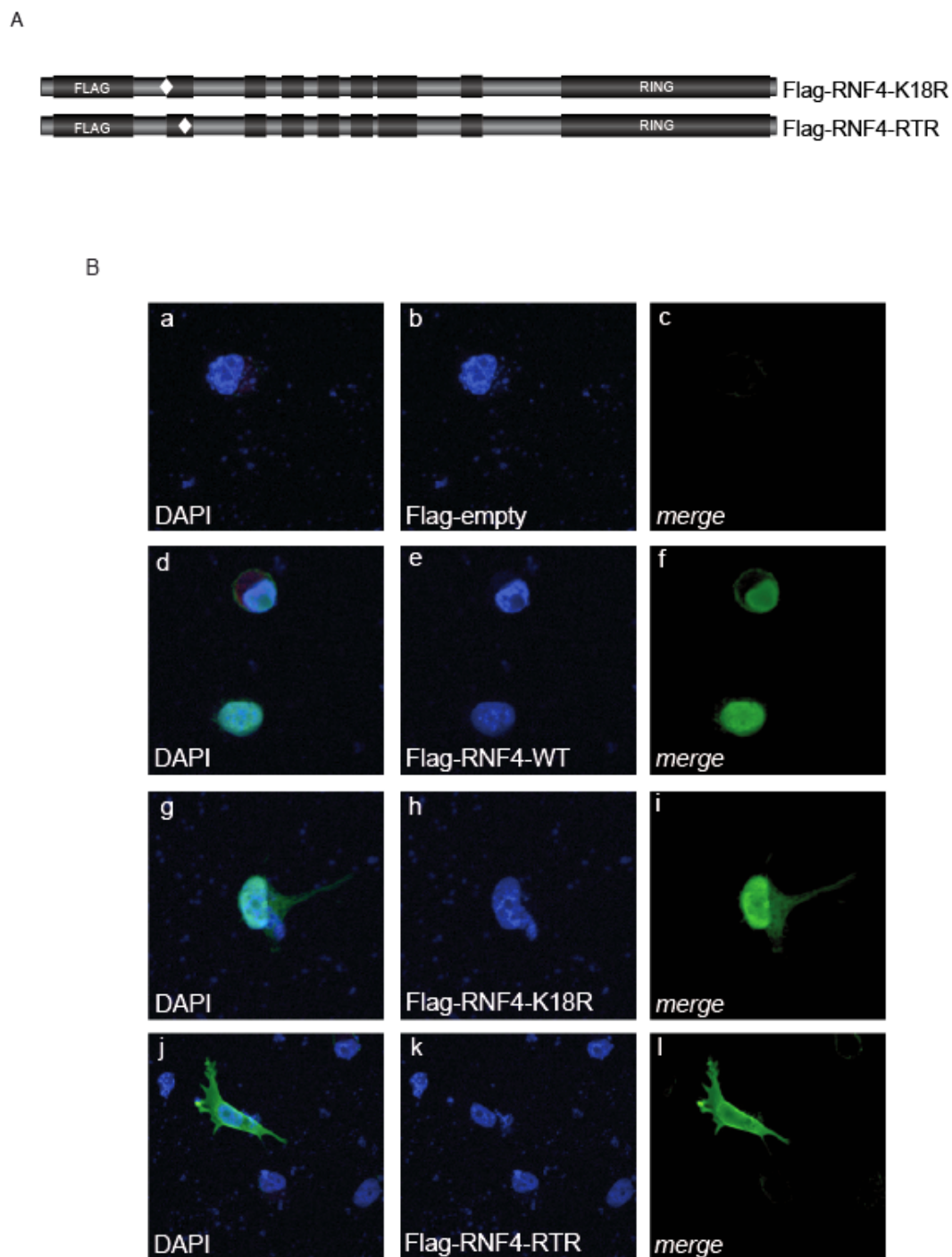
Fig. 18 AS changes in the putative RNF4 NLS show an effect on RNF4 subcellular localization

(A) Schematic representation of Flag-RNF4-K18R and -RTR (3 AS mutation in the putative NLS signal K192021R). (B) H1299 cells were transfected with 2 μg of pFlag-empty, Flag-RNF4-WT, K18R or -RTR. Cells were fixed with 4% PFA 48 h p.t. and labeled with α-Flag mouse mAb detected with *Alexa488* (α-Flag; green) conjugated secondary Ab. α-Flag (green; Bb, Be, Bh, Bk), DAPI (blue; Ba, Bd, Bg, Bj) staining patterns and overlays of the single images (merge; Bc, Bf, Bi, Bl) are shown (magnification x 7600). The represented phenotypes were observed in the major amount of analyzed cells from repeated experiments.

Results

5.1.9 E1B-55K/RNF4 interaction and relocalization is independent of RNF4 functional domains

As described previously, SIM, ARM and RF domains are very important for RNF4 function. RNF4 binds via its SIM domain to SUMOylated proteins by recognizing specific SUMO chains at the target protein (181, 182). Upon binding, RNF4 monomers get activated by dimerization of the RF domains. This activation either leads to substrate Ubiquitinylation, Ubiquitinylation of the SUMO c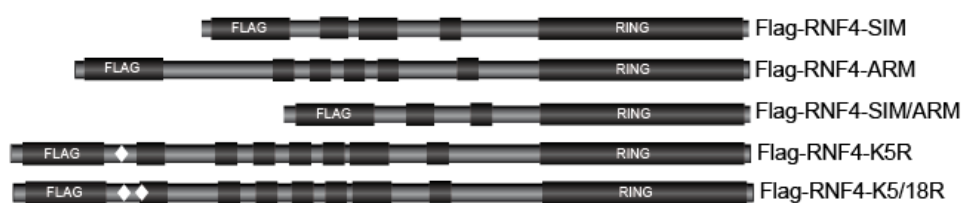hain directly or RNF4 auto-Ubiquitinylation (114, 180). Interestingly Kuo *et al.* published, at least for SUMO-KAP1 that the ARM region of RNF4 enhanced the SUMO/SIM interaction of RNF4 and KAP1 (134). By deletion of this region a 50% loss in SUMO/SIM binding capacity was observed (182). Additionally, the SUMO/SIM interaction synergized with ARM upon target Phosphorylation (134). Since the ARM domain of RNF4 also seems to be involved in the SUMO/SIM binding activity of the protein, this region can also be important for the interaction between RNF4 and E1B-55K.
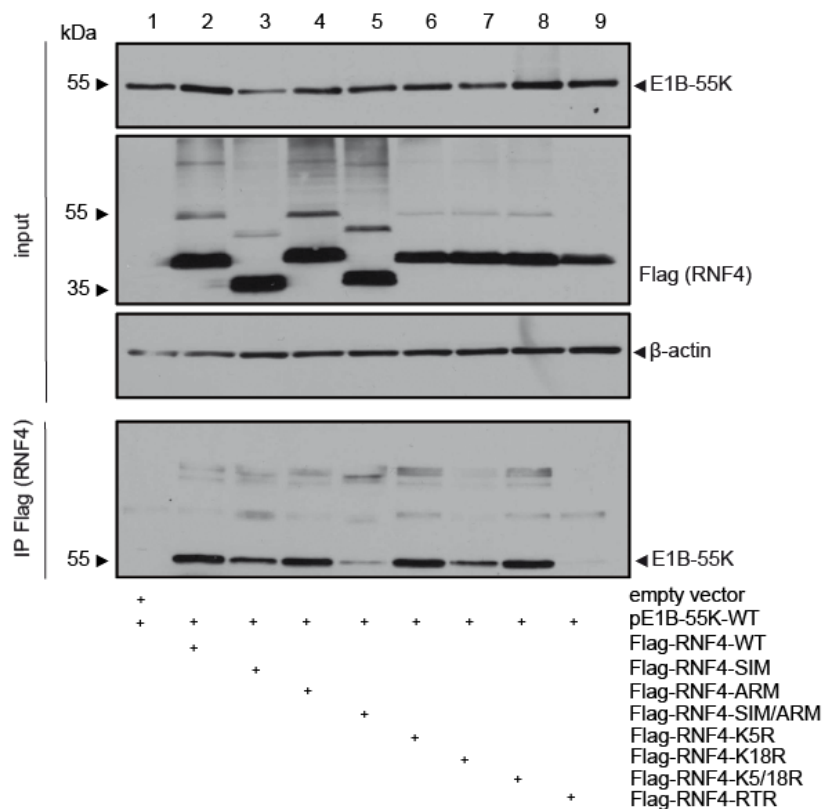
To test whether these domains are crucial for E1B-55K interaction, H1299 cells were cotransfected with a plasmid encoding E1B-55K and Flag-RNF4-WT, -SIM, -ARM, -SIM/ARM, -K5R (*in silico* predicted Ubiquitinylation site of RNF4), -K18R, -K5/18R and -RTR. Again, immunofluorescence and IP analyzes were performed (Fig. 19). In order to precisely determine the colocalization of RNF4 and E1B-55K and to compare the mutants quantifiable, colocalization was analyzed using colocthreshold and coloc2 in Fiji (167) and the Pearson's correlation coefficient (R-Value) was calculated. Intriguingly, all RNF4 mutants showed binding to E1B-55K (Fig. 19B; lanes 2-9), except the RNF4-SIM/ARM mutant and RNF4-RTR mutant, which showed a weaker binding to E1B-55K compared to the WT (Fig. 19B, lanes 5, and 9). Immunofluorescence assays supported and confirmed the results obtained by IP analysis (Fig. 19C). The R-values of all mutants were comparable to the previous results (Fig. 19C; panels Ci, Cn, Cs, Cy, Cdd, Cii, Cmm), except the R-value for the RTR-mutant indicated an opposite result (Fig. 19B; lane 9 + Fig. 19C; panels Cnn, Coo, Cpp, Cqq, Crr). This can be explained by the method used for IP, by which all insoluble proteins were centrifuged (4.6.5) and therefore an IP with insoluble proteins was not observed. Especially, the RTR-mutant of RNF4 showed a dramatic relocalization into insoluble E1B-55K containing aggregates (Fig. 19C; panel Cqq) and therefore it is most likely that no immunoprecipitated RNF4-RTR and E1B-55K are visible.

Results

A

B

empty vector	+									
pE1B-55K-WT	+	+	+	+	+	+	+	+	+	
Flag-RNF4-WT		+								
Flag-RNF4-SIM			+							
Flag-RNF4-ARM				+						
Flag-RNF4-SIM/ARM					+					
Flag-RNF4-K5R						+				
Flag-RNF4-K18R							+			
Flag-RNF4-K5/18R								+		
Flag-RNF4-RTR									+	

C

60
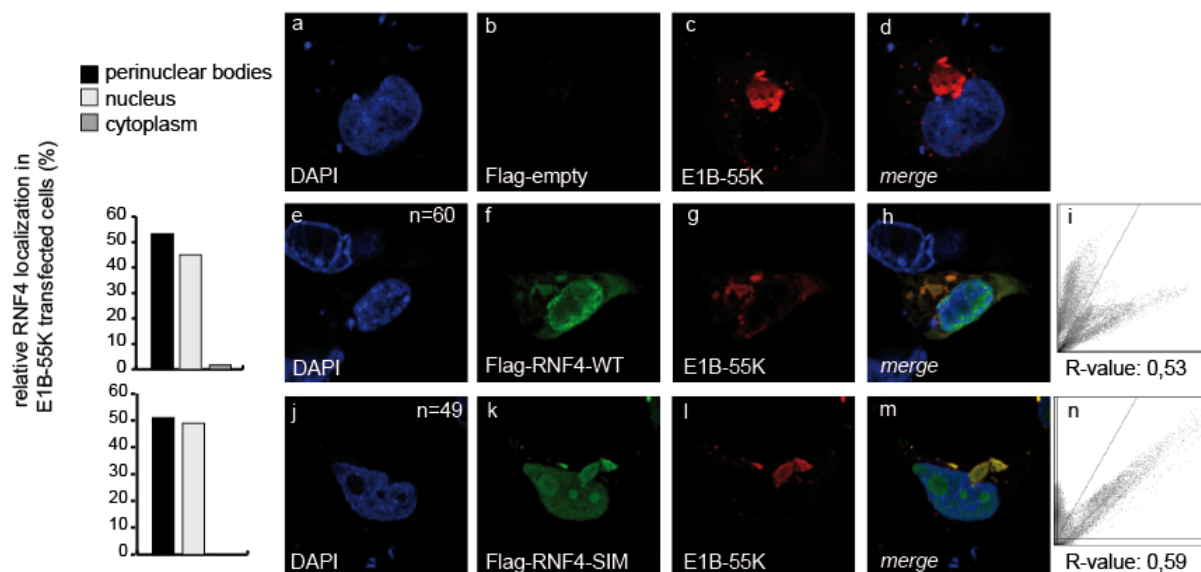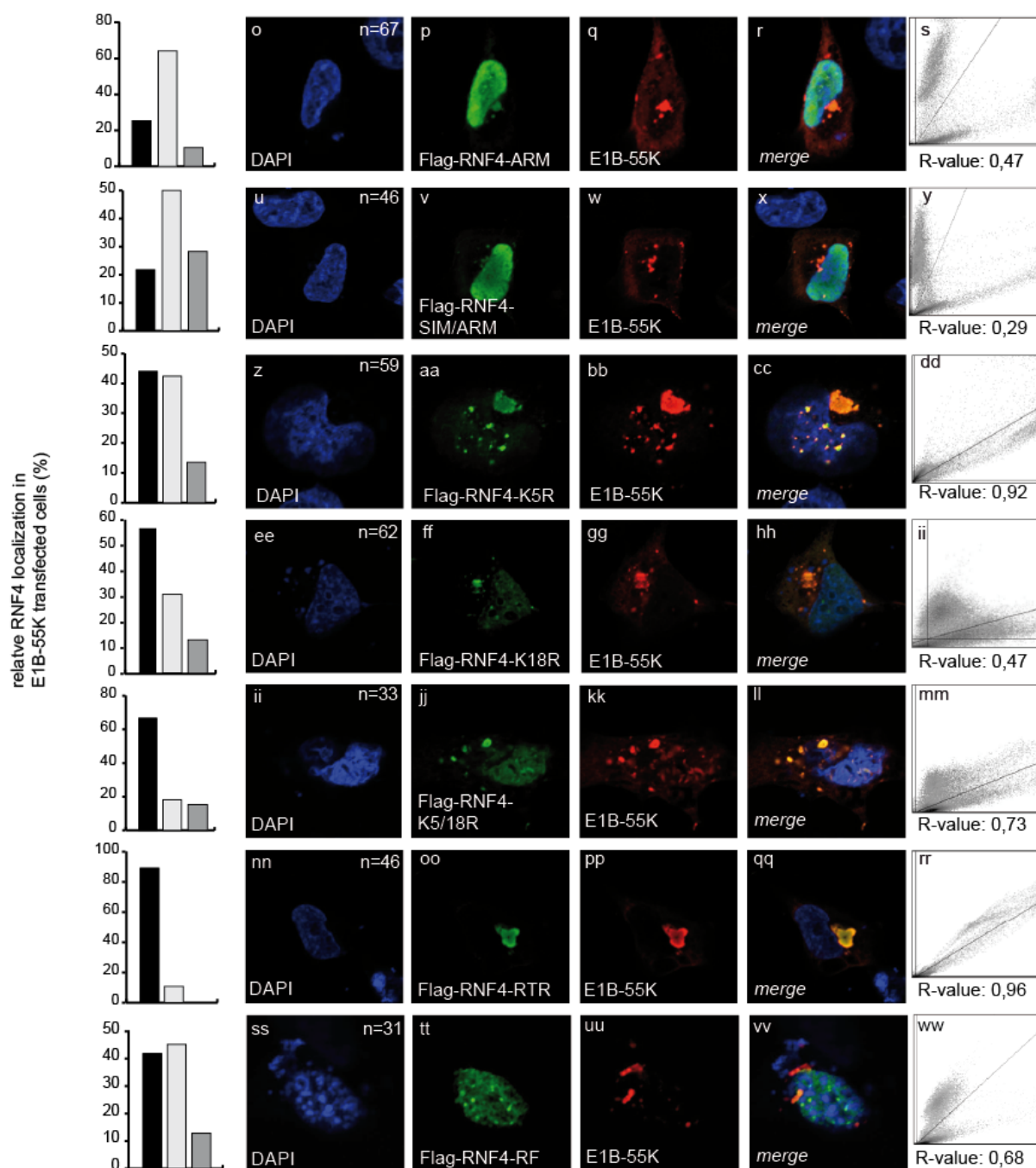
Fig. 19 E1B-55K/RNF4 interaction and relocalization is independent of RNF4 functional domains

(A) Schematic representation of the mutated Flag-RNF4 constructs SIM (deletion of SIM 1-4), ARM (deletion of ARM, position 73-83), SIM/ARM (deletion of SIM 1-4 and ARM), K5R and K5/18R. (B) H1299 cells were cotransfected with a plasmid encoding E1B-55K and Flag-RNF4-WT, -SIM, -ARM, -SIM/ARM, -K5R, -K18R, -K5/18R or -RTR and harvested 48 h p.t. and total-cell extracts were prepared. IP of Flag-RNF4 was performed using α-Flag mouse mAb, proteins were separated by SDS-PAGE and subjected to immunoblotting. Input levels of total-cell lysates and IP proteins were detected using E1B-55K mouse mAb, α-Flag mouse mAb and β-actin mouse mAb as loading controls. Molecular weights in kDa are indicated on the *left*, relevant proteins on the *right*. These blots represent the result of several repeated experiments.

Results

(C) H1299 cells were cotransfected with 2 μg of pE1B-55K and 2 μg pFlag-empty, Flag-RNF4-WT, -SIM, -ARM, -SIM/ARM, -K5R, -K18R, -K5/18R, -RTR Flag-RNF4-RF. Cells were fixed with 4% PFA 48 h p.t. and labeled as indicated in (Fig. 18B). α-Flag (green; Cb, Cf, Ck, Cp, Cv, Caa, Cff, Cjj, Coo, Ctt), α-E1B-55K (red; Cc, Cg, Cl, Cq, Cw, Cbb, Cgg, Ckk, Cpp, Cuu), DAPI (blue; Ca, Ce, Cj, Co, Cu, Cz, Cee, Cii, Cnn, Css) staining patterns, overlays of the single images (merge; Cd, Ch, Cm, Cr, Cx, Ccc, Chh, Cll, Cqq, Cvv) and 2D intensity Histograms (Ci, Cn, Cs, Cy, Cdd, Cii, Cmm, Crr, Cww) are shown. Colocalization of Flag-RNF4 and E1B-55K was analyzed using colocthreshold and coloc2 in Fiji (167) and calculated using Pearson's correlation coefficient (R-Value). On average, 50 positive transfected cells per batch were counted for calculation. The exact numbers are indicated as n=x.

The fact that all E1B-55K mutants as well as all tested RNF4 mutants possess the ability to interact with each other supports the assumption that colocalization of E1B-55K with RNF4 is mediated by direct or indirect interaction.

Taken together, these data show for the first time that RNF4 is a cellular binding partner of HAdV-C5 E1B-55K. Moreover, they strongly support the idea that the STUbL may play a key role in the E1B-55K-induced degradation of Daxx and possibly other host cell targets during productive infection and cell transformation.

5.2 RNF4 promotes the E1B-55K dependent Daxx restriction in HAdV-C5 infected cells

5.2.1 RNF4 is a positive regulator of HAdV-C5 infection

5.2.1.1 Depletion of RNF4 does not affect cell growth

The previous results identified RNF4 as a new interaction partner of E1B-55K. To analyze the effect of RNF4 on the E1B-55K dependent Daxx degradation during HAdV-C5 infection, a RNF4 depleted cell line was generated, by the usage of a lentivirus system to express shRNA against the human RNF4 protein (shRNF4). A non-targeted shRNA (shscrambled) was used as a control. In order to check the comparability of the RNF4 depleted cell line with the parental cell line, both cell lines were first characterized for cell growth, protein expression, viral mRNA synthesis and viral progeny production.

In the knockdown cells, RNF4 was efficiently depleted, as shown by Western Blot analysis (Fig. 20A; lane 2) and quantitative RT-PCR (Fig. 20B). Additionally, the generation of the RNF4 knockdown did not substantially affect the growth rate of the cells line (Fig. 20C).
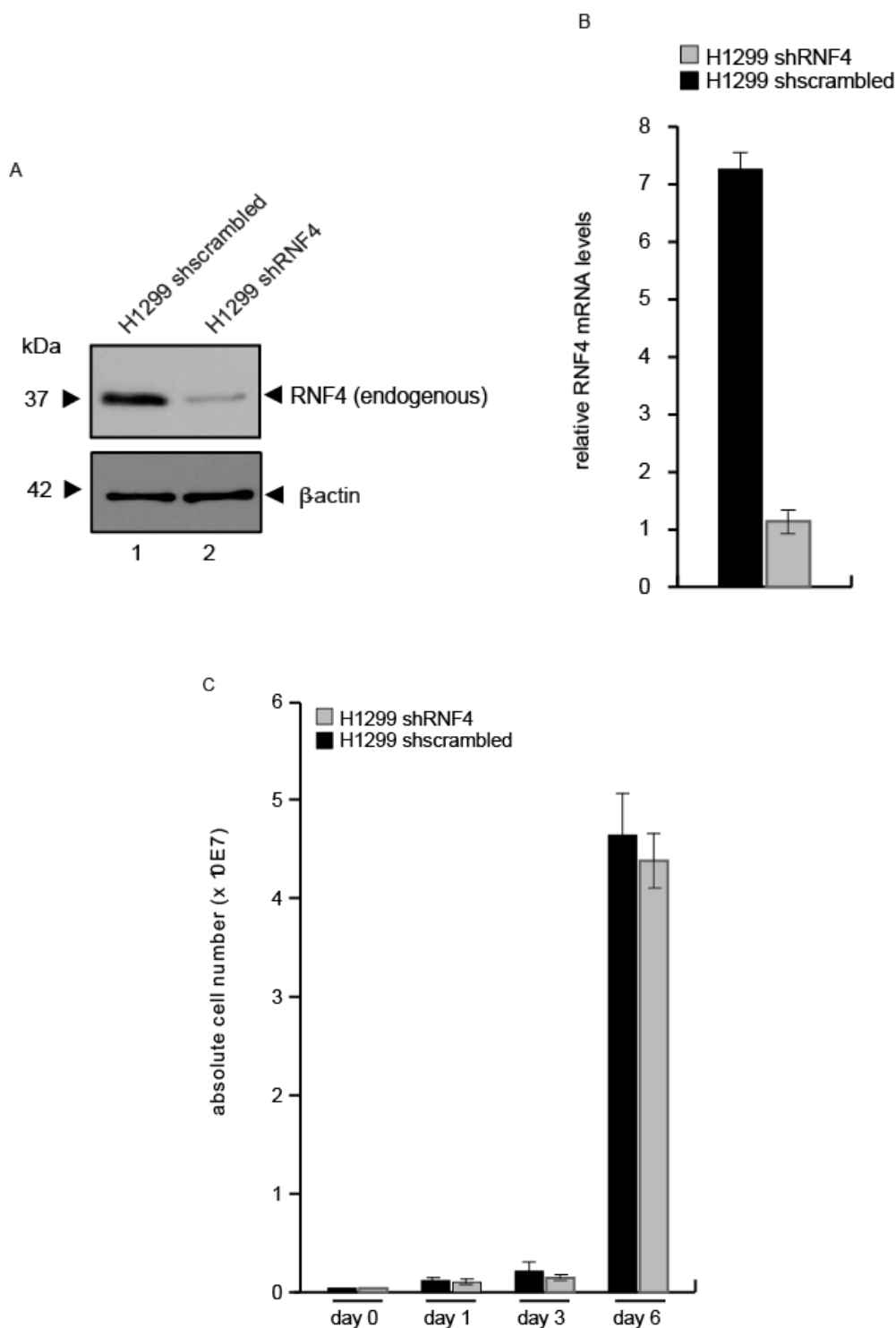
Fig. 20 Depletion of RNF4 does not affect cell growth

(A) Endogenous RNF4 protein levels in H1299 shscrambled and H1299 shRNF4 cells were determined by preparing whole-cell extracts followed by SDS-PAGE and immunoblotting using RNF4 mouse mAb and mouse mAb (anti-β-actin) as loading controls. Molecular weights in kDa are indicated on the *left*, relevant proteins on the *right*. These blots represents the result of several repeated experiments. (B) H1299 shscrambled and H1299 shRNF4 cells were harvested and total RNA was extracted, reverse transcribed and quantified by RT-PCR analysis using primers specific for RNF4. The data are presented as relative RNF4 mRNA levels, compared between H1299 shRNF4 and control cells H1299 shscrambled and were normalized to 18S rRNA levels. (C) H1299 shscrambled and H1299 shRNF4 were cultivated and absolute cell numbers were determined after the indicated time points. The mean and standard deviations are presented for three independent experiments (n=3).

Results

5.2.1.2 RNF4 enhances HAdV-C5 progeny production

To narrow down the effect of RNF4 on the virus life cycle, virus particle release, viral mRNA synthesis and protein expression were analyzed in the next experiments. The production of infectious viral particles was analyzed in parental and RNF4 depleted cells (Fig. 21A). Since the amount of progeny production depends on the cell line as well as an intact E1B-55K protein (183), it would be interesting to investigate the influence of RNF4 on the virus progeny production. Interestingly, the RNF4 depleted cell line showed a decreased viral progeny production at 48 and 72 h p.i., compared to the parental cell line (Fig. 21A).

As E2A/DBP is known as a marker for viral replication centers (184), immunofluorescence analysis were used to investigate the formation of replication centers in RNF4 depleted cells. As expected, the majority of RNF4 depleted cells showed a different E2A/DBP staining pattern compared to the parental cell line (Fig. 21B). Here, the replication centers were formed 48 h p.i (Fig. 21B; panels Bc, Bd), whereas the RNF4 depleted cell line showed a diffuse E2A/DBP staining at the respective time points (Fig. 21B; panels Bg, Bh). However, quantitative analysis of E2A/DPB staining showed a more diffuse staining of E2A/DBP in RNF4 depleted cells and a clear replication center staining of E2A/DBP in parental cells (Fig. 21C). Furthermore, a change in the PML protein staining could be observed in the RNF4 depleted cell line. According to the literature (107), punctate nuclear PML staining in uninfected cells could be detected (Fig. 21B; panels Ba, Bb, Be, Bf). However, in HAdV-C5 infected cells, PML could be detected in nuclear filamentous structures, so-called "track-like-structure" (Fig. 21B; panels Bc, Bd, Bg, Bh). Yet, weaker expression levels of PML in the RNF4 depleted cell line were observed, compared to the parental cell line (Fig. 21B; panels Ba, Bb, Be, Bf)

A
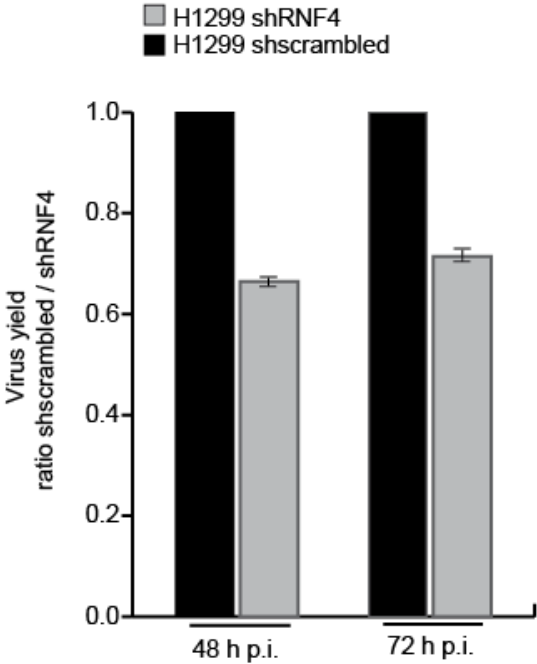
B
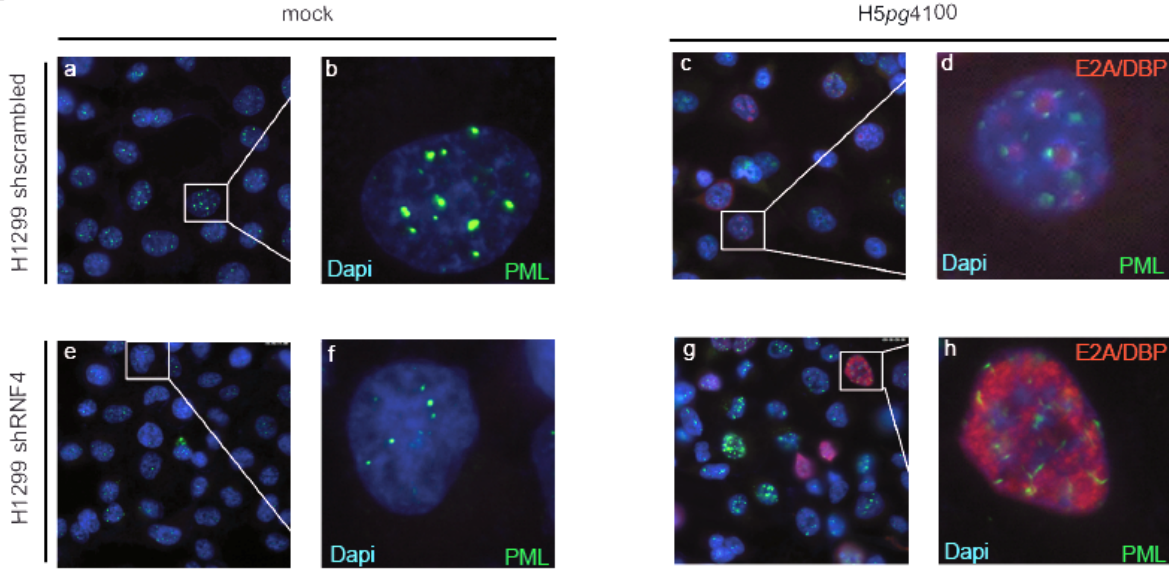
Results

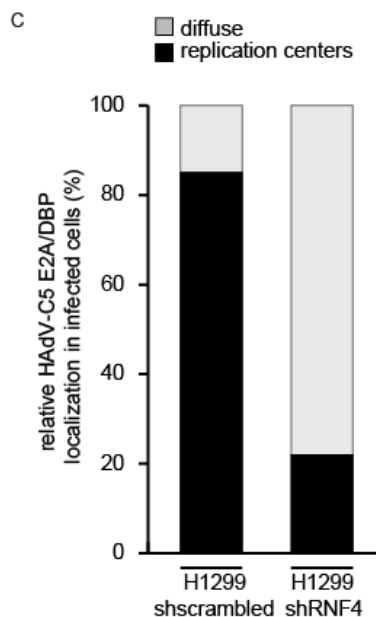**Fig. 21 RNF4 enhances HAdV-C5 progeny production**

(A) H1299 shscrambled and H1299 shRNF4 cells were infected with WT virus (H5*pg*4100) at a MOI of 50. Viral particles were harvested 48 and 72 h p.i. and virus yield was determined by quantitative E2A/DBP immunofluorescence staining on HEK293 cells. The mean and standard deviation are presented for three independent experiments. Values are shown as a ratio shscrambled/shRNF4. (B) H1299 cells were infected with WT virus (H5*pg*4100) at a MOI of 20 and fixed with ice-cold methanol 48 h p.i. Cells were labeled with PML pAb and E2A/DBP mouse mAb, detected with *Alexa488* (α-PML; green) and Cy3 (α-E2A/DBP; red) conjugated secondary Ab. Nuclei are labeled with DAPI. Overlay of images (merge; Ba, Bc, Be, Bg) and corresponding enlarged overlay (merge; Bb, Bd, Bf, Bh) staining patterns are shown (magnification x 7600). The represented phenotypes were observed in the major amount of analyzed cells from repeated experiments. and the E2A/DBP staining was quantified and analyzed by counting the ratio between diffuse and replication center localization in infected cells (C).

5.2.1.3 RNF4 positively regulates mRNA synthesis of HAdV-C5 E1A and Hexon

To examine the effect of RNF4 depletion on mRNA synthesis, the mRNA expression of E1A and Hexon genes were analyzed 16 and 48 h p.i (16 h p.i. data not shown). For this, parental and RNF4 depleted cells were analyzed by quantitative RT-PCR. The cellular 18S rRNA was used as an internal control. Compared to the parental cell line, the knockdown of RNF4 decreases E1A mRNA synthesis by 2.5 fold (Fig. 22; left panel) and Hexon mRNA synthesis by 10 fold at 48 h p.i. (Fig. 22; right panel). These results indicate a positive effect of RNF4 on the E1A and Hexon mRNA synthesis. Whether the RNF4 dependent regulation may take place via increased mRNA stability or alteration of mRNA transport has not been clarified yet and needs to be further investigated.
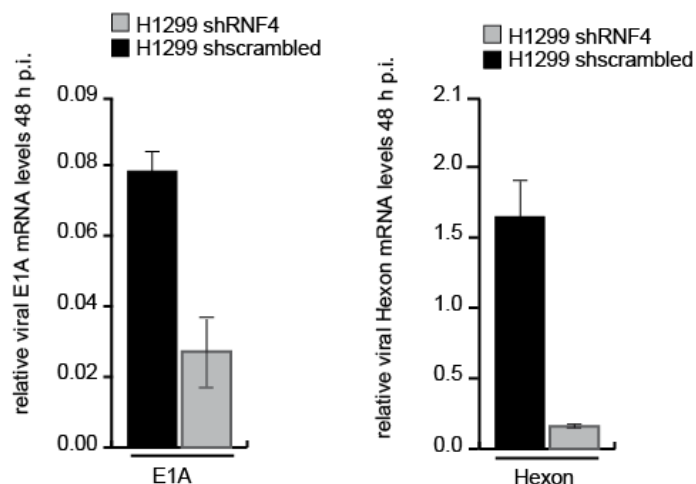
Fig. 22 RNF4 positively regulates mRNA synthesis of HAdV-C5 E1A and Hexon

H1299 shscrambled and H1299 shRNF4 cells were infected with WT virus (H5*pg*4100) at a MOI of 20. The cells were harvested 16 and 48 h p.i., total RNA was extracted, reverse transcribed, and quantified by RT-PCR analysis using primers specific for HAdV-C5 E1A and Hexon. The data were normalized to 18S rRNA levels and the mean and standard deviations are presented for three independent experiments (n=3).

5.2.1.4 RNF4 supports viral protein expression in HAdV-C5 infected cells

To study the role of RNF4 on general protein expression levels of cellular and viral proteins, the expression of early and late viral proteins as well as the known HAdV-C5 target proteins Daxx and Mre11 were analyzed (Fig. 23A). For this, parental and RNF4 depleted cell lines were infected with HAdV-C5 WT virus and harvested at indicated time points. Unfortunately, the Daxx specific-Ab used in Western Blot alaysis showed a high background signal (>100 kDa higher migrating bands). However, in previous experiments the specific Daxx protein band could be determined at 100 kDa.

Compared to the parental cell line, knockdown of RNF4 affects the expression of viral proteins at late time points of infection (Fig. 23; lanes 5-6, 11-12). As expected from the previous results, E1A, E1B-55K, E2A/DBP, HAdV capsid and L4-100K showed a delayed expression already 16 h p.i. (Fig. 23; lanes 1-12). Interestingly, Daxx and Mre11 protein levels decreased substantially later in the RNF4 depleted cell line 48 and 72 h p.i. (Fig. 23; lanes 5-6 and lanes 11-12).

Results
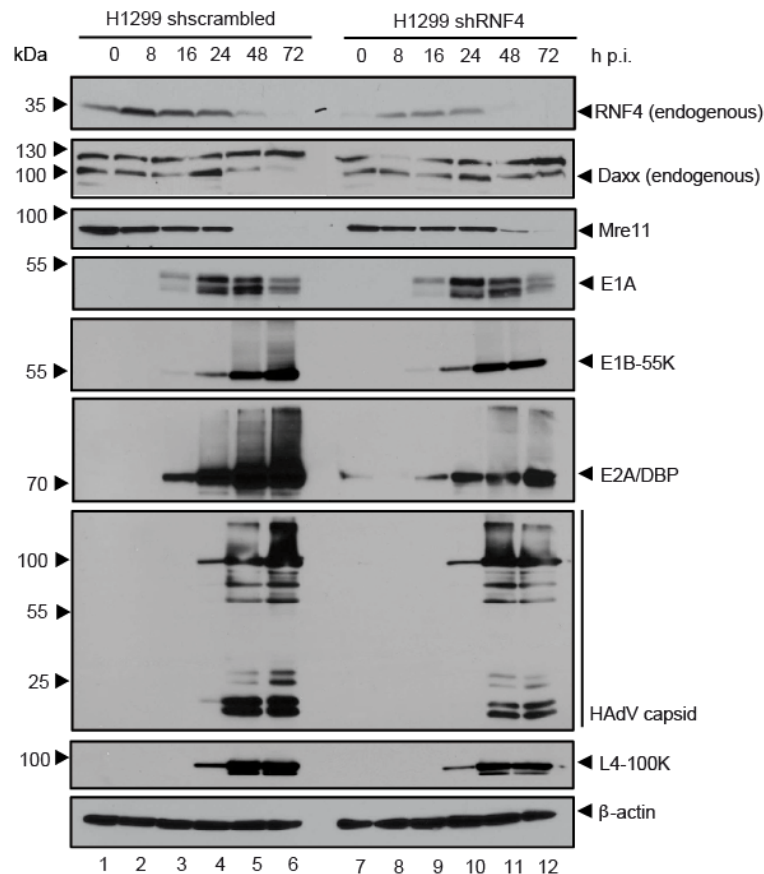
Fig. 23 RNF4 supports viral protein expression in HAdV-C5 infected cells

H1299 shscrambled and H1299 shRNF4 cells were infected with WT virus (H5*pg*4100) at a MOI of 50 and harvested at the indicated time points post infection. Total-cell extracts were prepared, separated by SDS-PAGE and subjected to immunoblotting using RNF4 mouse mAb, Daxx rabbit pAb, E1B-55K mouse mAb, E4orf6 mouse mAb (163), HAdV-C5 rabbit polyclonal serum (40), Mre11 rabbit pAb, E2A/DBP mouse mAb and β-actin mouse mAb as loading controls. Molecular weights in kDa are indicated on the *left*, relevant proteins on the *right*. These blots represent the result of several repeated experiments.

Summarized, these data point to RNF4 being a positive factor for HAdV-C5 productive replication. Additionally, the results of the RNF4 depleted cell line support the hypothesis that RNF4 might play a role in the HAdV-C5 dependent degradation of Daxx and possibly other host cell targets. On the basis of these facts, it was investigated whether RNF4 has an effect on Daxx degradation in HAdV-C5 infected cells. RNF4 has been shown to influence the Daxx protein levels in HAdV-C5 infected cells. Furthermore an interaction between E1B-55K and RNF4 could be observed in this work for the first time, which supports the hypothesis of an E1B-55K and RNF4 dependent Daxx degradation.

Results

5.2.2 RNF4 colocalization with Daxx is altered in HAdV-C5 infected cells

To determine the interplay of RNF4 with Daxx, the localization of both proteins in HAdV-C5 infected cells was analyzed by immunofluorescence staining.

RNF4 colocalized with Daxx in a punctate nuclear staining in uninfected cells, most presumably represent PML-NBs (Fig, 24; panels Ab, Ac, Ad). Furthermore, in HAdV-C5 infected cells, RNF4 colocalized with Daxx in track-like structures within the nucleus (Fig. 24; panels Af, Ag, Ah). Interestingly, a localization of Daxx similar to PML, consistent with the current literature on PML localization could be observed (107, 108).
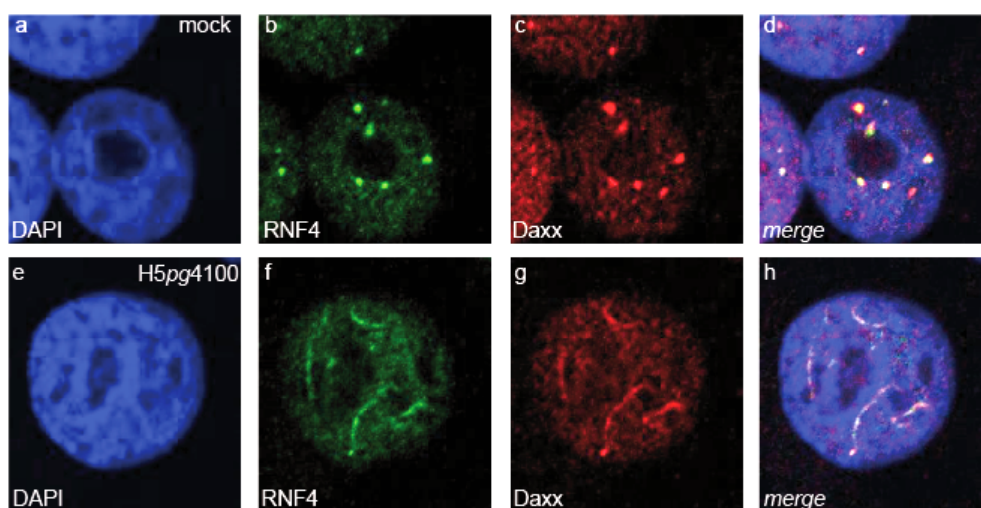
Fig. 24 RNF4 colocalization with Daxx is altered in HAdV-C5 infected cells

H1299 cells were infected with WT virus (H5*pg*4100) at a MOI of 20 and fixed with 4% PFA 48 h p.i. Cells were labeled with α-Flag mouse mAb, detected with *Alexa488* (α-Flag; green) conjugated secondary Ab and Daxx rabbit pAb, detected with Cy3 (α-Daxx; red) conjugated secondary Ab. Nuclei are labeled with DAPI. α-Flag (green; Ab, Af), α-Daxx (red; Ac, Ag), DAPI (blue; Aa, Ae) staining patterns and overlay of the single images (merge; Ad, Ah) are shown (magnification x 7600). The represented phenotypes were observed in the major amount of analyzed cells from n=2 experiments.

5.2.3 HAdV-C5 infection promotes E1B-55K/RNF4/Daxx complex formation

To evaluate the RNF4/Daxx interaction in the presence or absence of E1B-55K, IP experiments were performed at different time points of WT virus infection (Fig. 25A), as well as with either WT or an E1B-55K mutant virus 24 h p.i. (Fig. 25B). In uninfected cells, the endogenous RNF4 protein showed no binding to Daxx (Fig. 25A, lower panel, lane 4). Even 16 h p.i., no binding to Daxx was observed (Fig. 25A, lane lower panel, 5). After 36 h p.i., binding between Daxx and RNF4 was detectable,

where also high amounts of E1B-55K proteins were detectable (Fig. 25A, lane 3 and 6). An E1B-55K dependent interaction between Daxx and RNF4 was observed by IP in HAdV-C5 WT and E1B-55K. lacking virus infected cells (Fig. 25B). Here, binding of RNF4 to Daxx was only observed in the WT virus infection in the presence of E1B-55K (Fig. 25B, lane 2 and 5) but not in the E1B-55K mutant virus infected cells (Fig. 25B, lane 3 and 6).

In sum these data indicate that the binding of Daxx to RNF4 is mediated by E1B-55K possibly through multiple interactions in a trimeric complex.
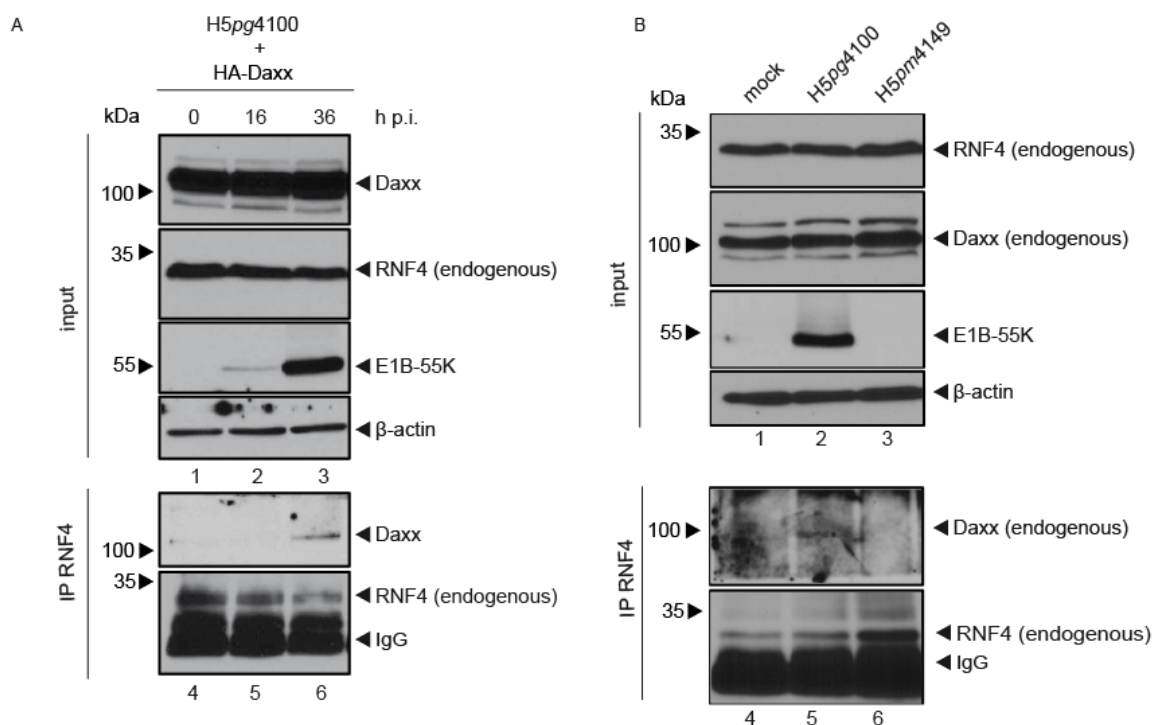
Fig. 25 HAdV-C5 infection promotes E1B-55K/RNF4/Daxx complex formation

(A) H1299 cells were infected with WT virus (H5*pg*4100) at a MOI of 50, harvested 16 and 36 h p.i. and total-cell extracts were prepared. IP of endogenous RNF4 was performed using RNF4 mouse pAb. Proteins were separated by SDS-PAGE and subjected to immunoblotting. Input levels of total-cell lysates and IP proteins were detected using E1B-55K mouse mAb, RNF4 mouse pAb, Daxx rabbit pAb and ß-actin mouse mAb as loading controls. Note that light chains (IgG) were detected at 25 kDa. (B) H1299 cells were infected with WT virus (H5*pg*4100) or E1B-55K mutant virus (H5*pm*4149) at a MOI of 50, harvested 24 h p.i., and total-cell extracts were prepared. IP of endogenous RNF4 was performed using RNF4 mouse pAb, proteins were separated by SDS-PAGE and subjected to immunoblotting. Input levels of total-cell lysates and IP proteins were detected using E1B-55K mouse mAb, RNF4 mouse pAb, Daxx rabbit pAb and ß-actin mouse mAb as loading controls. Note that light chains (IgG) were detected at 25 kDa. Molecular weights in kDa are indicated on the *left*, relevant proteins on the *right*. These blots represent the result of several repeated experiments.

Results

5.2.4 HAdV-C5 infection enhances Daxx SUMOylation

Daxx is a constitutive member of the PML-NBs, which is significantly involved in the generation of PML-NBs (96, 104). Recently published data revealed that the assembly of PML-NBs, induced by oxidative stress, controls the SUMOylation of PML partner proteins (185). In addition, the SIM domain of Daxx is important for the association with PML-NBs. Even more, an irreversible fusion of Daxx with SUMO-1 or SUMO-2 enhanced Daxx association to PML-NBs.

It is well known that SUMO is covalently attached to a small subset of Daxx proteins (186, 187). Furthermore, it has been shown that viruses can alter the SUMOylation of Daxx upon infection. As an example, it has been published that pp71 of HCMV enhanced Daxx SUMOylation via a viral protein upon infection but the role of this enhanced modification on the virus life cycle remains unclear (188). On the basis of these facts and additionally that the SUMOylation of target proteins is necessary for a STUbL dependent degradation, the SUMOylation status of Daxx in HAdV-C5 infected cells was investigated

For this, a model system developed by Tatham *et al*. was used to purify His-SUMO-2 conjugated proteins (Ni-NTA pulldown) (155) after HAdV-C5 WT and E1B-55K mutant virus infection (Fig. 26). A stronger, SUMO-2 modified form of Daxx with high molecular weight was detected with both viruses, irrespective of E1B-55K expression (Fig. 26; lanes 2-3). Similar but weaker bands were observed in the uninfected cells (Fig. 26; lane 1). The high molecular weight bands (Fig. 26, lanes 2-3) most likely present a SUMO modified Daxx protein. Furthermore, a HAdV-C5 dependent enhanced SUMOylation of Daxx seems to be independent of E1B-55K expression. However, to investigate whether other viral factors can impair the Daxx SUMOylation, infection studies with different HAdV-C5 mutant viruses could be used to address this question.

Results
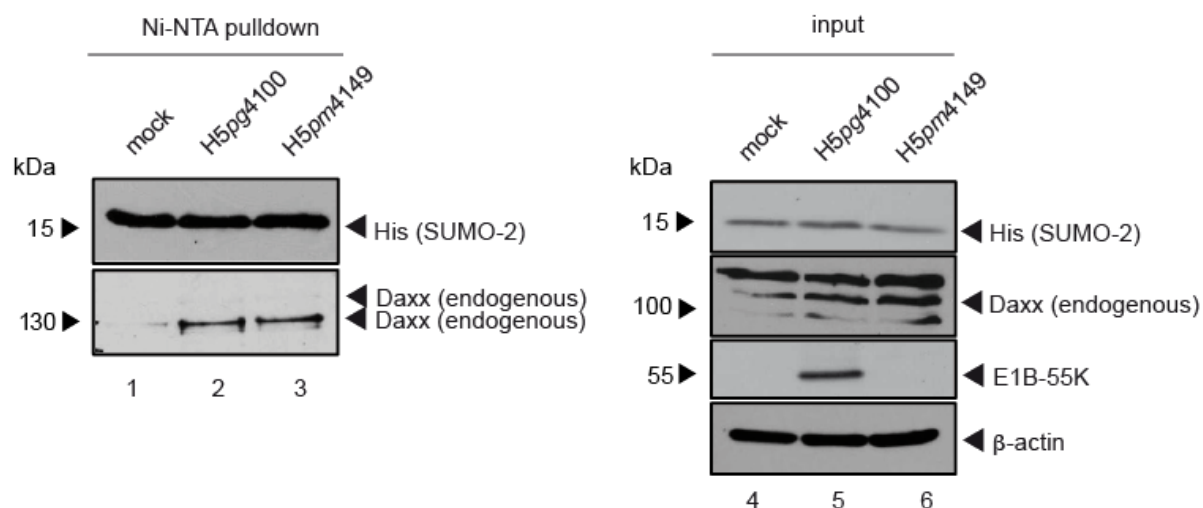
Fig. 26 HAdV-C5 infection enhances Daxx SUMOylation

HeLa cells stably expressing 6His-SUMO-2 were infected with WT virus (H5*pg*4100) or E1B-55K mutant virus (H5*pm*4149) at a MOI of 20. Whole-cell lysates were prepared with guanidine hydrochloride buffer 48 h p.i. and subjected to Ni-NTA purification of 6His-SUMO conjugated proteins. Proteins were separated by SDS-PAGE and subjected to immunoblotting. Input levels of total-cell lysates and Ni-NTA purified proteins were detected using Daxx rabbit pAb, His mouse mAb, ß-actin mouse mAb and E1B-55K mouse mAb. Molecular weights in kDa are indicated on the *left*, relevant proteins on the *right*. These blots represent the result of several repeated experiments.

5.2.5 RNF4/E1B-55K interaction is required for Daxx Ubiquitinylation

So far it could be shown that HAdV-C5 infection, more precisely E1B-55K, affects the subcellular localization of RNF4 and is important for the interaction of RNF4 with Daxx. This, along with the fact that Daxx gets degraded proteasomally via a novel E1B-55K-dependent pathway, led to the question whether binding of RNF4 to E1B-55K induces Ubiquitinylation of Daxx.

Daxx and Ubiquitin constructs were cotransfected with plasmids containing E1B-55K (Fig. 27, lanes 2 and 5) or E1B-55K plus RNF4 (Fig. 27, lanes 3 and 6). To stabilize Ubiquitinylated proteins and to prevent their degradation, cells were treated with the proteasome inhibitor MG-132. Ubiquitinylated Daxx was detected by IP using a HA specific-Ab, recognizing the HA-tagged Daxx protein and an Ubiquitin specific-Ab. E1B-55K coexpressed with RNF4 significantly enhanced Ubiquitinylation of Daxx (Fig. 27, left panel, lane 3, asterisks), were E1B-55K alone has no influence on Daxx Ubiquitinylation (Fig. 27, left panel, lane 2). Altogether, these results imply that Daxx Ubiquitinylation by E1B-55K is supported by the presence of RNF4.
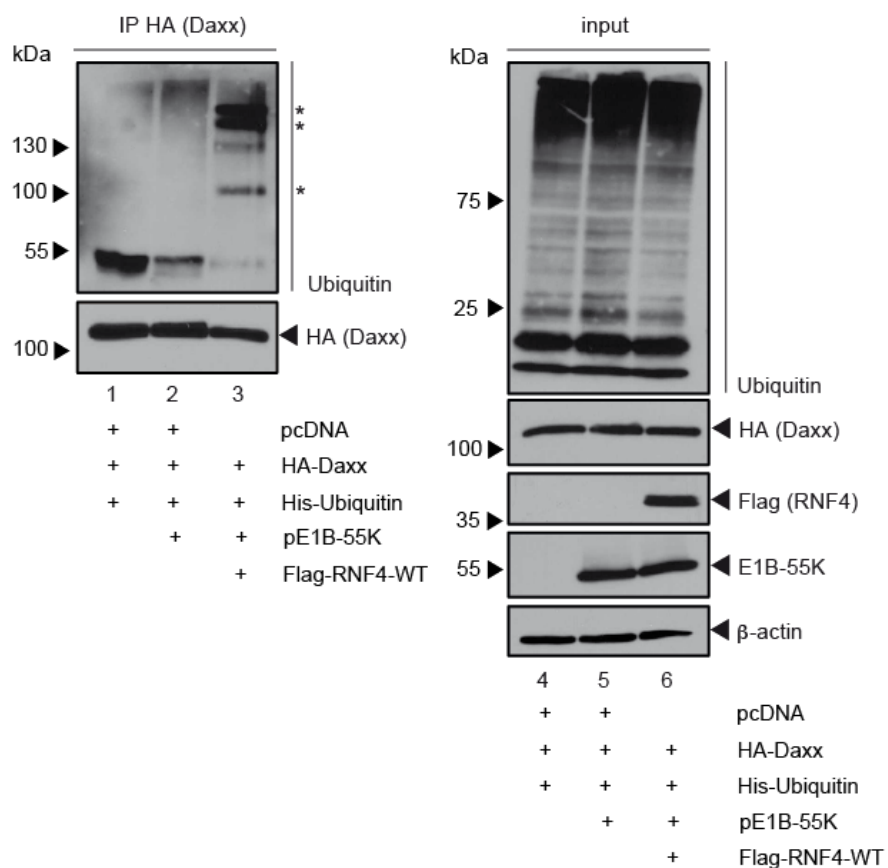
Fig. 27 RNF4/E1B-55K interaction is required for Daxx Ubiquitinylation

H1299 cells were cotransfected with 5 μg of HA-Daxx, 5 μg Flag-RNF4-WT, 5 μg His-Ubiquitin and 5 μg pE1B-55K, as indicated. Cells were harvested 24 h p.t., prior to preparation of IP assays and total-cell extracts. IP proteins and input levels of total-cell lysates were detected using Ubiquitin mouse mAb, Daxx rabbit pAb, ß-actin mouse mAb, E1B-55K mouse mAb and α-Flag mouse mAb. 4 hours prior harvesting, transfected cells were treated with MG-132 to inhibit proteasomal degradation of Ubiquitinylated proteins. Molecular weights in kDa are indicated on the *left*, relevant proteins on the *right*. These blots represent the result of several repeated experiments.

5.2.6 RNF4 promotes E1B-55K dependent Daxx Ubiquitinylation

Due to the observation that RNF4 enhances the Ubiquitinylation of Daxx together with E1B-55K, it was evaluated whether the enhanced Ubiquitinylation also triggers proteasomal degradation of Daxx (Fig, 28). To answer this question, a modified Ubiqitinylation assay was performed, where the cells were not treated with MG-132 to allow proteasomal degradation of Ubiquitinylated proteins. In addition it was tested whether the enhanced Ubiquitinylation is dependent on both RNF4 and E1B-55K. Because it is known that PML-IV isoform can act as a SUMO E3 ligase for p53 (72, 73) and the E3 Ubiquitin ligase Mdm2 (189), PML-IV was used to test if overexpression of any additional SUMO E3 ligase leads to enhanced Ubiquitinylation of Daxx.

In line with data shown in Figure 27, a reduction of Ubiquitinylated Daxx was observed in the presence of RNF4 and E1B-55K, independent of PML-IV (Fig. 28; lane 3 and 5). Furthermore, neither RNF4 alone (Fig. 28; Lane 2), nor RNF4 and PML-IV (Fig. 28; lane 4), induced a reduction of Ubiquitinylated Daxx. A slightly decrease of Daxx protein levels already at 24 h p.t. (Fig. 28; lanes 8, 10) strengthens the hypothesis that RNF4 is an important cofactor for E1B-55K dependent reduction of Daxx steady-state concentrations. Interestingly, also a slightly decreased in protein levels of RNF4 was observed in whole cell lysates containing E1B-55K (Fig. 28; lanes 7-8). This could be RNF4 auto-Uquitinylation and consequently proteasomal degradation due to RNF4 activation or E1B-55K dependent relocalization of RNF4 into the insoluble nuclear matrix as already shown in Fig. 11.
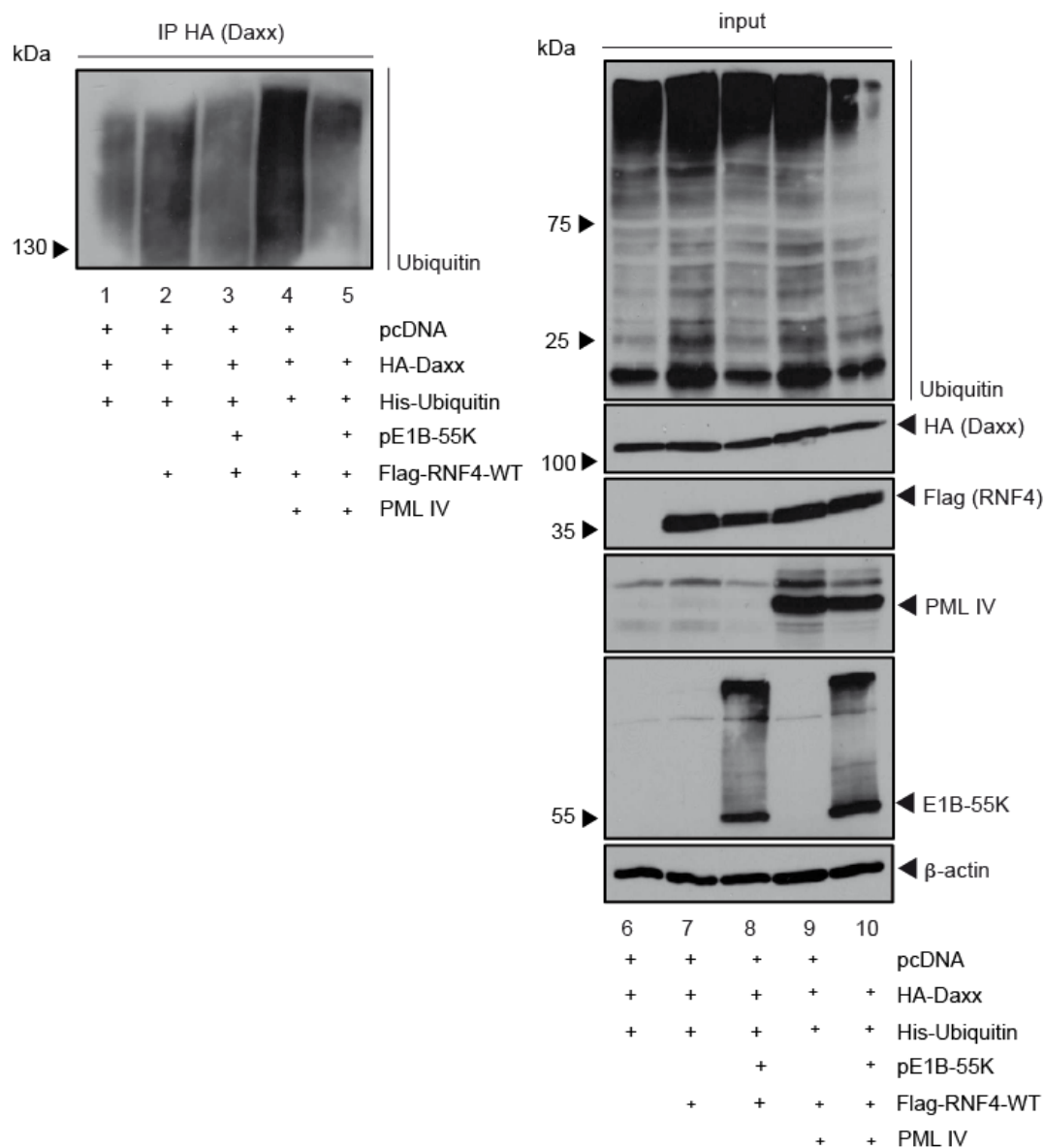
Fig. 28 RNF4 promotes E1B-55K dependent Daxx Ubiquitinylation

H1299 cells were cotransfected with 5 μg of HA-Daxx, 5 μg Flag-RNF4-WT, 5 μg His-Ubiquitin, 5 μg pPML-IV and 5 μg pE1B-55K, as indicated. Cells were harvested 24 h p.t., prior to preparation of IP assays and total-cell extracts. IP proteins and input levels of total-cell lysates were detected using mAb Ubiquitin, Daxx rabbit pAb, ß-actin mouse mAb, PML rabbit pAb, α-Flag mouse mAb and E1B-55K mouse mAb. Transfected cells were not treated with MG-132 to allow proteasomal degradation of Ubiquitinylated proteins. Molecular weights in kDa are indicated on the *left*, relevant proteins on the *right*. These blots represent the result of several repeated experiments.

5.2.7 Proteasome subunit 19S is relocalized into E1B-55K containing aggregates in HAdV-C5 infected cells

Due to the fact that E1B-55K is the main viral protein involved in proteasomal degradation of proteins in HAdV-C5 infected cells, immunofluorescence analyzes were performed to evaluate whether changes of the proteasome localization in HAdV-C5 infected cells could be observed (Fig. 29). Recent reports conclude that changes in the distribution and general intracellular localization of proteasomes truly depend on the host cell cycle (190). Furthermore, it could be shown that during progression of the cell cycle, increased levels of proteasomes remain bound to the nuclear matrix (191). Since also the localization of SUMOylated E1B-55K was observed in the nuclear matrix fraction, it was investigated whether the proteasome localization is altered in the presence of E1B-55K.

H1299 cells were infected with WT virus and stained for E1B-55K as well as proteasome with specific-Ab. Uninfected cells were used for control staining. No E1B-55K staining was observed in the uninfected cells, whereas E1B-55K exhibited characteristic nuclear staining in WT virus infected cells (Fig. 29; panels c and g). In uninfected cells, the proteasome subunit 19S showed a widely, diffuse nuclear staining (Fig. 29; panels b and d). Interestingly, in the majority of HAdV-C5 infected cells, the proteasome subunit 19S is relocalized from its diffuse nuclear staining into track-like structures juxtaposed to E1B-55K aggregates within the nucleus (Fig. 29; panels f, g, h, i). Interestingly, a similar staining could also be observed of RNF4 and Daxx, which supports previous results that RNF4 is involved in proteasomal degradation of Daxx in HAdV-C5 infected cells.

Results
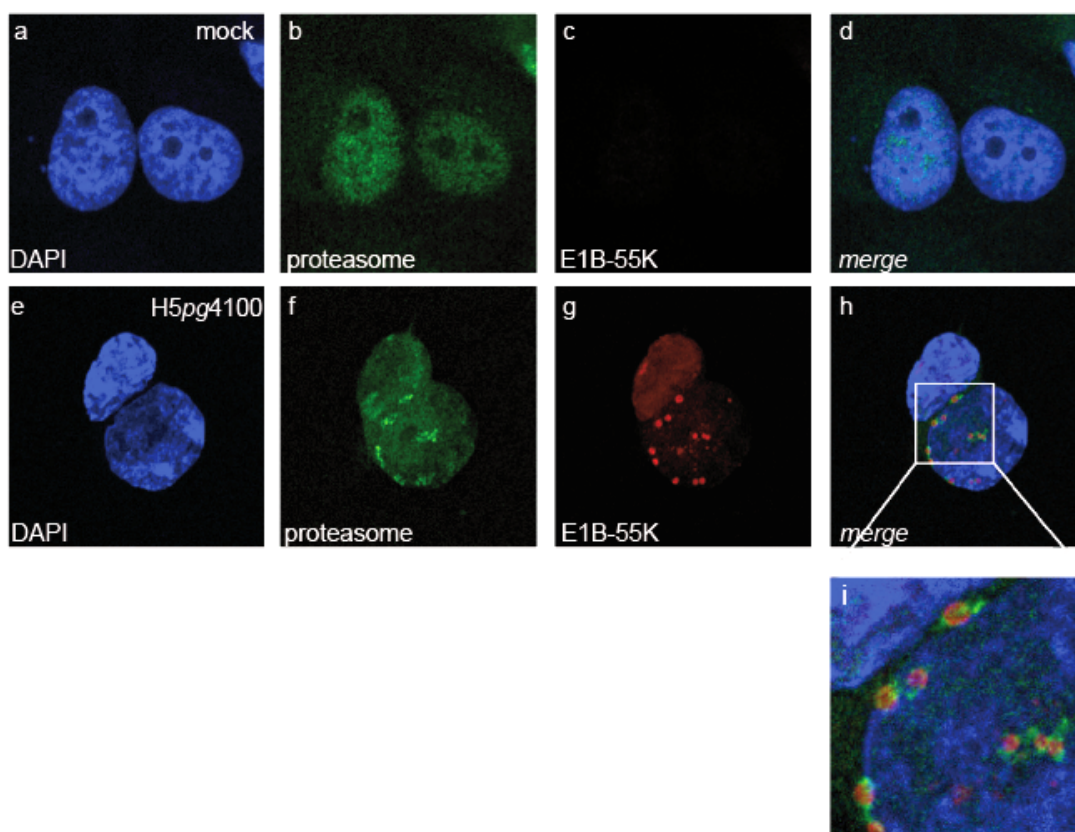
Fig. 29 Proteasome subunit 19S is relocalized into E1B-55K containing aggregates in HAdV-C5 infected cells

H1299 cells were infected with WT virus (H5*pg*4100) at a MOI of 20 and fixed with 4% PFA 48 h p.i. Cells were labeled with proteasome rabbit pAb, detected with *Alexa488* (α-Flag; green) conjugated secondary Ab and E1B-55K mouse mAb, detected with Cy3 (α-E1B-55K; red) conjugated secondary Ab. Nuclei are labeled with DAPI. α-proteasome (green; Bb, Bf), α-E1B-55K (red; Bc, Bg), DAPI (blue; Ba, Be) staining patterns, overlay of the single images (merge; Bd, Bh) and enlarged overlay (merge; Bi) are shown (magnification x 7600). The represented phenotypes were observed in the major amount of analyzed cells from repeated experiments.

Altogether, these results support published data that the host proteasome pathway is used in HAdV-C5 infected cell for degradation of cellular proteins (45, 46, 192). In the case of Daxx, this pathway seems to be dependent on E1B-55K expression and and RNF4 activity. Moreover, the observation that E1B-55K induced degradation of Daxx promotes *focus*-formation in pBRK cells (51, 52), suggests that the E1B-55K/RNF4 interaction may play an important role in HAdV induced oncogenesis. Therefore the effect of RNF4 on HAdV-C5 E1A/E1B mediated transformation was investigated.

Results

5.3 RNF4 effects HAdV-C5 E1 region mediated cell transformation

5.3.1 RNF4 overexpression suppresses the *focus*-forming activity of E1A and E1B

In classical transformation experiments, non-permissive pBRK cells start to grow in multilayer colonies (*foci*) after transduction with HAdV-C5 oncogenes. This effect can already be observed macroscopically 3-4 weeks after cultivation. The colony-shaped growth is due to the loss of contact inhibition, followed by the ability of unlimited cell growth (193). In contrast, primary cells are limited in growth and reach senescence after a certain number of divisions (194). The oncogenic properties of HAdV-C5 were attributed to the E1A and E1B products of the E1 region (59, 62). Some years later, oncogenic properties of the viral proteins E4orf3 and E4orf6 could additionally be observed (193, 195, 196).

It has been well established that RNF4 has an important role in the maintenance of genome stability by preventing chromosome loss through the interaction with the cellular DNA repair machinery. Interestingly it could be observed that RNF4 is down regulated during cellular transformation in germ cell tumors and ectopically expressed RNF4 inhibits cell proliferation (197, 198). To investigate the biological function of RNF4 in the HAdV-C5 E1A/E1B mediated transformation of rodent cells, transformation assays in pBRK cells were performed.

Human and rat RNF4-WT and RNF4-SIM mutants were cotransfected with an E1A/E1B encoding plasmid as indicated (Fig. 30). For quantitative analysis of *focus*-formation, pBRK cells were stained as described (4.2.5) and single *foci* were counted on each plate. Later, the relative *focus*-formation activity was determined (Fig. 30A). Consistent with published data, the relative *focus*-formation activity was almost 25 times lower, when E1A was transfected alone, compared to transfection of a plasmid encoding for both proteins (Fig. 30B) (196). Interestingly, cotransfection of RNF4, either human, rat, RNF4-WT or RNF4-SIM mutant, showed a reduced *focus*-formation activity compared to the positive control (Fig. 30B). Over all, the highest reduction was observed in cells cotransfected with the SIM mutant of human and rat RNF4 (Fig. 30B). In this case, an almost seven fold reduction was noticed.

A

B
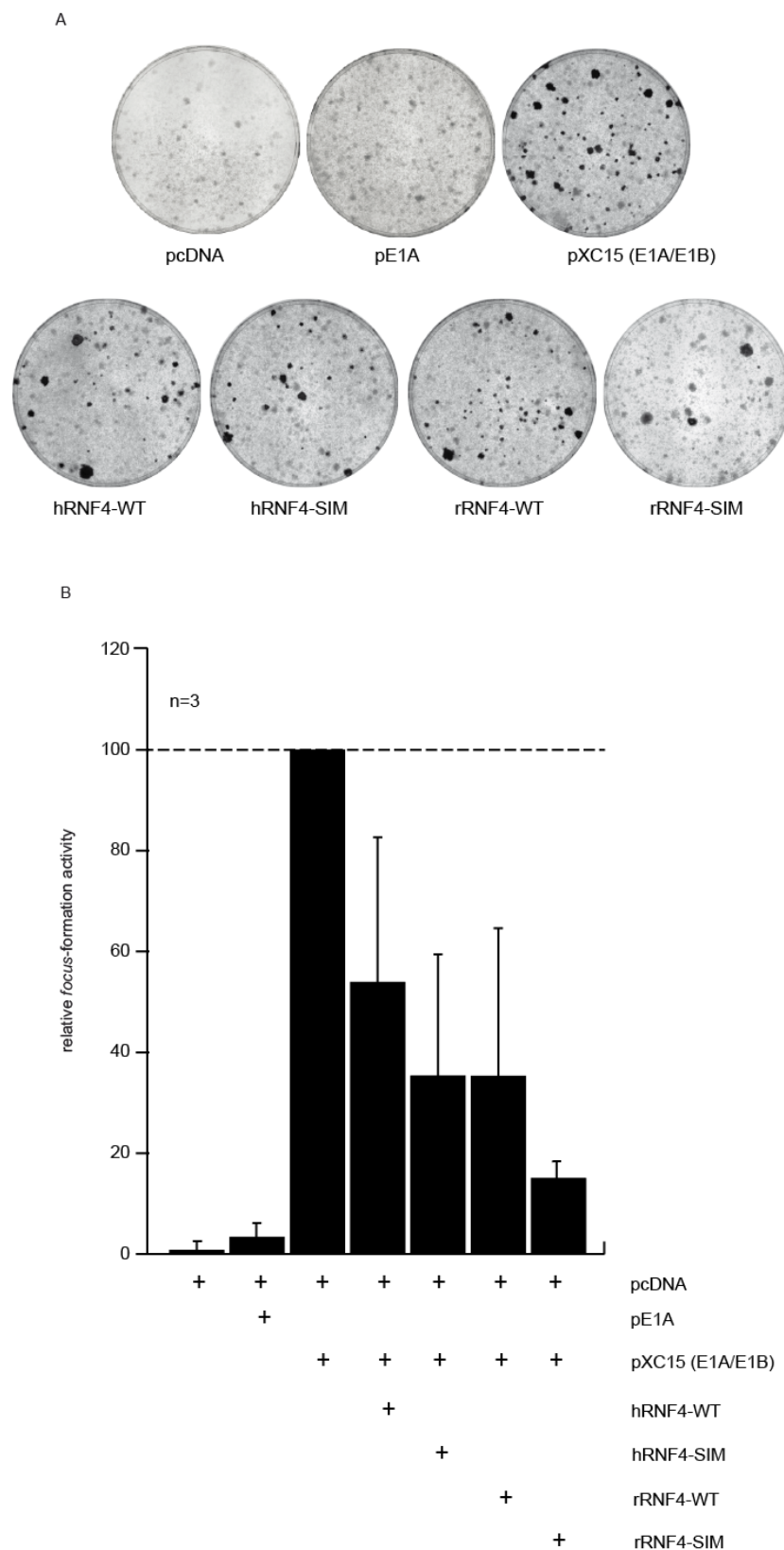
Fig. 30 RNF4 overexpression suppresses the *focus*-forming activity of E1A and E1B

(A) pBRK cells were cotransfected with 1.5 μg pE1A, 6 μg pXC15, 6 μg Flag-hRNF4-WT, Flag-hRNF4-SIM, Flag-rRNF4-WT or Flag-rRNF4-SIM as indicated. After cultivation for four weeks, cells were stained with a crystal violet staining solution (4.2.5). (B) The transformation activity was presented as relative *focus*-formation activity to the activity of pXC15. The mean values with standard deviation from three independent tests are shown (n=3).

Results

This experiment demonstrates that RNF4 has a negative effect on the HAdV-C5 E1A/E1B dependent transformation of rodent cells. Moreover, in contrast to the binding studies with E1B-55K (Fig. 24), the SIM domain of RNF4 appears to play a role in counteracting E1A/E1B mediated transformation, at least in primary rodent cells.

In summary, RNF4 appears to positively regulate lytic replication of HAdV-C5 but exhibits a negativ effect on HAdV-C5 E1A/E1B *focus*-forming activity.

5.4 Arkadia protein expression and localization is modulated in HAdV-C5 infected cells

5.4.1 Arkadia protein levels are decreased during HAdV-C5 infection

Humans are so far known to express two STUbLs, namely RNF4 and Arkadia (151, 175). It could be shown that Arkadia interacts with polySUMOylated PML via a SUMO/SIM interaction and depletion of Arkadia contributes to PML accumulation in response to As_2O_3 treatment (175). Furthermore, it has been described that Arkadia undergoes homodimerization upon activation, but concurrently a heterodimerization with RNF4 could be excluded (175). While Arkadia has also been implicated in PML degradation, it is also shown to be involved in DNA damage response by Ubiquitinylation of the SUMOylated XPC, which promotes NER (151).

To initially investigate the role of Arkadia during HAdV-C5 life cycle, H1299 cells were infected with WT virus and harvested at the indicated time points (Fig. 31). Interestingly, Arkadia protein levels were increased at 24 h p.i. (Fig. 31; lanes 1-2) and decreased upon 48 h p.i. with WT virus (Fig. 31; lanes 3-4), comparable to the data obtained for RNF4 (Fig. 11). Furthermore, Arkadia protein levels decreased, when E1B-55K protein levels started to increase (Fig. 31; lanes 2-4).
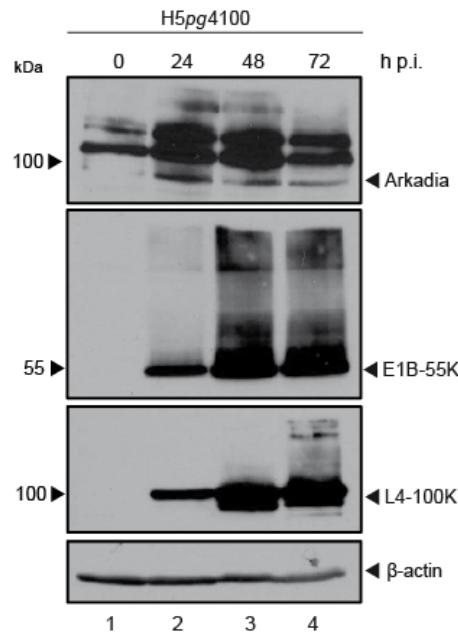
Fig. 31 Arkadia protein levels are decreased during HAdV-C5 infection

H1299 cells were infected with WT virus (H5*pg*4100) at a MOI of 50 and harvested at the indicated time points post infection. Total-cell extracts were prepared, separated by SDS-PAGE and subjected to immunoblotting using Arkadia mouse mAb, E1B-55K mouse mAb, L4-100K rat mAb (164) and ß-actin mouse mAb as loading controls. Molecular weights in kDa are indicated on the *left*, relevant proteins on the *right*. These blots represent the result of several repeated experiments.

5.4.2 Arkadia is relocalized in the insoluble nuclear matrix fraction in HAdV-C5 infected cells

Since the protein amount of Arkadia decreased at late time points of infection, it was investigated, whether this is due to a HAdV-C5 dependent degradation or a virus dependent relocalization into insoluble aggregates (Fig. 32A).

H1299 cells were infected with WT virus and stained for Arkadia 24 and 48 h p.i. Interestingly, a HAdV-C5 induced relocalization of Arkadia from the cytoplasm to the nucleus was observed already 24 h p.i. (Fig. 32A; panels Ab, Ac, Ae and Af), previously seen before for the RNF4 (Fig. 13). Preliminary data show that Arkadia localized in a punctate staining within the nucleus in HAdV-C5 infected cells, which was slightly reduced 48 h p.i. (Fig. 32A; panels h and i). Still, a partial fraction of Arkadia was present in the cytoplasm in late time points of infection (Fig. 32A; panels Ah and Ai). To analyze the punctate localization of Arkadia in more detail, a fractionation assay was performed (Fig. 32B) as described in Figure 12. As expected, Arkadia protein levels were observed in the insoluble nuclear matrix fraction in uninfected cells and 16 h p.i. (Fig. 32B; lanes 1 and 2). Consistent with the result seen

before (Fig. 31), Arkadia protein levels were also reduced in the insoluble nuclear fraction 48 h p.i. (Fig. 32B; lane 3).

In sum, these data indicate a HAdV-C5 dependent reduction of Arkadia upon infection. However, it must be mentioned here that it would be better to repeat the experiments with another, more Arkadia specific-Ab or overexpression of a tagged Arkadia construct, since high background signal were obtained with the used Ab.
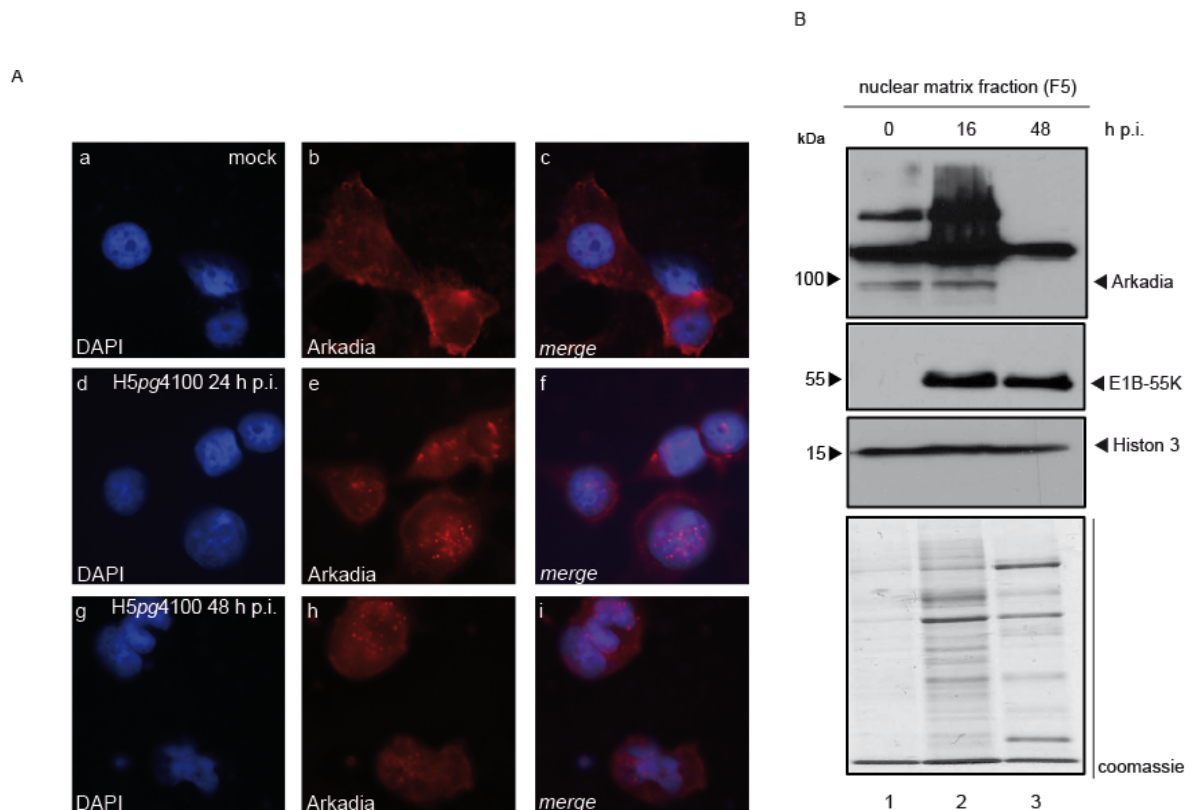
Fig. 32 Arkadia is relocalized in the insoluble nuclear matrix fraction in HAdV-C5 infected cells

(A) H1299 cells were infected with WT virus (H5*pg*4100) at a MOI of 20 and fixed with 4% PFA 24 and 48 h p.i. Cells were labeled with Arkadia mouse mAb detected with Cy3 (α-Arkadia; red) conjugated secondary Ab. Nuclei are labeled with DAPI. α-Arkadia (red; Ab, Ae, Ah) and DAPI (blue; Aa, Ad, Ag) staining patterns and overlay of the single images (merge; Ac, Af, Ai) are shown (magnification x 7600). The represented phenotypes were observed in the major amount of analyzed cells from n=2 experimets. (B) H1299 cells were infected with WT virus (H5*pg*4100) at a MOI of 50 and harvested at the indicated time points. Cell extracts were fractionated into cytoplasm, soluble nuclear, nuclear membrane, chromatin and insoluble nuclear factions, separated by SDS-PAGE and subjected to immunoblotting using the Ab indicated in (Fig. 12). Protein levels in the insoluble nuclear fraction are shown. Molecular weights in kDa are indicated on the *left*, relevant proteins on the *right*. These blots represent the result of several repeated experiments.

Results

5.4.3 Arkadia is relocalized juxtaposed to E1B-55K aggregates in HAdV-C5 infected cells

Since Arkadia protein levels were decreased in HAdV-C5 infected cells and relocalized into the insoluble nuclear matrix fraction, it was tested whether Arkadia and E1B-55K colocalize in HAdV-C5 infected cells. Immunofluorescence analysis was performed to visualize the localization of Arkadia (Fig. 33). For this, cells were infected with HAdV-C5 WT virus and stained 48 h p.i. Uninfected cells were used to control the immunostaining. As expected, no E1B-55K staining was observed in the uninfected cells, whereas Arkadia exhibited mainly cytoplasmic localization as described in the literature (199, 200) (Fig. 33; panels Ab and Ac). As observed previously (Fig. 32A), Arkadia is relocalized from its cytoplasmic staining into a punctate nuclear staining 48 h p.i. (Fig. 33; panel Af). Interestingly, the punctate Arkadia was observed juxtaposed to E1B-55K aggregates in the nucleus 48 h p.i in the majority of cells. (Fig. 33A; panels h and i). Noticeably, the same localization was as well observed for RNF4 in HAdV-C5 infected cells (Fig. 13).
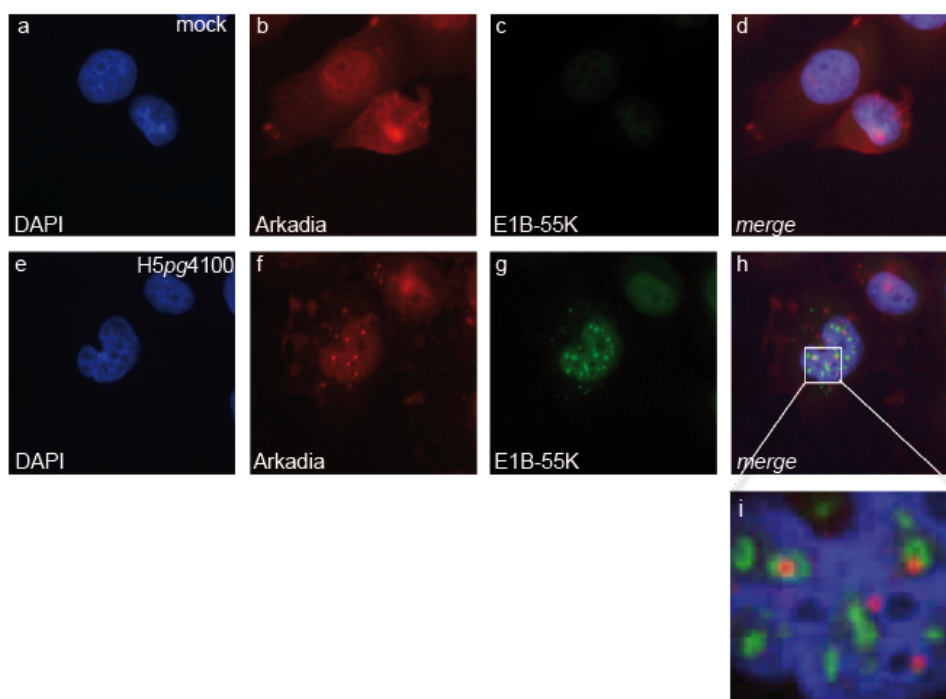
Fig. 33 Arkadia is relocalized juxtaposed to E1B-55K aggregates in HAdV-C5 infected cells

H1299 cells were infected with WT virus (H5*pg*4100) at a MOI of 20 and fixed with 4% PFA 48 h p.i. Cells were labeled with Arkadia mouse mAb, detected with *Alexa488* (α-Arkadia; green) conjugated secondary Ab and E1B-55K mouse mAb, detected with Cy3 (α-E1B-55K; red) conjugated secondary Ab. Nuclei are labeled with DAPI. α-Arkadia (green; Ab, Af), α-E1B-55K (red; Ac, Ag), DAPI (blue; Aa, Ae) staining patterns, overlay of the single images (merge; Ad, Ah) and enlarged overlay (merge; Ai) are shown (magnification x 7600). The represented phenotypes were observed in the major amount of analyzed cells from repeated experiments.

5.4.4 E1B-55K PTM influences the interaction with Arkadia

Published work from Cao *et al*. could identify Arkadia and Arkadia-like 1 protein (ARKL1) as new interaction partners of CK2, which seems to have an important role for EBV reactivation (201). Besides Ubiquitinylation and SUMOylation, Phosphorylation is the most prevalent PTM that can alter protein function, localization and stability of proteins. Many studies have shown that, besides SUMOylation, E1B-55K can also be phosphorylated at highly conserved serine and threonine residues at the C-terminus (202) and that the cellular CK2 kinase is responsible for E1B-55K Phosphorylation at a specific CK2 consensus motif (117, 203). Furthermore, a phospho- and SUMO-E1B-55K dependency on target degradation (Mre11, DNA ligase IV), leading to inefficient degradation of antiviral targets, could be observed (117). In order to investigate whether the interaction of E1B-55K and Arkadia is influenced by Phosphorylation or even directly by CK2, IP analysis with Arkadia and E1B-55K SUMO- and Phosphorylation mutants were performed (Fig. 34). Surprisingly, Arkadia interacts with all transfected E1B-55K mutants (Fig. 34; lanes 8-12). However, a weaker binding signal was observed in E1B-55K-SCS and E1B-55K-delP mutant transfection (Fig. 34; lanes 9, 11). Comparable signals were obtained for E1B-55K-WT, -NES and -pM mutant transfection (Fig. 34; lanes 8, 10, 12). In sum, these data revealed a SUMO-, and phospho-E1B-55K dependency of binding with Arkadia.
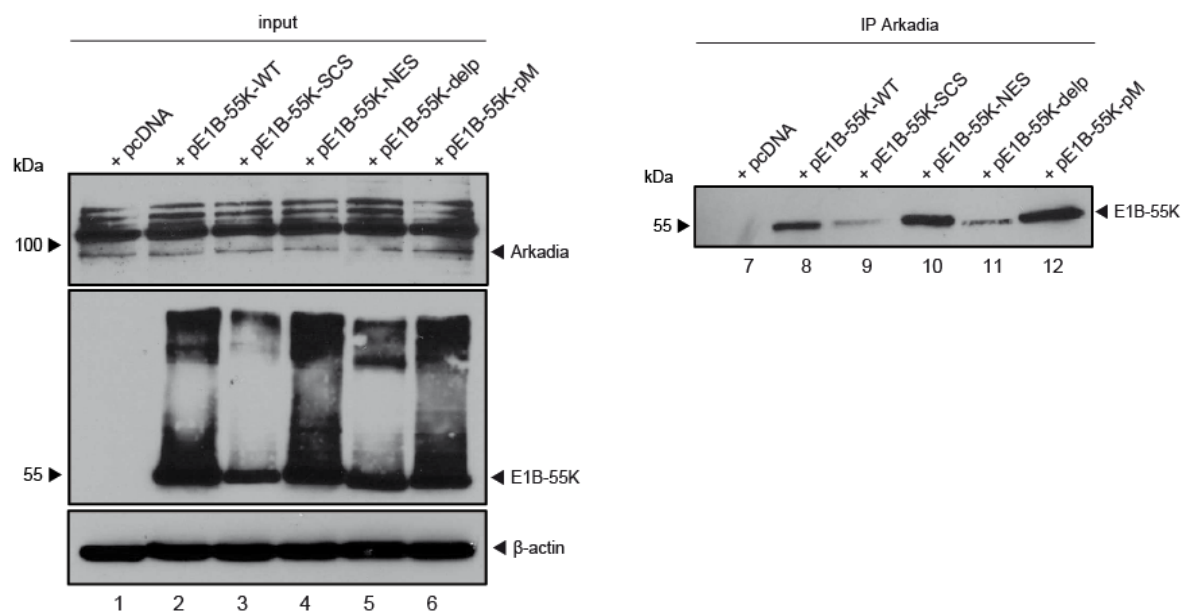
Fig. 34 E1B-55K PTM influences the interaction with Arkadia

H1299 cells were cotransfected with 6 μg pE1B-55K-WT, -SCS, -NES, -delp (phospho-mutant S490/91A, T495A, (202)) or -pM (phospho-mimic-mutant S490/91D, T495D, (111)) and harvested 48 h p.t. and total-cell extracts were prepared. IP of Arkadia was performed using Arkadia mouse mAb, proteins were separated by SDS-PAGE and subjected to immunoblotting. Input levels of total-cell lysates and IP proteins were detected using E1B-55K mouse mAb, Arkadia mouse mAb and ß-actin mouse mAb as loading controls. Molecular weights in kDa are indicated on the *left*, relevant proteins on the *right*. These blots represent the result of n=2 repeated experiments.

5.4.5 CK2α is a novel interaction partner of Arkadia in HAdV-C5 infected cells

Since Arkadia could also influence the Phosphorylation of E1B-55K, the interaction of Arkadia and CK2 in HAdV-C5 infected cells was investigated (Fig. 35). Preliminary IP analysis of CK2 with Arkadia revealed an interaction between both factors in HAdV-C5 infected cells (Fig. 35; lane 4). Surprisingly, no CK2 signal was observed in the uninfected cells (Fig. 35; lane 5). To address the question if E1B-55K mediates the CK2/Arkadia interaction or Arkadia directly influence CK2 mediated E1B-55K Phosphorylation, an E1B-55K mutant virus could be used for further experiments.
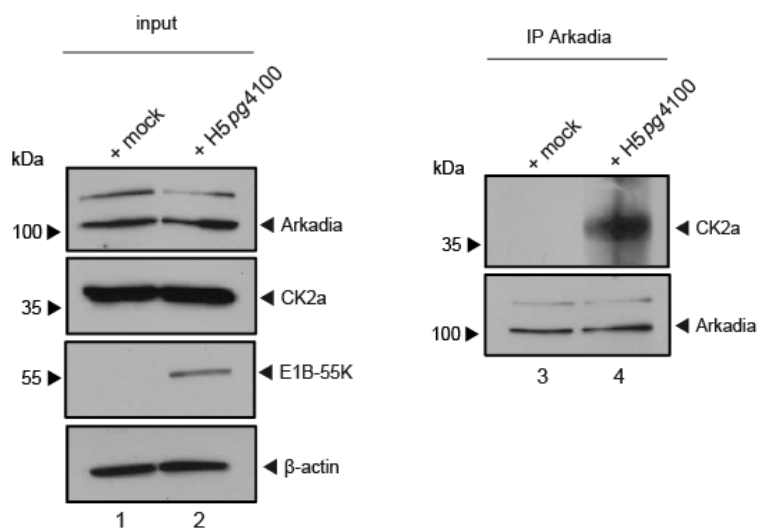
Fig. 35 CK2α is a novel interaction partner of Arkadia in HAdV-C5 infected cells

H1299 cells were infected with WT virus (H5*pg*4100) at a MOI of 50, harvested 24 h p.i. and total-cell extracts were prepared. IP of endogenous Arkadia was performed using Arkadia mouse mAb, proteins were separated by SDS-PAGE and subjected to immunoblotting. Input levels of total-cell lysates and IP proteins were detected using anti-CK2α rabbit pAb, Arkadia mouse mAb, E1B-55K mouse mAb and ß-actin mouse mAb as loading controls. Molecular weights in kDa are indicated on the *left*, relevant proteins on the *right*. These blots represent the result of n=2 repeated experiments.

6 Discussion

6.1 Role of STUbLs during productive infection of HAdV-C5

RNF4 belongs to the family of SIM containing RING-finger proteins. It consists of 190 AS, has a molecular weight of 31 kDa and is expressed in the nucleus of mammalian cells (129). The main function of RNF4 is the Ubiquitinylation of SUMOylated proteins, prior to proteasomal degradation (122, 204). A recent study characterized over 300 proteins as potential RNF4 substrates using a non-denaturing affinity pull down approach combined with mass spectrometry analysis (139). Known targets of RNF4 are mainly involved in the DNA damage response, transcriptional control and cell cycle regulation such as kinetochore assembly (145, 205, 206).

The first substrate identified for the human STUbL RNF4 was the PML-NB name-giving protein PML (204). RNF4 interacts with the cellular protein PML via SUMO/SIM binding and induces proteasomal degradation of PML. This mechanism is also used in the treatment of APL patients. Here, As_2O_3 leads to RNF4 mediated Ubiquitinylation and proteasomal degradation of PML (125, 204). The interaction of RNF4 with the SUMO modified PML protein furthermore indicates that RNF4 is recruited into PML-NBs (136). So far, more than 80 proteins are known, which localize together with PML in the PML-NBs, most of them are transiently associated with the PML-NBs (97-99, 108). The cellular transcription factor Daxx for instance was confirmed in previous studies as a direct interaction partner of PML (100, 101).

With regard to virus infection, it is known from earlier studies that PML-NBs are located in the immediate vicinity of viral replication centers in many DNA and RNA viruses. For this reason, many viruses express gene products that reorganize or destroy PML-NBs in order to eliminate potential antiviral protection mechanisms. The role of PML-NBs in infection processes was examined a long time ago and turned out to be an important step to back up viral replication of different viruses (207, 208).

HAdV-C5 targets the PML-NBs to directly prevent the intrinsic antiviral immune response mediated by PML-NB components. An interaction of E1B-55K with PML-NB key components, like Daxx and Sp100A was already observed in HAdV-C5 infected cells (51, 105, 106). There are numerous indications of a Daxx dependent repression of HAdV-C5 replication, which is reflected in a significant increase in viral gene expression upon degradation of Daxx (119, 192). Among others, the viral

structural protein pVI was identified as an interaction factor of Daxx (32). It is assumed that pVI subsequently mediates a relocalization of the Nedd-4 Ubiquitin ligase as well as Daxx to the PML-NBs in order to initiate a specific Ubiquitinylation of Daxx, thus ensuring the productive HAdV-C5 infection (32). Furthermore, the viral protein E1B-55K was identified as an interaction partner of Daxx. In infected cells, PML and Daxx usually provide the initiation of apoptosis in the nucleus and it could be shown that the repressive property of Daxx is weakened by its localization to the PML-NBs (109). However, the viral protein E1B-55K prevents this apoptotic mechanism through proteasomal degradation of Daxx during HAdV-C5 infection. The negative effect of Daxx on viral gene expression is moreover closely related to its interaction with ATRX. Both of these factors are capable of recruiting HDACs to amplify the chromatin structure at the respective promoter (53, 54). Apparently, this function is blocked in HAdV-C5 infected cells by interactions with pVI and E1B-55K (119, 192).

This study investigates the role of RNF4 in the E1B-55K mediated degradation of Daxx and the general influence of RNF4 during HAdV-C5 infection. In first experiments, RNF4 could be identified as a new interaction partner of E1B-55K, which seems to be independent of E1B-55K PTM (Fig. 18). This is an interesting observation, since numerous reports suggest that important functions of E1B-55K rely on the PTM of the protein, including SUMOylation and Phosphorylation (39, 40, 105, 110, 111, 202). Mutational inactivation of both PTM motifs within E1B-55K abrogates key functions, most notably repression of p53-stimulated transcription and, consequently, complete transformation of primary rodent cells. Furthermore, E1B-55K itself is a substrate for SUMOylation and furthermore is involved in protein SUMOylation as an E3 SUMO1 ligase for p53 (73).

In HAdV-C5 infected cells, E1B-55K locates in the aggresome and sequesters other proteins in this compartment (113). As seen in Figure 14, RNF4 is also relocalized into E1B-55K containing perinuclear structures that presumably represent the aggresome or also called perinuclear body. The perinuclear body is known to harbor important proteins, among others Ubiquitin for protein degradation. In contrast to the model that proteasomes are distributed throughout the cyto- and nucleoplasm, current data show an accumulation of proteasomes upon catalytic activation in so called proteolysis centers. These are formed juxtaposed to the nucleus in discrete regions, also called aggresomes or perinuclear bodies (190). Since E1B-55K is involved in the degradation of proteins during HAdV-C5 infection, it can be

Discussion

assumed that E1B-55K recruits proteins, including RNF4, into the proteasome containing aggregates, where they are then degraded. Supportive to the relocalization of RNF4, it was also shown that the proteasome subunit 19S was located juxtaposed to E1B-55K in HAdV-C5 infected cells (Fig. 29).

Interaction studies performed in this work did not identify binding regions in RNF4 or E1B-55K required for their interaction (Fig. 19). Nevertheless, some areas in both proteins were excluded to be involved in binding. It was demonstrated here that the important SIM domains of RNF4 are not essential for binding to E1B-55K. It is known from other studies that RNF4 binds indirectly to polySUMOylated PML via its multiple SIMs (125, 137, 204) and that the RNF4-SIM/PML interaction is apart required for RNF4 mediated Ubiquitinylation of PML. Interestingly, the initial binding between RNF4 and polySUMOylated PML is also a SIM independent step (209). This observation supports the idea that RNF4 interacts with E1B-55K indirectly via possible other proteins. Besides the SIM domains in RNF4, the RING domain also plays a significant role for the E3 Ubiquitin ligase function of RNF4. It was shown that the RING domain alone is responsible for the activation of the protein, where two monomers are combined to form a dimer. Activation of RNF4 not only leads to the Ubiquitinylation of SUMOylated proteins, but further to auto-Ubiquitinylation of RNF4. Despite that, a direct interaction between RNF4 and E1B-55K via the RING domain or any other functional domain could not be confirmed. After all, the exact binding between RNF4 and other proteins is also not fully understood. It was published that loss of RNF4 is associated with a global increase of DNA methylation and consequently higher levels of DNA damage (210). Interestingly, in the presence of RNF4, distinct mismatch processing enzyme activity increases, which is important for the correction of G:T mismatches upon demethylation, serving as a DNA repair process (210). It is known that these enzymes have the ability to bind to RNF4. Again, the interaction neither depends on the RING domain, nor on the SIM motif. How RNF4 regulates these enzymes in the course of DNA repair remains to be determined.

Another difficulty in finding the exact binding site between E1B-55K and RNF4 can be the still unsolved structure of E1B-55K. E1B-55K appears to be non-globular, with an elongated structure and a lack of discrete structural domains (211). In contrast to this, the HAdV-C5 protein E1A has a limited structure and it is possible to map specific binding sites on E1A for partner proteins, such as Rb and p300 (212, 213). Up to now, only one proof has been provided to indicate the extent of the E1B-55K

protein structures. An intrinsic disorder in the common N-terminus of E1B-55K was published in 2011 (214). Observations that small deletions or insertions, scattered throughout the HAdV-C5 E1B-55K protein, already interfere with p53, Daxx and E4orf6 protein interactions suggest that binding sites are likely to consist of short sequences or single AS within the protein (52, 215). Although the exact binding between E1B-55K and RNF4 was not identified here, an E1B-55K dependent recruitment of RNF4 into proteasome containing aggregates could be observed. This finding further supports the idea of a role of RNF4 on the E1B-55K dependent Daxx degradation. It is known that HAdV-C5 infection leads to an altered integrity of the PML-NBs by which PML-NB associated proteins are relocalized into track-like structures (107). Since Daxx is a constitutive factor of the PML-NBs, it can be assumed that it is also relocalized into track-like structures in order to inhibit its antiviral functions. This is supported by the fact that colocalization of RNF4 and Daxx was observed in punctuate staining in uninfected cells whereas in HAdV-C5 infected cells both proteins are relocalized in track-like structures (Fig. 24). Thus, it is likely that RNF4 regulates the proteasomal degradation of Daxx through a complex formation with E1B-55K. In fact, this work supported this hypothesis by an E1B-55K dependent complex formation between RNF4 and Daxx (Fig. 25). To further address this question of RNF4 influence on Daxx degradation, a RNF4 depleted cell line was used and interestingly, a decreased degradation of Daxx in the RNF4 depleted cell line in HAdV-C5 infected cells was observed (Fig. 23). According to this, a decrease of Ubiquitinylated Daxx protein could be detected in the presence of E1B-55K and RNF4 in cells, where the proteasome was not inhibited. In MG-132 treated cells however, Ubiquitinylated Daxx was accumulated in the presence of RNF4 and E1B-55K. These results highly support the hypothesis of a Daxx degradation that is dependent on the STUbL RNF4. It is already known that Daxx gets SUMOylated in HAdV-C5 infected cells. Thus, Daxx SCS mutants (mutation sites personally discussed with R. Hay) were generated and tested for SUMOylation in HAdV-C5 infection (Data not shown). Unfortunately, these mutants only partially inhibited the SUMOylation of Daxx and where therefore not suitable for internal controls in the Ubiquitinylation assay. A further *in silico* screen for possible SCS in Daxx would be useful to clearly show that SUMOylated Daxx is degraded in dependency of the STUbL RNF4 in HAdV-C5 infected cells. Nevertheless, a direct proof of an E1B-55K and RNF4 dependent Daxx Ubiquitinylation was only observed under cell culture conditions, where it cannot be excluded that other cellular proteins are involved in this process. An *in vitro* Ubiquitinylation assay with purified proteins needs to be

Discussion

established to confirm the hypothesis of an RNF4 triggered E1B-55K dependent Daxx Ubiquitinylation during HAdV-C5 infection.

Analysis of the RNF4 depleted cell line additionally revealed an effect of RNF4 on other HAdV-C5 viral proteins. On the one hand, a general change in PML-NB formation was detected via immunofluorescence analysis (Fig. 21). It is known that E4orf3 is important for PML disruption in HAdV-C5 infected cells (107) Additionally, a recent study has shown that E4orf3 can act itself as a SUMO E3 ligase for cellular proteins and induces proteasomal degradation of the general transcription factor II-I (TFII-I) in virus infected cells (216, 217). Due to these observations, an interesting research focus could be set to the possible interaction of RNF4 with E4orf3 in the lytic HAdV-C5 infection. Therefore, an E4orf3 deletion mutant virus or an E1B-55K/E4orf3 mutant virus could be used to examine the protein amount of RNF4 and moreover the HAdV-C5 dependent relocalization of RNF4 juxtaposed to E1B-55K aggregates. Moreover, it would be of great interest to investigate the E4orf3 SUMO ligase functions on RNF4 SUMO dependent degradation of cellular factors in HAdV-C5 infection. On the other hand, an influence of replication center formation was observed in the RNF4 depleted cell line. It is known that the establishment of HAdV-C5 replication centers primarily depends on the expression of E2A/DBP (162, 218). Results from this work conclude that depletion of RNF4 induces a decreased viral progeny production and viral protein expression (Figs. 21 and 23) as well as delayed formation of replication centers. Due to these findings, a potential interaction between RNF4 and the viral E2A/DBP is conceivable. An interaction between RNF4 and E2A/DBP has indeed been confirmed in a preliminary experiment via IP analysis of HAdV-C5 infected cells (data not shown).

Finally, it is shown that HAdV-C5 might use the SUMO dependent Ubiquitinylation of RNF4 for degradation of proteins. In case of Daxx, this mechanism can be used to enhance the viral transcription and to achieve efficient viral progeny production. The current model proposed here indicates a crosstalk between RNF4 and E1B-55K, illustrating the E1B-55K dependent Daxx restriction in the early infection of HAdV-C5 (Fig. 36). Upon RNF4 recruitment into the nucleus, it is assumed that SUMOylated Daxx gets Ubiquitinylated and proteasomally degraded in HAdV-C5 infected cells. This, in turn, happens to counteract the repressive function of the Daxx/ATRX chromatin complex and to ensure efficient viral gene expression (Fig. 36).

Discussion
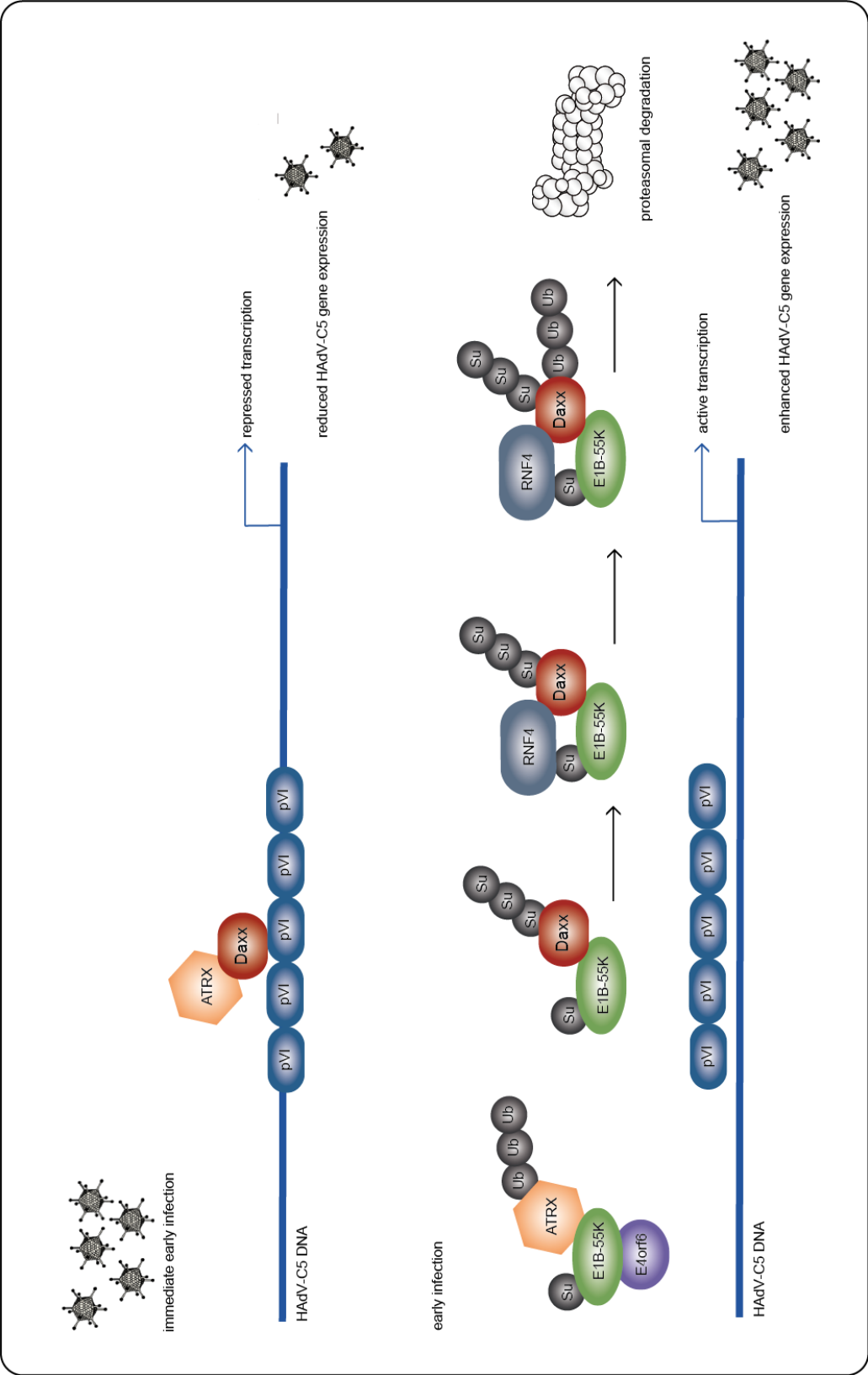
Fig. 36 Model of complex formation between RNF4, Daxx and E1B-55K

Schematic representation illustrating a proposed model linking the E1B-55K dependent Daxx restriction and modulation by cellular factor RNF4. In HAdV-C5 infected cells, RNF4 is recruited to the nucleus in an E1B-55K dependent manner and antiviral factor Daxx gets Ubiquitinylated and proteasomally degraded to counteract the cellular chromatin complex and therefore to ensure enhanced viral gene expression.

92

Discussion

In addition to RNF4, the cellular RING-finger protein 111, also called Arkadia, was identified as the second cellular STUbL binding SIM dependent to SUMOylated proteins (149). To date, no functions of Arkadia are known during viral infections. Nonetheless, a repressive function in the EBV reactivation pathway was observed for ARKL1 that possesses only the SIM domains of Arkadia and lacks the RING domain. Additionally, ARKL1 has been shown to be a restriction factor for influenza virus infection. Domingues and coworkers showed an increased influenza A virus titer upon ARKL1 depletion (219). ARKL1, as well as Arkadia, harbor a binding site for the CK2 KSSR binding motif. Interestingly, Epstein-Barr nuclear antigen 1 (EBNA1) is known to bind to the same binding motif, which is essential for EBV episome maintenance during latency (220).

Furthermore, the interaction between EBNA1 and CK2 increases the Phosphorylation of PML proteins, thereby inducing proteasomal degradation of PML upon EBV infection (221). The HAdV-C5 protein E1B-55K reveals similar functions to EBNA1 that plays a major role in transcriptional regulation and degradation of antiviral proteins upon EBV infection. Moreover, E1B-55K also interacts with CK2 (222), which leads to Phosphorylation and following SUMOylation of E1B-55K. The CK2 dependent Phosphorylation of E1B-55K provides the basis for many E1B-55K dependent functions in the HAdV-C5 life cycle (111).

Based on these findings, it was questioned whether Arkadia acts as an Ubiquitin ligase in the course of HAdV-C5 infection to trigger proteasomal degradation of HAdV-C5 dependent phosphorylated proteins. Therefore, the protein levels of Arkadia during HAdV-C5 infection were analyzed. An increased amount of protein could be observed, which decreased in the course of infection (Fig. 31).

These findings suggest a HAdV-C5 dependent activation of Arkadia, resulting in increased steady-state levels early in infection. To evaluate the decrease of Arkadia in late time points of infection, fractionation assays were performed. Notably, a reduction of Arkadia protein levels was also detected in the insoluble nuclear matrix fraction, which indicates a degradation of the protein (Fig. 32B). Similar to RNF4, a reduction of the protein could also be detected in the late phase of HAdV-C5 infection in whole cell lysates (Fig. 11). However in contrast, fractionation experiments showed that RNF4 has not been degraded upon infection but has been completely localized into the insoluble nuclear matrix fraction (Fig. 12).

Discussion

Interaction studies could identify E1B-55K as a new interaction partner for Arkadia and moreover, a weaker binding between Arkadia and a non-SUMOylated E1B-55K as well as a non-phosphorylated E1B-55K was observed (Fig. 34). Interestingly, an interaction between Arkadia and CK2 was only observed in HAdV-C5 infected cells (Fig. 35), pointing to an influence of Arkadia on the viral infection in a still unknown way. It is possible that the influence of Arkadia on the CK2 dependent Phosphorylation of E1B-55K is directly prevented via degradation of the protein in HAdV-C5 infected cells, which could explain the reduced amount of the Arkadia protein levels in HAdV-C5 infected cells.

6.2 Role of RNF4 during HAdV-C5 E1A/E1B mediated cell transformation

In addition to the STUbL function of RNF4, the protein is involved in the cellular DNA repair machinery by preventing chromosome loss and in the maintenance of genome stability. These activities play an important role in the induction of oncogenic processes (82, 130, 141, 223). Interestingly, RNF4 is down regulated during cellular transformation in vitro and in germ cell tumors and ectopically expressed RNF4 inhibits cell proliferation (197, 198). Data from Hakli *et al.* indicate that RNF4 and PML can cooperate in the regulation of transcription and cell growth (136).

Cell transformation by HAdV from species A, B and C is a multistep process, which is mediated by the viral oncoproteins E1A (E1A-12S and E1A-13S) and E1B (E1B-19K and E1B-55K) and two proteins from E4, E4orf6 and E4orf3 (59, 65, 193, 224, 225). The additive functions of E1B-55K and E1B-19K against E1A-induced anti-proliferative mechanisms in order to maintain a transformed phenotype and progression were intensively examined and are fairly well understood. Additionally, the interaction of E1B-55K with PML-NB associated proteins p53, Mre11 and Daxx is known to directly influence the E1A/E1B mediated cell transformation (52, 110, 113, 226). Previous studies have shown that the E1B-55K dependent degradation of Daxx indeed plays a decisive role in the E1A/E1B mediated transformation of pBRKs. Despite of the positive effect on lytic replication, it has been shown that E1B-55K mutants unable to degrade Daxx exhibit substantially reduced *focus*-forming activity (52).

The SUMO-E1B-55K dependent interaction of RNF4 and Daxx shown in this work suggests that RNF4 is used in HAdV-C5 infected cells to promote viral replication through the E1B-55K triggered Daxx degradation. In the context of viral

Discussion

transformation, the E1B-55K dependent inhibition of RNF4 functions in DNA repair provides another possible use from the interaction of both proteins. To investigate the role of RNF4 in the context of HAdV-C5 mediated cell transformation, *focus*-forming assays in pBRK were performed (Fig. 30). The results from these studies showed a decreased *focus*-formation activity by overexpression of both human and rat wild type RNF4 (Fig. 33). Interestingly, a further reduction of *foci* was observed by overexpression of the RNF4-SIM mutants, indicating that the RNF4 SIM domain may regulate the interaction of RNF4 and E1B-55K in primary rat cells. Apparently, this result is in contrast to the interaction of both proteins observed in productively infected human tumor cell lines. Here, the interaction seems to be SIM independent.

Since some data reveal a down regulation of RNF4 during cellular transformation and in germ cell tumors (198), it would be interesting to perform transformation assays again in RNF4 depleted pBRK. Further, it would be interesting to check RNF4 protein levels in different HAdV-C5 transformed rodent cells to investigate the role of E1B-55K on RNF4 in HAdV-C5 mediated cell transformation.

Another interesting function of RNF4 linked to transformation is the RNF4 dependent oncogene activation through protein Phosphorylation dependent atypical Ubiquitinylation (227). Thomas *et al.* highlighted that RNF4 is essential for epithelial cancer cell survival triggered by atypical Ubiquitinylation of oncogenes and high levels of RNF4 are correlated with a poor survival rate in patients. Based on this function, it would be very interesting to investigate whether Ubiquitinylation of known oncogenes occurs during the course of HAdV-C5 E1A/E1B mediated transformation. In first experiments, a PTM dependent effect of RNF4 on Ubiquitinylation of E1B-55K was already observed (Data not shown). This raised the question if SUMOylation or even Phosphorylation of E1B-55K might regulate Ubiquitinylation or vice versa. Ubiquitinylation assays with E1B-55K SUMO-, NES- or phosphor-mutants would be interesting to answer these questions. Encouraging this idea, it was shown that RNF4 impairs the cellular oncogene activation machinery by phosphor dependent Ubiquitinylation of oncogenes directly via the ARM-motif. RNF4 binds to phosphorylated β-catenin, c-Jun and c-myc, and enhances the activity as well as stability of these oncogenes, which seem to be essential for cancer cell survival at least in distinct subsets of human cancers (227, 228). To provide further insight into this issue, it would be interesting to investigate the role of the RNF4-ARM mutant in Ubiquitinylation assays as well as transformation assays in pBRKs. Overall, it is possible that RNF4 is directly involved in the stabilization of the HAdV-

Discussion

C5 oncogenes. Further investigation in this direction could help to analyze the exact mechanism of the E1A/E1B cell transformation in more detail.

In sum, the data from this work indicate that HAdV-C5 efficiently uses the cellular STUbL machinery to establish a productive viral infection. On the one hand, the best studied STUbL RNF4 seems to represent a positive factor for HAdV-C5 infection due to interaction with E1B-55K, supporting its functions in protein degradation. On the other hand, HAdV-C5 infection induces protein reduction of the second cellular STUbL Arkadia. In this work, it could be shown for the first time that the viral protein E1B-55K is a new interaction partner of RNF4 and Arkadia. Furthermore, this interaction triggers an important role of RNF4 in HAdV-C5 infection, as depletion of the protein shows a negative effect not only on the protein expression but also on viral progeny production. Nevertheless, more experiments are needed to understand the direct link between the productive infection and the cellular SUMO dependent Ubiquitin machinery.

Transformation based assays in this work investigated a negative effect of RNF4 on the HAdV-C5 E1A/E1B mediated *focus*-forming activity. These different findings of RNF4 on HAdV-C5 infection and transformation provide the basis to find out how exactly HAdV-C5 oncogenes could use the functions of cellular proteins. This could be either to support productive infection by protein-protein interaction, or to inhibit cellular proteins, to promote cell transformation.

However, the differences between the cellular STUbLs RNF4 and Arkadia and the involvement of other viral proteins are very interesting subjects for further investigations. Especially the possible interactions between the two STUbLs and E4orf3 and E2A/DBP might be helpful in understanding how exactly HAdVs use the cellular PTM machinery to ensure an efficient lytic infection and mediate cell transformation.

7 Literature

1. **Enders JF, Bell JA, Dingle JH, Francis T, Jr., Hilleman MR, Huebner RJ, Payne AM.** 1956. Adenoviruses: group name proposed for new respiratory-tract viruses. Science **124:**119-120.
2. **Berk AJ.** 2007. Adenoviridae: The Viruses and Their Replication.
3. **Benkö M, Harrach B.** 1998. A proposal for a new (third) genus within the family Adenoviridae. Arch. Virol. **143:**829-837.
4. **Davison AJ, Telford EA, Watson MS, McBride K, Mautner V.** 1993. The DNA sequence of adenovirus type 40. J. Mol. Biol. **234:**1308-1316.
5. **Davison AJ, Benko M, Harrach B.** 2003. Genetic content and evolution of adenoviruses. The Journal of general virology **84:**2895-2908.
6. **Bailey A, Mautner V.** 1994. Phylogenetic relationships among adenovirus serotypes. Virology **205:**438-452.
7. **Wadell G.** 1984. Molecular epidemiology of human adenoviruses. Curr Top Microbiol Immunol **110:**191-220.
8. **Jones MS, 2nd, Harrach B, Ganac RD, Gozum MM, Dela Cruz WP, Riedel B, Pan C, Delwart EL, Schnurr DP.** 2007. New adenovirus species found in a patient presenting with gastroenteritis. Journal of virology **81:**5978-5984.
9. **Lion T.** 2014. Adenovirus infections in immunocompetent and immunocompromised patients. Clinical microbiology reviews **27:**441-462.
10. **Shenk T.** 2001. Adenoviridae: the viruses and their replication, p. 2265-2300. *In* Knipe DM, Howley PM (ed.), Virology, Fourth ed, vol. 2. Lippincott-Raven, New York.
11. **Yabe Y, Trentin JJ, Taylor G.** 1962. Cancer induction in hamsters by human type 12 adenovirus. Effect of age and of virus dose. Proceedings of the Society for Experimental Biology and Medicine. Society for Experimental Biology and Medicine **111:**343-344.
12. **Jawetz E, Hanna L, Sonne M, Thygeson P.** 1959. A laboratory infection with adenovirus type 8; laboratory and epidemiologic observations. American journal of hygiene **69:**13-20.
13. **Mautner V, Steinthorsdottir V, Bailey A.** 1995. Enteric adenoviruses. Curr Top Microbiol Immunol **199 (Pt 3):**229-282.
14. **Yolken RH, Lawrence F, Leister F, Takiff HE, Strauss SE.** 1982. Gastroenteritis associated with enteric type adenovirus in hospitalized infants. The Journal of pediatrics **101:**21-26.
15. **Russel WC.** 2000. Update on adenovirus and its vectors. J. Gen. Virol. **81:**2573-2604.
16. **Carrigan DR.** 1997. Adenovirus infections in immunocompromised patients. The American journal of medicine **102:**71-74.
17. **Abe S, Miyamura K, Oba T, Terakura S, Kasai M, Kitaori K, Sasaki T, Kodera Y.** 2003. Oral ribavirin for severe adenovirus infection after allogeneic marrow transplantation. Bone marrow transplantation **32:**1107-1108.
18. **Lewis PF, Schmidt MA, Lu X, Erdman DD, Campbell M, Thomas A, Cieslak PR, Grenz LD, Tsaknardis L, Gleaves C, Kendall B, Gilbert D.** 2009. A community-based outbreak of severe respiratory illness caused by human adenovirus serotype 14. The Journal of infectious diseases **199:**1427-1434.
19. **Alharbi S, Van Caeseele P, Consunji-Araneta R, Zoubeidi T, Fanella S, Souid AK, Alsuwaidi AR.** 2012. Epidemiology of severe pediatric adenovirus lower

respiratory tract infections in Manitoba, Canada, 1991-2005. BMC infectious diseases **12:**55.

20. **Berciaud S, Rayne F, Kassab S, Jubert C, Faure-Della Corte M, Salin F, Wodrich H, Lafon ME, Typadeno Study M.** 2012. Adenovirus infections in Bordeaux University Hospital 2008-2010: clinical and virological features. Journal of clinical virology : the official publication of the Pan American Society for Clinical Virology **54:**302-307.

21. **Yang X, Wang Q, Liang B, Wu F, Li H, Liu H, Sheng C, Ma Q, Yang C, Xie J, Li P, Jia L, Wang L, Du X, Qiu S, Song H.** 2017. An outbreak of acute respiratory disease caused by a virus associated RNA II gene mutation strain of human adenovirus 7 in China, 2015. PloS one **12:**e0172519.

22. **Gavin PJ, Katz BZ.** 2002. Intravenous ribavirin treatment for severe adenovirus disease in immunocompromised children. Pediatrics **110:**e9.

23. **Ganapathi L, Arnold A, Jones S, Patterson A, Graham D, Harper M, Levy O.** 2016. Use of cidofovir in pediatric patients with adenovirus infection. F1000Research **5:**758.

24. **San Martin C, Burnett RM.** 2003. Structural studies on adenoviruses. Curr Top Microbiol Immunol **272:**57-94.

25. **Rux JJ, Burnett RM.** 2004. Adenovirus structure. Human gene therapy **15:**1167-1176.

26. **Russell WC.** 2009. Adenoviruses: update on structure and function. The Journal of general virology **90:**1-20.

27. **Vellinga J, Van der Heijdt S, Hoeben RC.** 2005. The adenovirus capsid: major progress in minor proteins. The Journal of general virology **86:**1581-1588.

28. **Russell WC, Matthews DA.** 2003. Nuclear perturbations following adenovirus infection. Curr Top Microbiol Immunol **272:**399-413.

29. **Gaggar A, Shayakhmetov DM, Lieber A.** 2003. CD46 is a cellular receptor for group B adenoviruses. Nature medicine **9:**1408-1412.

30. **Bergelson JM, Cunningham JA, Droguett G, Kurt-Jones EA, Krithivas A, Hong JS, Horwitz MS, Crowell RL, Finberg RW.** 1997. Isolation of a common receptor for coxsackie B viruses and adenoviruses 2 and 5. Science **275:**1320-1323.

31. **Wu E, Pache L, Von Seggern DJ, Mullen TM, Mikyas Y, Stewart PL, Nemerow GR.** 2003. Flexibility of the adenovirus fiber is required for efficient receptor interaction. Journal of virology **77:**7225-7235.

32. **Schreiner S, Martinez R, Groitl P, Rayne F, Vaillant R, Wimmer P, Bossis G, Sternsdorf T, Marcinowski L, Ruzsics Z, Dobner T, Wodrich H.** 2012. Transcriptional activation of the adenoviral genome is mediated by capsid protein VI. PLoS pathogens **8:**e1002549.

33. **Weinmann R, Raskas HJ, Roeder RG.** 1974. Role of DNA-dependent RNA polymerases II and III in transcription of the adenovirus genome late in productive infection. Proceedings of the National Academy of Sciences of the United States of America **71:**3426-3439.

34. **Flint SJ, Racaniello R, Enquist E, Rall GF, Skalka AM, Enquist LW, American Society for M.** 2015. Principles of Virology: Molecular Biology. ASM Press.

35. **Kosulin K, Haberler C, Hainfellner JA, Amann G, Lang S, Lion T.** 2007. Investigation of adenovirus occurrence in pediatric tumor entities. Journal of virology **81:**7629-7635.

36. **Nevins JR, Darnell JE.** 1978. Groups of adenovirus type 2 mRNA's derived from a large primary transcript: probable nuclear origin and possible common 3' ends. Journal of virology **25:**811-823.

37. **Beltz GA, Flint SJ.** 1979. Inhibition of HeLa cell protein synthesis during adenovirus infection. Restriction of cellular messenger RNA sequences to the nucleus. Journal of molecular biology **131:**353-373.

38. **Berk AJ.** 2005. Recent lessons in gene expression, cell cycle control, and cell biology from adenovirus. Oncogene **24:**7673-7685.

39. **Endter C, Hartl B, Spruss T, Hauber J, Dobner T.** 2005. Blockage of CRM1-dependent nuclear export of the adenovirus type 5 early region 1B 55-kDa protein augments oncogenic transformation of primary rat cells. Oncogene **24:**55-64.

40. **Kindsmüller K, Groitl P, Härtl B, Blanchette P, Hauber J, Dobner T.** 2007. Intranuclear targeting and nuclear export of the adenovirus E1B-55K protein are regulated by SUMO1 conjugation. Proc. Natl. Acad. Sci. USA **104:**6684-6689.

41. **Kratzer F, Rosorius O, Heger P, Hirschmann N, Dobner T, Hauber J, Stauber RH.** 2000. The adenovirus type 5 E1B-55K oncoprotein is a highly active shuttle protein and shuttling is independent of E4orf6, p53 and Mdm2. Oncogene **19:**850-857.

42. **Blanchette P, Cheng CY, Yan Q, Ketner G, Ornelles DA, Dobner T, Conaway RC, Conaway JW, Branton PE.** 2004. Both BC-box motifs of adenovirus protein E4orf6 are required to assemble an E3 ligase complex that degrades p53. Mol. Cell. Biol. **24:**9619-9629.

43. **Harada JN, Shevchenko A, Pallas DC, Berk AJ.** 2002. Analysis of the adenovirus E1B-55K-anchored proteome reveals its link to ubiquitination machinery. J. Virol. **76:**9194-9206.

44. **Querido E, Morisson MR, Chu-Pham-Dang H, Thirlwell SW, Boivin D, Branton PE.** 2001. Identification of three functions of the adenovirus E4orf6 protein that mediate p53 degradation by the E4orf6-E1B55K complex. J. Virol. **75:**699-709.

45. **Stracker TH, Carson CT, Weitzman MD.** 2002. Adenovirus oncoproteins inactivate the Mre11 Rad50 NBS1 DNA repair complex. Nature **418:**348-352.

46. **Schreiner S, Burck C, Glass M, Groitl P, Wimmer P, Kinkley S, Mund A, Everett RD, Dobner T.** 2013. Control of human adenovirus type 5 gene expression by cellular Daxx/ATRX chromatin-associated complexes. Nucleic acids research **41:**3532-3550.

47. **Schreiner S, Kinkley S, Burck C, Mund A, Wimmer P, Schubert T, Groitl P, Will H, Dobner T.** 2013. SPOC1-mediated antiviral host cell response is antagonized early in human adenovirus type 5 infection. PLoS pathogens **9:**e1003775.

48. **Baker A, Rohleder KJ, Hanakahi LA, Ketner G.** 2007. Adenovirus E4 34k and E1b 55k oncoproteins target host DNA ligase IV for proteasomal degradation. Journal of virology **81:**7034-7040.

49. **Gupta A, Jha S, Engel DA, Ornelles DA, Dutta A.** 2012. Tip60 degradation by adenovirus relieves transcriptional repression of viral transcriptional activator EIA. Oncogene.

50. **Orazio NI, Naeger CM, Karlseder J, Weitzman MD.** 2011. The adenovirus E1b55K/E4orf6 complex induces degradation of the Bloom helicase during infection. Journal of virology **85:**1887-1892.

51. **Schreiner S, Wimmer P, Sirma H, Everett RD, Blanchette P, Groitl P, Dobner T.** 2010. Proteasome-dependent degradation of Daxx by the viral E1B-55K protein in human adenovirus-infected cells. Journal of virology **84:**7029-7038.

52. **Schreiner S, Wimmer P, Groitl P, Chen SY, Blanchette P, Branton PE, Dobner T.** 2011. Adenovirus type 5 early region 1B 55K oncoprotein-dependent degradation of cellular factor Daxx is required for efficient transformation of primary rodent cells. Journal of virology **85:**8752-8765.

53. **Hollenbach AD, McPherson CJ, Mientjes EJ, Iyengar R, Grosveld G.** 2002. Daxx and histone deacetylase II associate with chromatin through an interaction with core histones and the chromatin-associated protein Dek. Journal of cell science **115:**3319-3330.

54. **Muromoto R, Sugiyama K, Yamamoto T, Oritani K, Shimoda K, Matsuda T.** 2004. Physical and functional interactions between Daxx and TSG101. Biochemical and biophysical research communications **316:**827-833.

55. **Mackey JK, Rigden PM, Green M.** 1976. Do highly oncogenic group A human adenoviruses cause human cancer? Analysis of human tumors for adenovirus 12 transforming DNA sequences. Proceedings of the National Academy of Sciences of the United States of America **73:**4657-4661.

56. **Mackey JK, Green M, Wold WS, Rigden P.** 1979. Analysis of human cancer DNA for DNA sequences of human adenovirus type 4. Journal of the National Cancer Institute **62:**23-26.

57. **Chauvin C, Suh M, Remy C, Benabid AL.** 1990. Failure to detect viral genomic sequences of three viruses (herpes simplex, simian virus 40 and adenovirus) in human and rat brain tumors. Italian journal of neurological sciences **11:**347-357.

58. **Hahn WC, Counter CM, Lundberg AS, Beijersbergen RL, Brooks MW, Weinberg RA.** 1999. Creation of human tumour cells with defined genetic elements. Nature **400:**464-468.

59. **Graham FL, Rowe DT, McKinnon R, Bacchetti S, Ruben M, Branton PE.** 1984. Transformation by human adenoviruses. Journal of cellular physiology. Supplement **3:**151-163.

60. **Speiseder T, Hofmann-Sieber H, Rodriguez E, Schellenberg A, Akyuz N, Dierlamm J, Spruss T, Lange C, Dobner T.** 2017. Efficient Transformation of Primary Human Mesenchymal Stromal Cells by Adenovirus Early Region 1 Oncogenes. Journal of virology **91**.

61. **Endter C, Dobner T.** 2004. Cell transformation by human adenoviruses. Curr Top Microbiol Immunol **273:**163-214.

62. **Graham FL, Smiley J, Russel WC, Nairn R.** 1977. Characteristics of a human cell line transformed by DNA from human adenovirus type 5. J. Gen. Virol. **36:**59-72.

63. **Fallaux FJ, Kranenburg O, Cramer SJ, Houweling A, Van Ormondt H, Hoeben RC, Van Der Eb AJ.** 1996. Characterization of 911: a new helper cell line for the titration and propagation of early region 1-deleted adenoviral vectors. Human gene therapy **7:**215-222.

64. **Tauber B, Dobner T.** 2001. Molecular regulation and biological function of adenovirus early genes: the E4 ORFs. Gene **278:**1-23.

65. **Täuber B, Dobner T.** 2001. Adenovirus early E4 genes in viral oncogenesis. Oncogene **20:**7847-7854.

66. **Jung MS, Jin DH, Chae HD, Kang S, Kim SC, Bang YJ, Choi TS, Choi KS, Shin DY.** 2004. Bcl-xL and E1B-19K proteins inhibit p53-induced irreversible growth arrest and senescence by preventing reactive oxygen species-dependent p38 activation. The Journal of biological chemistry **279:**17765-17771.

67. **Han J, Sabbatini P, Perez D, Rao L, Modha D, White E.** 1996. The E1B 19K protein blocks apoptosis by interacting with and inhibiting the p53-inducible and death-promoting Bax protein. Genes & development **10:**461-477.

68. **White E.** 1996. Life, death, and the pursuit of apoptosis. Genes & development **10:**1-15.

69. **Blanchette P, Cheng CY, Yan Q, Ketner G, Ornelles DA, Dobner T, Conaway RC, Conaway JW, Branton PE.** 2004. Both BC-box motifs of adenovirus protein E4orf6 are required to efficiently assemble an E3 ligase complex that degrades p53. Molecular and cellular biology **24:**9619-9629.

70. **Kao CC, Yew PR, Berk AJ.** 1990. Domains required for in vitro association between the cellular p53 and the adenovirus 2 E1B 55K proteins. Virology **179:**806-814.

71. **Yew PR, Berk AJ.** 1992. Inhibition of p53 transactivation required for transformation by adenovirus early 1B protein. Nature **357:**82-85.

72. **Muller S, Dobner T.** 2008. The adenovirus E1B-55K oncoprotein induces SUMO modification of p53. Cell cycle **7:**754-758.

73. **Pennella MA, Liu Y, Woo JL, Kim CA, Berk AJ.** 2010. Adenovirus E1B 55-kilodalton protein is a p53-SUMO1 E3 ligase that represses p53 and stimulates its nuclear export through interactions with promyelocytic leukemia nuclear bodies. Journal of virology **84:**12210-12225.

74. **Liu Y, Colosimo AL, Yang XJ, Liao D.** 2000. Adenovirus E1B 55-kilodalton oncoprotein inhibits p53 acetylation by PCAF. Molecular and cellular biology **20:**5540-5553.

75. **Ciechanover A.** 1998. The ubiquitin-proteasome pathway: on protein death and cell life. EMBO J **17:**7151-7160.

76. **Haglund K, Dikic I.** 2005. Ubiquitylation and cell signaling. EMBO J **24:**3353-3359.

77. **Andreou AM, Tavernarakis N.** 2009. SUMOylation and cell signalling. Biotechnology journal **4:**1740-1752.

78. **Johnson ES.** 2004. Protein modification by SUMO. Annual review of biochemistry **73:**355-382.

79. **Miteva M, Keusekotten K, Hofmann K, Praefcke GJ, Dohmen RJ.** 2010. Sumoylation as a signal for polyubiquitylation and proteasomal degradation. Sub-cellular biochemistry **54:**195-214.

80. **Weisshaar SR, Keusekotten K, Krause A, Horst C, Springer HM, Gottsche K, Dohmen RJ, Praefcke GJ.** 2008. Arsenic trioxide stimulates SUMO-2/3 modification leading to RNF4-dependent proteolytic targeting of PML. FEBS letters **582:**3174-3178.

81. **Uzunova K, Gottsche K, Miteva M, Weisshaar SR, Glanemann C, Schnellhardt M, Niessen M, Scheel H, Hofmann K, Johnson ES, Praefcke GJ, Dohmen RJ.** 2007. Ubiquitin-dependent proteolytic control of SUMO conjugates. The Journal of biological chemistry **282:**34167-34175.

82. **Prudden JP, Stephanie. Raffa, Grazia. Slavin, Daniela A. Perry, J Jefferson P. Trainer, John A. McGowan, Clare H. Boddy, Michael N.** 2007. SUMO-targeted ubiquitin ligases n genome stability. EMBO **26:**4089-4101.

83. **Tatham MH, Matic I, Mann M, Hay RT.** 2011. Comparative proteomic analysis identifies a role for SUMO in protein quality control. Science signaling **4:**rs4.

84. **Schulman BA, Harper JW.** 2009. Ubiquitin-like protein activation by E1 enzymes: the apex for downstream signalling pathways. Nat Rev Mol Cell Biol **10:**319-331.

85. **Wang J, Taherbhoy AM, Hunt HW, Seyedin SN, Miller DW, Miller DJ, Huang DT, Schulman BA.** 2010. Crystal structure of UBA2(ufd)-Ubc9: insights into E1-E2 interactions in Sumo pathways. PloS one **5:**e15805.

86. **Garza R, Pillus L.** 2013. STUbLs in chromatin and genome stability. Biopolymers **99:**146-154.
87. **Rodriguez MS, Dargemont C, Hay RT.** 2001. SUMO-1 conjugation in vivo requires both a consensus modification motif and nuclear targeting. The Journal of biological chemistry **276:**12654-12659.
88. **Hendriks IA, Vertegaal AC.** 2016. A comprehensive compilation of SUMO proteomics. Nat Rev Mol Cell Biol **17:**581-595.
89. **Saitoh H, Hinchey J.** 2000. Functional heterogeneity of small ubiquitin-related protein modifiers SUMO-1 versus SUMO-2/3. The Journal of biological chemistry **275:**6252-6258.
90. **Bayer P, Arndt A, Metzger S, Mahajan R, Melchior F, Jaenicke R, Becker J.** 1998. Structure determination of the small ubiquitin-related modifier SUMO-1. Journal of molecular biology **280:**275-286.
91. **Li SJ, Hochstrasser M.** 1999. A new protease required for cell-cycle progression in yeast. Nature **398:**246-251.
92. **Chau V, Tobias JW, Bachmair A, Marriott D, Ecker DJ, Gonda DK, Varshavsky A.** 1989. A multiubiquitin chain is confined to specific lysine in a targeted short-lived protein. Science **243:**1576-1583.
93. **Tatham MH, Jaffray E, Vaughan OA, Desterro JM, Botting CH, Naismith JH, Hay RT.** 2001. Polymeric chains of SUMO-2 and SUMO-3 are conjugated to protein substrates by SAE1/SAE2 and Ubc9. The Journal of biological chemistry **276:**35368-35374.
94. **Berman HM, Westbrook J, Feng Z, Gilliland G, Bhat TN, Weissig H, Shindyalov IN, Bourne PE.** 2000. The Protein Data Bank. Nucleic acids research **28:**235-242.
95. **Negorev D, Maul GG.** 2001. Cellular proteins localized at and interacting within ND10/PML nuclear bodies/PODs suggest functions of a nuclear depot. Oncogene **20:**7234-7242.
96. **Doucas V, Evans RM.** 1996. The PML nuclear compartment and cancer. Biochimica et biophysica acta **1288:**M25-29.
97. **Ferbeyre G, de Stanchina E, Querido E, Baptiste N, Prives C, Lowe SW.** 2000. PML is induced by oncogenic ras and promotes premature senescence. Genes & development **14:**2015-2027.
98. **LaMorte VJ, Dyck JA, Ochs RL, Evans RM.** 1998. Localization of nascent RNA and CREB binding protein with the PML-containing nuclear body. Proceedings of the National Academy of Sciences of the United States of America **95:**4991-4996.
99. **Torok D, Ching RW, Bazett-Jones DP.** 2009. PML nuclear bodies as sites of epigenetic regulation. Front Biosci **14:**1325-1336.
100. **Maul GG, Negorev D, Bell P, Ishov AM.** 2000. Review: Properties and assembly mechanisms of ND10, PML bodies, or PODs. J. Struct. Biol. **129:**278-287.
101. **Dellaire G, Bazett-Jones DP.** 2004. PML nuclear bodies: dynamic sensors of DNA damage and cellular stress. Bioessays **26:**963-977.
102. **Zhong S, Salomoni P, Pandolfi PP.** 2000. The transcriptional role of PML and the nuclear body. Nature cell biology **2:**E85-90.
103. **Zhong S, Muller S, Ronchetti S, Freemont PS, Dejean A, Pandolfi PP.** 2000. Role of SUMO-1-modified PML in nuclear body formation. Blood **95:**2748-2752.
104. **Ishov AM, Sotnikov AG, Negorev D, Vladimirova OV, Neff N, Kamitani T, Yeh ET, Strauss JF, 3rd, Maul GG.** 1999. PML is critical for ND10 formation and recruits the PML-interacting protein daxx to this nuclear structure when modified by SUMO-1. The Journal of cell biology **147:**221-234.

105. **Wimmer P, Schreiner S, Everett RD, Sirma H, Groitl P, Dobner T.** 2010. SUMO modification of E1B-55K oncoprotein regulates isoform-specific binding to the tumour suppressor protein PML. Oncogene **29:**5511-5522.

106. **Berscheminski J, Brun J, Speiseder T, Wimmer P, Ip WH, Terzic M, Dobner T, Schreiner S.** 2016. Sp100A is a tumor suppressor that activates p53-dependent transcription and counteracts E1A/E1B-55K-mediated transformation. Oncogene **35:**3178-3189.

107. **Carvalho T, Seeler JS, Ohman K, Jordan P, Pettersson U, Akusjarvi G, Carmo-Fonseca M, Dejean A.** 1995. Targeting of adenovirus E1A and E4-ORF3 proteins to nuclear matrix-associated PML bodies. The Journal of cell biology **131:**45-56.

108. **Doucas V, Ishov AM, Romo A, Juguilon H, Weitzman MD, Evans RM, Maul GG.** 1996. Adenovirus replication is coupled with the dynamic properties of the PML nuclear structure. Genes & development **10:**196-207.

109. **Li H, Leo C, Zhu J, Wu X, O'Neil J, Park EJ, Chen JD.** 2000. Sequestration and inhibition of Daxx-mediated transcriptional repression by PML. Molecular and cellular biology **20:**1784-1796.

110. **Endter C, Kzhyshkowska J, Stauber R, Dobner T.** 2001. SUMO-1 modification is required for transformation by adenovirus type 5 early region 1B 55-kDa oncoprotein. Proc. Natl. Acad. Sci. USA **98:**11312-11317.

111. **Wimmer P, Blanchette P, Schreiner S, Ching W, Groitl P, Berscheminski J, Branton PE, Will H, Dobner T.** 2013. Cross-talk between phosphorylation and SUMOylation regulates transforming activities of an adenoviral oncoprotein. Oncogene **32:**1626-1637.

112. **Wimmer P, Berscheminski J, Blanchette P, Groitl P, Branton PE, Hay RT, Dobner T, Schreiner S.** 2015. PML isoforms IV and V contribute to adenovirus-mediated oncogenic transformation by functionally inhibiting the tumor-suppressor p53. Oncogene.

113. **Hartl B, Zeller T, Blanchette P, Kremmer E, Dobner T.** 2008. Adenovirus type 5 early region 1B 55-kDa oncoprotein can promote cell transformation by a mechanism independent from blocking p53-activated transcription. Oncogene **27:**3673-3684.

114. **Liew CW, Sun H, Hunter T, Day CL.** 2010. RING domain dimerization is essential for RNF4 function. The Biochemical journal **431:**23-29.

115. **Borden KL, Freemont PS.** 1996. The RING finger domain: a recent example of a sequence-structure family. Current opinion in structural biology **6:**395-401.

116. **Deshaies RJ, Joazeiro CA.** 2009. RING domain E3 ubiquitin ligases. Annual review of biochemistry **78:**399-434.

117. **Ching W, Dobner T, Koyuncu E.** 2012. The human adenovirus type 5 E1B 55-kilodalton protein is phosphorylated by protein kinase CK2. Journal of virology **86:**2400-2415.

118. **Schreiner S, Wimmer P, Groitl P, Chen SY, Blanchette P, Branton PE, Dobner T.** 2011. Adenovirus type 5 early region 1B 55K oncoprotein-dependent degradation of cellular factor Daxx is required for efficient transformation of primary rodent cells. Journal of virology **85:**8752-8765.

119. **Schreiner S, Wimmer P, Sirma H, Everett RD, Blanchette P, Groitl P, Dobner T.** 2010. Proteasome-dependent degradation of Daxx by the viral E1B-55K protein in human adenovirus-infected cells. Journal of virology **84:**7029-7038.

120. **Kawai T, Akira S, Reed JC.** 2003. ZIP kinase triggers apoptosis from nuclear PML oncogenic domains. Molecular and cellular biology **23:**6174-6186.

121. **Sudharsan R, Azuma Y.** 2012. The SUMO ligase PIAS1 regulates UV-induced apoptosis by recruiting Daxx to SUMOylated foci. Journal of cell science **125:**5819-5829.

122. **Sun HL, Joel D. Hunter, Tony.** 2007. Conserved function of RNF4 family proteins in eukaryotes: targeting a ubiquitin ligase to SUMOylated proteins. EMBO **26:**4102-4112.

123. **Erker Y, Neyret-Kahn H, Seeler JS, Dejean A, Atfi A, Levy L.** 2013. Arkadia, a Novel SUMO-Targeted Ubiquitin Ligase Involved in PML Degradation. Molecular and cellular biology **33:**2163-2177.

124. **Xu Y, Plechanovova A, Simpson P, Marchant J, Leidecker O, Kraatz S, Hay RT, Matthews SJ.** 2014. Structural insight into SUMO chain recognition and manipulation by the ubiquitin ligase RNF4. Nature communications **5:**4217.

125. **Tatham MH, Geoffroy MC, Shen L, Plechanovova A, Hattersley N, Jaffray EG, Palvimo JJ, Hay RT.** 2008. RNF4 is a poly-SUMO-specific E3 ubiquitin ligase required for arsenic-induced PML degradation. Nature cell biology **10:**538-546.

126. **Staudinger JL.** 2017. The Molecular Interface Between the SUMO and Ubiquitin Systems. Advances in experimental medicine and biology **963:**99-110.

127. **Moilanen A-MP, Hetti. Karvonen, Ulla. Häkli, Marika. Jänne, Olli A. Palvimo, Jorma J.** 1998. Identification of a Novel RING Finger Protein as a Coregulator in Steroid Receptor-Mediated Gene Transcription. Molecular and cellular biology **18:**5128-5139.

128. **Häkli M, Lorick KL, Weissman AM, Jänne OA, Palvimo JJ.** 2004. Transcriptional coregulator SNURF (RNF4) possesses ubiquitin E3 ligase activity. FEBS Letters **560:**56-62.

129. **Chiariotti LB, Giovanna. Fedel, Monica. Santoro, Massimo. Simeone, Antonio. Fusco, Alfredo. Bruni, Carmelo B.** 1998. Identification and Characterization of a Novel RING-Finger Gene (RNF4) Mapping at 4p16.3. Genomics **47:**258-265.

130. **Galanty YB, Rimma. Coates, Julia. Jackson, Stephen P.** 2012. RNF4, a SUMO-targeted ubiquitin E3 ligase, promotes DNA double-strand break repair. Genes & development **26:**1179-1195.

131. **Liew CW, Sun H, Hunter T, Day CL.** 2010. RING domain dimerization is essential for RNF4 function. The Biochemical journal **431:**23-29.

132. **Plechanovova A, Jaffray EG, McMahon SA, Johnson KA, Navratilova I, Naismith JH, Hay RT.** 2011. Mechanism of ubiquitylation by dimeric RING ligase RNF4. Nature structural & molecular biology **18:**1052-1059.

133. **Plechanovova A, Jaffray EG, Tatham MH, Naismith JH, Hay RT.** 2012. Structure of a RING E3 ligase and ubiquitin-loaded E2 primed for catalysis. Nature **489:**115-120.

134. **Kuo CY, Li X, Kong XQ, Luo C, Chang CC, Chung Y, Shih HM, Li KK, Ann DK.** 2014. An arginine-rich motif of ring finger protein 4 (RNF4) oversees the recruitment and degradation of the phosphorylated and SUMOylated Kruppel-associated box domain-associated protein 1 (KAP1)/TRIM28 protein during genotoxic stress. The Journal of biological chemistry **289:**20757-20772.

135. **Lallemand-Breitenbach V, Jeanne M, Benhenda S, Nasr R, Lei M, Peres L, Zhou J, Zhu J, Raught B, de The H.** 2008. Arsenic degrades PML or PML-RARalpha through a SUMO-triggered RNF4/ubiquitin-mediated pathway. Nature cell biology **10:**547-555.

136. **Hakli M, Karvonen U, Janne OA, Palvimo JJ.** 2005. SUMO-1 promotes association of SNURF (RNF4) with PML nuclear bodies. Experimental cell research **304:**224-233.

137. **Percherancier Y, Germain-Desprez D, Galisson F, Mascle XH, Dianoux L, Estephan P, Chelbi-Alix MK, Aubry M.** 2009. Role of SUMO in RNF4-mediated promyelocytic leukemia protein (PML) degradation: sumoylation of PML and phospho-switch control of its SUMO binding domain dissected in living cells. The Journal of biological chemistry **284:**16595-16608.

138. **Maroui MA, Kheddache-Atmane S, El Asmi F, Dianoux L, Aubry M, Chelbi-Alix MK.** 2012. Requirement of PML SUMO interacting motif for RNF4- or arsenic trioxide-induced degradation of nuclear PML isoforms. PloS one **7:**e44949.

139. **Bruderer R, Tatham MH, Plechanovova A, Matic I, Garg AK, Hay RT.** 2011. Purification and identification of endogenous polySUMO conjugates. EMBO reports **12:**142-148.

140. **Williams RS, Dodson GE, Limbo O, Yamada Y, Williams JS, Guenther G, Classen S, Glover JN, Iwasaki H, Russell P, Tainer JA.** 2009. Nbs1 flexibly tethers Ctp1 and Mre11-Rad50 to coordinate DNA double-strand break processing and repair. Cell **139:**87-99.

141. **Yin Y, Seifert A, Chua JS, Maure JF, Golebiowski F, Hay RT.** 2012. SUMO-targeted ubiquitin E3 ligase RNF4 is required for the response of human cells to DNA damage. Genes & development **26:**1196-1208.

142. **Vyas R, Kumar R, Clermont F, Helfricht A, Kalev P, Sotiropoulou P, Hendriks IA, Radaelli E, Hochepied T, Blanpain C, Sablina A, van Attikum H, Olsen JV, Jochemsen AG, Vertegaal AC, Marine JC.** 2013. RNF4 is required for DNA double-strand break repair in vivo. Cell death and differentiation **20:**490-502.

143. **Kuo CY, Li X, Stark JM, Shih HM, Ann DK.** 2016. RNF4 regulates DNA double-strand break repair in a cell cycle-dependent manner. Cell cycle **15:**787-798.

144. **Lamsoul I, Lodewick J, Lebrun S, Brasseur R, Burny A, Gaynor RB, Bex F.** 2005. Exclusive ubiquitination and sumoylation on overlapping lysine residues mediate NF-kappaB activation by the human T-cell leukemia virus tax oncoprotein. Molecular and cellular biology **25:**10391-10406.

145. **Fryrear KAG, Xin. Kerscher, Oliver. Semmes, O. John.** 2012. The Sumo-targeted ubiquitin ligase RNF4 regulates the localization and function of the HTLV-1 oncoprotein Tax. Blood **119:**1173-1181.

146. **Dassouki Z, Sahin U, El Hajj H, Jollivet F, Kfoury Y, Lallemand-Breitenbach V, Hermine O, de The H, Bazarbachi A.** 2015. ATL response to arsenic/interferon therapy is triggered by SUMO/PML/RNF4-dependent Tax degradation. Blood **125:**474-482.

147. **Yang YC, Yoshikai Y, Hsu SW, Saitoh H, Chang LK.** 2013. Role of RNF4 in the Ubiquitination of Rta of Epstein-Barr Virus. The Journal of biological chemistry **288:**12866-12879.

148. **Li J, Callegari S, Masucci MG.** 2017. The Epstein-Barr virus miR-BHRF1-1 targets RNF4 during productive infection to promote the accumulation of SUMO conjugates and the release of infectious virus. PLoS pathogens **13:**e1006338.

149. **Sun H, Hunter T.** 2012. Poly-small ubiquitin-like modifier (PolySUMO)-binding proteins identified through a string search. The Journal of biological chemistry **287:**42071-42083.

150. **Inoue Y, Imamura T.** 2008. Regulation of TGF-beta family signaling by E3 ubiquitin ligases. Cancer science **99:**2107-2112.

151. **Poulsen SL, Hansen RK, Wagner SA, van Cuijk L, van Belle GJ, Streicher W, Wikstrom M, Choudhary C, Houtsmuller AB, Marteijn JA, Bekker-Jensen S, Mailand N.** 2013. RNF111/Arkadia is a SUMO-targeted ubiquitin ligase that facilitates the DNA damage response. The Journal of cell biology **201:**797-807.

152. **Hanahan D, Meselson M.** 1983. Plasmid screening at high colony density. Methods Enzymol **100:**333-342.

153. **Mitsudomi T, Steinberg SM, Nau MM, Carbone D, D'Amico D, Bodner HK, Oie HK, Linnoila RI, Mulshine JL, Minna JD, Gazdar AF.** 1992. p53 gene mutations in non-small-lung cell cancer cell lines and their correlation with the presence of ras mutations and clinical features. Oncogene **7:**171-180.

154. **Gey GO, Coffman, WD, and Kubicek, MT.** 1952. TissueCulture Studies of the Proliferative Capacity of Cervical Carcinoma and Normal Epithelium. Cancer Research **12**.

155. **Tatham MH, Rodriguez MS, Xirodimas DP, Hay RT.** 2009. Detection of protein SUMOylation in vivo. Nature protocols **4:**1363-1371.

156. **Kindsmuller K, Groitl P, Hartl B, Blanchette P, Hauber J, Dobner T.** 2007. Intranuclear targeting and nuclear export of the adenovirus E1B-55K protein are regulated by SUMO1 conjugation. Proceedings of the National Academy of Sciences of the United States of America **104:**6684-6689.

157. **Blanchette P, Cheng CY, Yan Q, Ketner G, Ornelles DA, Dobner T, Conaway RC, Conaway JW, Branton PE.** 2004. Both BC-box motifs of adenovirus protein E4orf6 are required to efficiently assemble an E3 ligase complex that degrades p53. Molecular and cellular biology **24:**9619-9629.

158. **Beyer WR, Westphal M, Ostertag W, von Laer D.** 2002. Oncoretrovirus and lentivirus vectors pseudotyped with lymphocytic choriomeningitis virus glycoprotein: generation, concentration, and broad host range. Journal of virology **76:**1488-1495.

159. **Dull T, Zufferey R, Kelly M, Mandel RJ, Nguyen M, Trono D, Naldini L.** 1998. A third-generation lentivirus vector with a conditional packaging system. Journal of virology **72:**8463-8471.

160. **Harlow E, Franza BR, Jr., Schley C.** 1985. Monoclonal antibodies specific for adenovirus early region 1A proteins: extensive heterogeneity in early region 1A products. J. Virol. **55:**533-546.

161. **Sarnow P, Hearing P, Anderson CW, Reich N, Levine AJ.** 1982. Identification and characterization of an immunologically conserved adenovirus early region 11,000 Mr protein and its association with the nuclear matrix. J. Mol. Biol. **162:**565-583.

162. **Reich NC, Sarnow P, Duprey E, Levine AJ.** 1983. Monoclonal antibodies which recognize native and denatured forms of the adenovirus DNA-binding protein. Virology **128:**480-484.

163. **Marton MJ, Baim SB, Ornelles DA, Shenk T.** 1990. The adenovirus E4 17-kilodalton protein complexes with the cellular transcription factor E2F, altering its DNA-binding properties and stimulating E1A-independent accumulation of E2 mRNA. J. Virol. **64:**2345-2359.

164. **Kzhyshkowska J, Kremmer E, Hofmann M, Wolf H, Dobner T.** 2004. Protein arginine methylation during lytic adenovirus infection. The Biochemical journal **383:**259-265.

165. **Vojtesek B, Bartek J, Midgley CA, Lane DP.** 1992. An immunochemical analysis of the human nuclear phosphoprotein p53. New monoclonal antibodies and epitope mapping using recombinant p53. J. Immunol. Methods **151:**237-244.

166. **Wodrich H, Henaff D, Jammart B, Segura-Morales C, Seelmeir S, Coux O, Ruzsics Z, Wiethoff CM, Kremer EJ.** 2010. A capsid-encoded PPxY-motif facilitates adenovirus entry. PLoS pathogens **6:**e1000808.

167. **Schindelin J, Arganda-Carreras I, Frise E, Kaynig V, Longair M, Pietzsch T, Preibisch S, Rueden C, Saalfeld S, Schmid B, Tinevez JY, White DJ, Hartenstein V, Eliceiri K, Tomancak P, Cardona A.** 2012. Fiji: an open-source platform for biological-image analysis. Nature methods **9:**676-682.
168. http://www.lentigo-vectors.de/docs/Production.pdf, posting date. [Online.]
169. **Saiki RK, Gelfand DH, Stoffel S, Scharf SJ, Higuchi R, Horn GT, Mullis KB, Erlich HA.** 1988. Primer-directed enzymatic amplification of DNA with a thermostable DNA polymerase. Science **239:**487-491.
170. **Bradford LW.** 1976. Problems of ethics and behavior in the forensic sciences. Journal of forensic sciences **21:**763-768.
171. **Laemmli UK.** 1970. Cleavage of structural proteins during the assembly of the head of bacteriophage T4. Nature **227:**680-685.
172. **Hodge LD, Mancini P, Davis FM, Heywood P.** 1977. Nuclear matrix of HeLa S3 cells. Polypeptide composition during adenovirus infection and in phases of the cell cycle. The Journal of cell biology **72:**194-208.
173. **Long BH, Huang CY, Pogo AO.** 1979. Isolation and characterization of the nuclear matrix in Friend erythroleukemia cells: chromatin and hnRNA interactions with the nuclear matrix. Cell **18:**1079-1090.
174. **van Eekelen CA, van Venrooij WJ.** 1981. hnRNA and its attachment to a nuclear protein matrix. The Journal of cell biology **88:**554-563.
175. **Erker Y, Neyret-Kahn H, Seeler JS, Dejean A, Atfi A, Levy L.** 2013. Arkadia, a novel SUMO-targeted ubiquitin ligase involved in PML degradation. Molecular and cellular biology **33:**2163-2177.
176. **Xue Y, Gibbons R, Yan Z, Yang D, McDowell TL, Sechi S, Qin J, Zhou S, Higgs D, Wang W.** 2003. The ATRX syndrome protein forms a chromatin-remodeling complex with Daxx and localizes in promyelocytic leukemia nuclear bodies. Proceedings of the National Academy of Sciences of the United States of America **100:**10635-10640.
177. **Berscheminski J, Wimmer P, Brun J, Ip WH, Groitl P, Horlacher T, Jaffray E, Hay RT, Dobner T, Schreiner S.** 2014. Sp100 isoform-specific regulation of human adenovirus 5 gene expression. Journal of virology **88:**6076-6092.
178. **Hakli M, Karvonen U, Janne OA, Palvimo JJ.** 2005. SUMO-1 promotes association of SNURF (RNF4) with PML nuclear bodies. Experimental cell research **304:**224-233.
179. **Percherancier Y, Germain-Desprez D, Galisson F, Mascle XH, Dianoux L, Estephan P, Chelbi-Alix MK, Aubry M.** 2009. Role of SUMO in RNF4-mediated promyelocytic leukemia protein (PML) degradation: sumoylation of PML and phospho-switch control of its SUMO binding domain dissected in living cells. The Journal of biological chemistry **284:**16595-16608.
180. **Rojas-Fernandez A, Plechanovova A, Hattersley N, Jaffray E, Tatham MH, Hay RT.** 2014. SUMO chain-induced dimerization activates RNF4. Molecular cell **53:**880-892.
181. **Keusekotten K, Bade VN, Meyer-Teschendorf K, Sriramachandran AM, Fischer-Schrader K, Krause A, Horst C, Schwarz G, Hofmann K, Dohmen RJ, Praefcke GJ.** 2014. Multivalent interactions of the SUMO-interaction motifs in RING finger protein 4 determine the specificity for chains of the SUMO. The Biochemical journal **457:**207-214.
182. **Tatham MH, Geoffroy MC, Shen L, Plechanovova A, Hattersley N, Jaffray EG, Palvimo JJ, Hay RT.** 2008. RNF4 is a poly-SUMO-specific E3 ubiquitin ligase required for arsenic-induced PML degradation. Nature cell biology **10:**538-546.

183. **Goodrum FD, Ornelles DA.** 1998. p53 status does not determine outcome of E1B 55-Kilodalton mutant adenovirus lytic infection. J. Virol. **72:**9479-9490.
184. **Weitzman MD, Fisher KJ, Wilson JM.** 1996. Recruitment of wild-type and recombinant adeno-associated virus into adenovirus replication centers. Journal of virology **70:**1845-1854.
185. **Sahin U, Ferhi O, Jeanne M, Benhenda S, Berthier C, Jollivet F, Niwa-Kawakita M, Faklaris O, Setterblad N, de The H, Lallemand-Breitenbach V.** 2014. Oxidative stress-induced assembly of PML nuclear bodies controls sumoylation of partner proteins. The Journal of cell biology **204:**931-945.
186. **Jang MS, Ryu SW, Kim E.** 2002. Modification of Daxx by small ubiquitin-related modifier-1. Biochemical and biophysical research communications **295:**495-500.
187. **Lin DY, Huang YS, Jeng JC, Kuo HY, Chang CC, Chao TT, Ho CC, Chen YC, Lin TP, Fang HI, Hung CC, Suen CS, Hwang MJ, Chang KS, Maul GG, Shih HM.** 2006. Role of SUMO-interacting motif in Daxx SUMO modification, subnuclear localization, and repression of sumoylated transcription factors. Molecular cell **24:**341-354.
188. **Hwang J, Kalejta RF.** 2009. Human cytomegalovirus protein pp71 induces Daxx SUMOylation. Journal of virology **83:**6591-6598.
189. **Chu Y, Yang X.** 2011. SUMO E3 ligase activity of TRIM proteins. Oncogene **30:**1108-1116.
190. **Wojcik C, DeMartino GN.** 2003. Intracellular localization of proteasomes. The international journal of biochemistry & cell biology **35:**579-589.
191. **Wojcik C, Paweletz N, Schroeter D.** 1995. Localization of proteasomal antigens during different phases of the cell cycle in HeLa cells. European journal of cell biology **68:**191-198.
192. **Schreiner S, Burck C, Glass M, Groitl P, Wimmer P, Kinkley S, Mund A, Everett RD, Dobner T.** 2013. Control of human adenovirus type 5 gene expression by cellular Daxx/ATRX chromatin-associated complexes. Nucleic acids research **41:**3532-3550.
193. **Nevels M, Täuber B, Kremmer E, Spruss T, Wolf H, Dobner T.** 1999. Transforming potential of the adenovirus type 5 E4orf3 protein. J. Virol. **73:**1591-1600.
194. **Hayflick L.** 1968. Human cells and aging. Scientific American **218:**32-37.
195. **Moore M, Horikoshi N, Shenk T.** 1996. Oncogenic potential of the adenovirus E4orf6 protein. Proc. Natl. Acad. Sci. USA **93:**11295-11301.
196. **Nevels M, Rubenwolf S, Spruss T, Wolf H, Dobner T.** 1997. The adenovirus E4orf6 protein can promote E1A/E1B-induced focus formation by interfering with p53 tumor suppressor function. Proc. Natl. Acad. Sci. USA **94:**1206-1211.
197. **Pero R, Lembo F, Di Vizio D, Boccia A, Chieffi P, Fedele M, Pierantoni GM, Rossi P, Iuliano R, Santoro M, Viglietto G, Bruni CB, Fusco A, Chiariotti L.** 2001. RNF4 is a growth inhibitor expressed in germ cells but not in human testicular tumors. The American journal of pathology **159:**1225-1230.
198. **Hirvonen-Santti SJ, Rannikko A, Santti H, Savolainen S, Nyberg M, Janne OA, Palvimo JJ.** 2003. Down-regulation of estrogen receptor beta and transcriptional coregulator SNURF/RNF4 in testicular germ cell cancer. European urology **44:**742-747; discussion 747.
199. **Uhlen M, Fagerberg L, Hallstrom BM, Lindskog C, Oksvold P, Mardinoglu A, Sivertsson A, Kampf C, Sjostedt E, Asplund A, Olsson I, Edlund K, Lundberg E, Navani S, Szigyarto CA, Odeberg J, Djureinovic D, Takanen JO, Hober S, Alm T, Edqvist PH, Berling H, Tegel H, Mulder J, Rockberg J, Nilsson P, Schwenk**

JM, Hamsten M, von Feilitzen K, Forsberg M, Persson L, Johansson F, Zwahlen M, von Heijne G, Nielsen J, Ponten F. 2015. Proteomics. Tissue-based map of the human proteome. Science **347:**1260419.

200. http://www.proteinatlas.org 2017, posting date. Human Protein Atlas. [Online.]
201. **Cao JY, Shire K, Landry C, Gish GD, Pawson T, Frappier L.** 2014. Identification of a novel protein interaction motif in the regulatory subunit of casein kinase 2. Molecular and cellular biology **34:**246-258.
202. **Teodoro JG, Halliday T, Whalen SG, Takayesu D, Graham FL, Branton PE.** 1994. Phosphorylation at the carboxy terminus of the 55-kilodalton adenovirus type 5 E1B protein regulates transforming activity. Journal of virology **68:**776-786.
203. **Meggio F, Pinna LA.** 2003. One-thousand-and-one substrates of protein kinase CK2? FASEB journal : official publication of the Federation of American Societies for Experimental Biology **17:**349-368.
204. **Lallemand-Breitenbach V, Jeanne M, Benhenda S, Nasr R, Lei M, Peres L, Zhou J, Zhu J, Raught B, de The H.** 2008. Arsenic degrades PML or PML-RARalpha through a SUMO-triggered RNF4/ubiquitin-mediated pathway. Nature cell biology **10:**547-555.
205. **Wang YT, Yang WB, Chang WC, Hung JJ.** 2011. Interplay of posttranslational modifications in Sp1 mediates Sp1 stability during cell cycle progression. Journal of molecular biology **414:**1-14.
206. **Mukhopadhyay D, Arnaoutov A, Dasso M.** 2010. The SUMO protease SENP6 is essential for inner kinetochore assembly. The Journal of cell biology **188:**681-692.
207. **Maul GG, Guldner HH, Spivack JG.** 1993. Modification of discrete nuclear domains induced by herpes simplex virus type 1 immediate early gene 1 product (ICP0). The Journal of general virology **74 (Pt 12):**2679-2690.
208. **Kelly C, Van Driel R, Wilkinson GW.** 1995. Disruption of PML-associated nuclear bodies during human cytomegalovirus infection. The Journal of general virology **76 (Pt 11):**2887-2893.
209. **Nisole S, Maroui MA, Mascle XH, Aubry M, Chelbi-Alix MK.** 2013. Differential Roles of PML Isoforms. Frontiers in oncology **3:**125.
210. **Hu XV, Rodrigues TM, Tao H, Baker RK, Miraglia L, Orth AP, Lyons GE, Schultz PG, Wu X.** 2010. Identification of RING finger protein 4 (RNF4) as a modulator of DNA demethylation through a functional genomics screen. Proceedings of the National Academy of Sciences of the United States of America **107:**15087-15092.
211. **Martin ME, Berk AJ.** 1998. Adenovirus E1B 55K represses p53 activation in vitro. Journal of virology **72:**3146-3154.
212. **Pelka P, Ablack JN, Fonseca GJ, Yousef AF, Mymryk JS.** 2008. Intrinsic structural disorder in adenovirus E1A: a viral molecular hub linking multiple diverse processes. Journal of virology **82:**7252-7263.
213. **Frisch SM, Mymryk JS.** 2002. Adenovirus-5 E1A: paradox and paradigm. Nat Rev Mol Cell Biol **3:**441-452.
214. **Sieber T, Scholz R, Spoerner M, Schumann F, Kalbitzer HR, Dobner T.** 2011. Intrinsic disorder in the common N-terminus of human adenovirus 5 E1B-55K and its related E1BN proteins indicated by studies on E1B-93R. Virology **418:**133-143.
215. **Blackford AN, Grand RJ.** 2009. Adenovirus E1B 55-kilodalton protein: multiple roles in viral infection and cell transformation. Journal of virology **83:**4000-4012.

216. **Bridges RG, Sohn SY, Wright J, Leppard KN, Hearing P.** 2016. The Adenovirus E4-ORF3 Protein Stimulates SUMOylation of General Transcription Factor TFII-I to Direct Proteasomal Degradation. mBio **7:**e02184-02115.

217. **Sohn SY, Hearing P.** 2016. The adenovirus E4-ORF3 protein functions as a SUMO E3 ligase for TIF-1gamma sumoylation and poly-SUMO chain elongation. Proceedings of the National Academy of Sciences of the United States of America **113:**6725-6730.

218. **Puvion-Dutilleul F, Pedron J, Cajean-Feroldi C.** 1984. Identification of intranuclear structures containing the 72K DNA-binding protein of human adenovirus type 5. European journal of cell biology **34:**313-322.

219. **Domingues P, Golebiowski F, Tatham MH, Lopes AM, Taggart A, Hay RT, Hale BG.** 2015. Global Reprogramming of Host SUMOylation during Influenza Virus Infection. Cell reports **13:**1467-1480.

220. **Yates J, Warren N, Reisman D, Sugden B.** 1984. A cis-acting element from the Epstein-Barr viral genome that permits stable replication of recombinant plasmids in latently infected cells. Proceedings of the National Academy of Sciences of the United States of America **81:**3806-3810.

221. **Sivachandran N, Cao JY, Frappier L.** 2010. Epstein-Barr virus nuclear antigen 1 Hijacks the host kinase CK2 to disrupt PML nuclear bodies. Journal of virology **84:**11113-11123.

222. **Ching W, Dobner T, Koyuncu E.** 2012. The human adenovirus type 5 E1B 55-kilodalton protein is phosphorylated by protein kinase CK2. Journal of virology **86:**2400-2415.

223. **Hirota K, Tsuda M, Murai J, Takagi T, Keka IS, Narita T, Fujita M, Sasanuma H, Kobayashi J, Takeda S.** 2014. SUMO-targeted ubiquitin ligase RNF4 plays a critical role in preventing chromosome loss. Genes to cells : devoted to molecular & cellular mechanisms **19:**743-754.

224. **Nevels M, Spruss T, Wolf H, Dobner T.** 1999. The adenovirus E4orf6 protein contributes to malignant transformation by antagonizing E1A-induced accumulation of the tumor suppressor protein p53. Oncogene **18:**9-17.

225. **McLorie W, McGlade CJ, Takayesu D, Branton PE.** 1991. Individual adenovirus E1B proteins induce transformation independently but by additive pathways. The Journal of general virology **72 (Pt 6):**1467-1471.

226. **Sieber T, Dobner T.** 2007. Adenovirus type 5 early region 1B 156R protein promotes cell transformation independently of repression of p53-stimulated transcription. Journal of virology **81:**95-105.

227. **Thomas JJ, Abed M, Heuberger J, Novak R, Zohar Y, Beltran Lopez AP, Trausch-Azar JS, Ilagan MX, Benhamou D, Dittmar G, Kopan R, Birchmeier W, Schwartz AL, Orian A.** 2016. RNF4-Dependent Oncogene Activation by Protein Stabilization. Cell reports **16:**3388-3400.

228. **Diefenbacher M, Orian A.** 2017. Stabilization of nuclear oncoproteins by RNF4 and the ubiquitin system in cancer. Molecular & cellular oncology **4:**e1260671.

8 Abstract (German)

HAdV-C5 repräsentiert ein hervorragendes Modellsystem zur Analyse von Virus-Wirts Interaktionswegen. E1B-55K ist ein multifunktionales virales Protein, das zusammen mit dem viralen Protein E4orf6 und zellulären Komponenten, einen wichtigen Faktor für den Abbau antiviraler zellulärer Proteine durch einen E3 Ubiquitin-Ligase Komplex darstellt. Viele zelluläre Zielproteine es viralen E3 Ubiquitin-Ligase Komplexes wurden bereits identifiziert, wie z.B. p53, Mre11, ATRX und SPOC1. Darüber hinaus wurde der zelluläre Transkriptionsfaktor Daxx als Zielprotein eines E1B-55K induzierten Abbauweges identifiziert, der interessanterweise unabhängig von E4orf6 ist.

In diesem Zusammenhang wurde vor kurzem eine neue Gruppe von Proteinen beschrieben, die den proteasomalen Abbau von SUMOylierten Proteinen vermitteln und dementspechend als SUMO-targeted Ubiquitin ligases (STUbLs) bezeichnet werden. Zwei zelluläre STUbL Proteine wurden bisher identifiziert: RNF4 und Arkadia. Soweit bekannt, ist die STUbL Aktivität von RNF4 für die Homöostase von zentraler Bedeutung, um die Akkumulation von SUMOylierten Proteinen innerhalb der Zelle nach zellulärem Stress, einschließlich UV-induzierter DNA Schäden zu verhindern.

Im Hauptteil dieser Arbeit wurde die Rolle von RNF4 im produktiven Replikationszyklus von HAdV-C5 untersucht. Zuerst konnte die Interaktion zwischen E1B-55K und RNF4 in IPs bestätigt werden. Weiterhin konnte gezeigt werden, dass RNF4 in die Kernmatrix von infizierten Zellen, benachbart zu E1B-55K enthaltenden punktförmigen Aggregaten, lokalisiert wird. Die Ergebnisse RNF4 depletierter Zellen zeigen, dass RNF4 ein positiver Faktor für die lytische Replikation von HAdVC-5 ist. Dagegen weisen Transformationsversuche, auf einen negativen, inhibitorischen Effekt von RNF4 auf die HAdV-C5 E1A/E1B abhängige Transformation primärer Rattenzellen hin.

Der zweite Teil dieser Arbeit befasste sich mit Analysen zur Rolle der zellulären STUbL Arkadia während der produktiven HAdV-C5 Infektion. Arkadia wurde, wie auch RNF4, als neuer Interaktionspartner von E1B-55K identifiziert. Zusätzlich konnte eine Reduktion der Arkadia Proteinmengen während der HAdV-C5 Infektion gezeigt werden, was einen HAdV-C5 abhängigen Abbau von Arkadia während der Infektion vermuten lässt.

Abstract (German)

Zusammenfassend zeigt diese Arbeit erstmalig eine Interaktion zwischen E1B-55K und beiden STUbLs, die im Falle von RNF4 den produktiven Infektionsverlauf von HAdV-C5 fördert. Um die direkte Verbindung zwischen der produktiven Infektion und der zellulären SUMO-abhängigen Ubiquitin-Maschinerie zu verstehen sind noch weitere Experimente notwendig. Allerdings sind die Unterschiede zwischen den zellulären STUbLs RNF4 und Arkadia während der Infektion sehr interessant und werden die Grundlage für weitere wichtige Untersuchungen sein.

Publications

I Publications in scientific journals

- <u>Müncheberg S</u>, Hay R. T, Ip W. H, Meyer T, Dobner T, Schreiner S. (2017) RNF4 STUbL promotes HAdV gene expression by supporting E1B-55K functions. (Journal of Virology, in revision).

- Bürck C, Mund A, Berscheminksi J, Kieweg L, <u>Müncheberg S</u>, Dobner T, Schreiner S. (2015) KAP1 Is a Host Restriction Factor That Promotes Human Adenovirus E1B-55K SUMO Modification. Journal of Virology 90 (2): 930-46. doi: 10.1128/JVI.01836-15.

II Oral presentation at scientific meetings

- 12th International Adenovirus Meeting, Barsinghausen, Germany, 2016.

- DNA Tumor Virus Meeting, Montreal (Quebec), Canada, 2016.

- HPI Scientific Retreat, Hamburg, Germany, 2016.

- TUM Retreat - Institut für Virologie, Schliersee/Spitzungsee, Germany, 2016.

- TUM Retreat - Institut für Virologie, Tutzing, Germany, 2015.

- 3rd HPI Young Scientists Retreat, Hamburg, Germany, 2014.

III Poster presentations at scientific meetings

- EMBO conference on Ubiquitin and SUMO, Cavtat-Dubrovnik, Croatia, 2015.

- 25th Annual Meeting of the Society for Virology, Bochum, Germany, 2015.

- HPI Scientific Retreat, Hamburg, Germany, 2015.

- 4th HPI Young Scientists Retreat, Hamburg, Germany, 2016.

IV Participation in courses/workshops

- Workshop: Planung und Durchführung von Tierversuchen an der Maus, University Medical Center Eppendorf, Hamburg, 2016.

- Soft-skill course: Application Training and Job Analysis (Kepos), Hamburg, 2015.

Acknowledgements

First, I would sincerely like to thank my doctor father and first supervisor Thomas Dobner for giving me the opportunity to work on this interesting project. In addition to this also for his guidance and support during the whole time in the department of pretty pretty viruses and for the joint cheering of the HSV in the Volksparkstadion.

Second, my thanks go to Nicole Fischer for being my second supervisor and for the valuable and good discussions for my thesis. I would like to thank Julia Kehr for chairing my disputation.

Additionally, I would like to thank Sabrina Schreiner from Munich for her tireless personal und financial support during the whole project and for the great opportunity to participate in international meetings and nice retreats in Munich.

Particularly, I would like to thank all lab colleagues and especially the dungeon lab: Tina Meyer, Nora Freudenberger, Wing Hang Ip, Julia Gruhne, Carolin Bürck, Jana Kondrajew, Maggi Valdes-Aleman and Fabian Hausmann. Thank you for your help, good scientific discussions and for the good atmosphere in the lab at any time.

I would like to thank Thomas Speiseder for his helpful corrections and good comments. My special thanks go to Vicky, for her great help during the whole time being together in- and outside the lab!

Last but not least, I thank my husband Benny and my parents, for their endless support at any time and situation. Without their help and support, I would not have mastered this intense time. Thank you for always being at my side!